Auckland Regional Council
TE RAUHĪTANGA TAIAO

Hydraulic Effects of Riparian Plantings

July 2009 TR2009/096

Auckland Regional Council
Technical Report No.096 July 2009
ISSN 1179-0504 (Print)
ISSN 1179-0512 (Online)
ISBN 978-1-877540-09-7

Technical Report, First Edition

Reviewed by	Approved for Auckland Council Publication by
Name: Bodo Hellberg Position: Stormwater Technical Specialist Organisation: Auckland Regional Council Date: 25 July 2009	Name: Judy-Ann Ansen Position: Team Leader Stormwater Action Team Organisation: Auckland Regional Council Date: 25 July 2009

Recommended Citation:

Barnett, A.G., Shamseldin, A.Y. (2009). Hydraulic Effects of Riparian Plantings. Prepared by Barnett & MacMurray Ltd for Auckland Regional Council. Auckland Regional Council Document TR 2009/096.

Hydraulic Effects of Riparian Plantings

A.G. Barnett

A.Y. Shamseldin

Prepared for

Auckland Regional Council

Sections 2-8 of this report are based on “Hydraulic Resistance of Vegetation” Ref 13024.00 dated 4 February 2008, by Auckland Uniservices Ltd, Level 10, Uniservices House, 70 Symonds St, Auckland. (unpublished)

The remainder of this report incorporates and extends the report “Hydraulic Effects of Riparian Planting”, Project BM1-202 dated February 2008, by Barnett & MacMurray Ltd, 318 Grey St, Hamilton. (unpublished)

Contents

List of Symbols

γ specific weight

Δ difference over a reach

μ discharge coefficient

ν fluid kinematic viscosity

ξ deformation factor

ρ density of water

τ local boundary shear stress

τ_0 bed shear stress in conveyance modelling

A cross-section area

A_i frontal area of an individual plant blocking flow or projected plant area in the upstream direction

A_s total cross-sectional area of all of the stems of an individual plant measured at $H_p/4$

a dimensionless coefficient relating shear to velocity

C Chézy C

C_d Drag coefficient of vegetation

C_f Chezy coefficient for vegetated floodplain

C_g Chezy coefficient of grass covered floodplain without other vegetation

C_s manipulation variable

d_v, D pipe diameter

E plant stiffness modulus

f friction factor

g acceleration of gravity

H energy head

H_p average undeflected plant height

h local water depth

h_g average height of vegetation canopy

i subscript referring to the "ith" subsection across the floodplain

K cross-section conveyance

k equivalent grain size

k_{max}	maximum value of k when used for vegetation size
L	reach length
$\mathcal{M}$	dimensioned constant Manning formula coefficient = 1.000 $m^{1/3}$ s^{-1}
M	number of plants per m^2 (in Equation (6))
m	adjustment factor for meandering
MEI	vegetation stiffness factor
n	Manning n (roughness coefficient)
n_1	adjustment factor for surface irregularity
n_2	adjustment factor for variation in shape and size of the channel cross section
n_3	adjustment factor for obstruction
n_4	adjustment factor for vegetation
n_b	base n value for a straight, uniform, smooth channel
n_{eq}	equivalent/apparent/composite Manning roughness coefficient
n_l	Total unit Manning n
$n_{sur}, n_{veg}, n_{irr}$	Unit Manning n for surface, vegetation and irregularity respectively
n_s	Reference Manning n for section; base for relative roughness ratio
n_v	Manning roughness coefficient without vegetation
P	wetted perimeter
p	percentage of opening in hedgerow
Q	flow through section
R	hydraulic radius
rr	relative roughness
S	bed or energy slope
S_f	friction slope
s_v	spacing
u	approach velocity
u_w	wake velocity
V	local flow velocity
V_*	shear velocity
v	velocity causing shear
x	channel distance along axis

Executive Summary

The replanting of stream banks in native vegetation has been encouraged by the Auckland Regional Council as contributing strongly to improvements of freshwater habitats. To ensure that a flooding hazard is not created by providing environmental enhancement, the effect of riparian planting on design peak flows must be quantified. This publication reports the results of an investigation into the hydraulic effects of such plantings along a closely monitored test reach of the Opanuku Stream in west Auckland.

The investigation was undertaken in two parts. The first part, reported in Sections 2-8, evaluated theories about the hydraulic resistance of plants, and endorsed two published models, one for tall vegetation and one for short vegetation. The second part, reported in the remaining Sections, dealt with the practicalities of quantifying hydraulic resistance changes by modelling and field observation, including careful analysis of the sensitivity of results to model limitations.

Factors contributing to hydraulic resistance were analysed, with influences considered including bed surface irregularity, variation in shape and size of the channel cross-section, obstruction, and meandering as well as vegetation. A compound channel description was introduced to account for observed channel/floodplain flow interactions. Methods for estimating roughness were categorised into: visual assessment or remote sensing a priori, profile fitting, manual or automatic optimization, and residual flow methods.

Vegetation resistance was discussed for both submerged and partially submerged cases. For tall vegetation, the model of Kouwen and Fathi-Moghdam (2000) was preferred, while for short vegetation the model of Kouwen and Lin (1980) was chosen. A case study using data from the Opanuku test reach was undertaken, using the vegetation models as implemented in the *AULOS* package to compare resistances predicted a priori using the tall vegetation model with those calibrated in the field by residual flow analysis. A close match could be obtained, but only by assuming a stem wave speed of 0.5m/s, some ten times those measured in limited studies of Canadian tree species. Whether this difference is characteristic of relevant New Zealand tree species awaits investigation, requiring a suitable programme of laboratory testing.

Residual flow analysis was then introduced and demonstrated to be highly sensitive to resistance settings, making it an excellent tool for calibration. In parallel with resistance calibration, this approach was shown to synthesise catchment runoff hydrographs in catchments where field data acquisition includes at least two continuous water level recorders. These runoff hydrographs, deduced purely by hydraulic models, provide a valuable check on catchment rainfall-runoff modelling using more traditional hydrologic analysis.

This analysis concluded that between floods observed in October 2006 and August 2008, there was a measurable decrease of about 10% in the hydraulic resistance of the test reach, expressed in terms of the Manning n. This period coincided with significant

replacement of exotic riparian vegetation by native plantings along the test reach, but some of the resistance decrease may also be attributable to seasonal effects.

1. Introduction

In March 2007, Barnett & MacMurray Ltd was commissioned by the Auckland Regional Council to undertake modelling of the hydraulic effects of riparian planting. At the same time, a complementary report was commissioned from Dr Asaad Shamseldin of the University of Auckland, who as subconsultant to Barnett & MacMurray undertook a literature review of vegetation flow resistance models, recommended preferred models for implementation, and evaluated the outcomes from the resulting computational models.

HYDRA Software Ltd undertook the algorithmic analysis and coding of the selected vegetation flow resistance models, and implemented these in an alpha (research) enhancement of the commercial software package *AULOS* as already used for hydraulic analysis by both Barnett & MacMurray Ltd and the Engineering School of the University of Auckland.

Following an extensive search of available databases, a reach of the Opanuku Stream was selected as having the required combination of intensive hydraulic data monitoring and a significant current riparian planting programme.

The results were presented in February 2008, and an intention was expressed to go on to publish these in a Technical Report of the Regional Council. However the original reports lacked access to measurements of a flood event large enough for proper model verification, so were quickly superseded by the occurrence of a significant Opanuku flood in August 2008.

This report revises the two previous (unpublished) reports, incorporating reference to the full 2008 dataset, and to data collected subsequently.

2. Background

It is well known that the estimation of flow resistance of vegetation is important for many river management studies as it can have significant effects on channel conveyance (Järvelä, 2002). However, the estimation of this resistance is not an easy task. The hydraulic flow through and over vegetation involves complex physical interactions between flow, fluid properties and biophysical properties of vegetation.

The compound channel consisting of distinct channel subsections (e.g. a main channel with floodplains) is a common feature of natural rivers. The flow structure in a compound channel with overbank flow is more complex than that of a single channel due to the variation in cross-section shape and roughness (Yang et al., 2007). Indeed, the existence of vegetation in natural channels adds further complexity to the flow structure.

The report is structured as follows. Section 3 explains the flow structure in compound channels and discusses its complexity. Section 4 describes the roughness description in 1-D model. Section 5 briefly describes the various 1-D methods used for estimating the compound channel resistance. Section 6 discusses the various approaches used for estimating the hydraulic roughness coefficient. Section 7 provides a summary about the experimental and empirical studies concerned with the estimation of vegetation roughness. Section 8 of this report describes the preliminary results obtained by incorporating selected experimental equations into the *AULOS* software package when applied to the original Opanuku case study.

3. Flow Structure in Compound Channels

In the case of compound channels, the roughness of the main channel can be significantly different from that of the floodplains. As mentioned earlier, the flow structure in a compound channel with overbank flow is more complex than that of a single channel due to the variation in cross-section shape and roughness (Yang et al., 2007). The momentum transfer occurring between the main channel and floodplains decreases the discharge in the main channel and increases the discharge on the floodplains, resulting in a possible decrease in the total discharge capacity as the main channel capacity is exceeded. This was recognised in the 1960s by Sellin (1964). A schematic diagram of the mechanism of momentum transfer in a straight two-stage compound channel is shown in Figure 1. Knight et al. (1983) noted that due to strong lateral gradient of the longitudinal velocity, a bank of vortices rotating around a vertical axis may be formed along a vertical interface between the main channel and the floodplain. They also reported that “this mechanism allows for the slower moving water on the floodplain to interact with the faster moving water in the main channel”.

In the last few years, a significant amount of physical laboratory work on compound channels has been carried out (Yang et al., 2007). Knight and Sellin (1987) provided an overview of the work undertaken in the UK flood channel facility at Hydraulic Research (HR), Wallingford. An excellent summary of similar works carried out in the German universities in the 1980’s can be found in Helmiö (2004). In addition to physical laboratory works, numerical (3-D) computational fluid dynamic (CFD) models have also been used to improve the understanding of the flow structure in compound channels (Pezzinga, 1994; Naot et al. , 1996; Sofialidis and Prinos, 1998, 1999; Stoessor et al. 2003; Nicholas and McLelland, 2004).

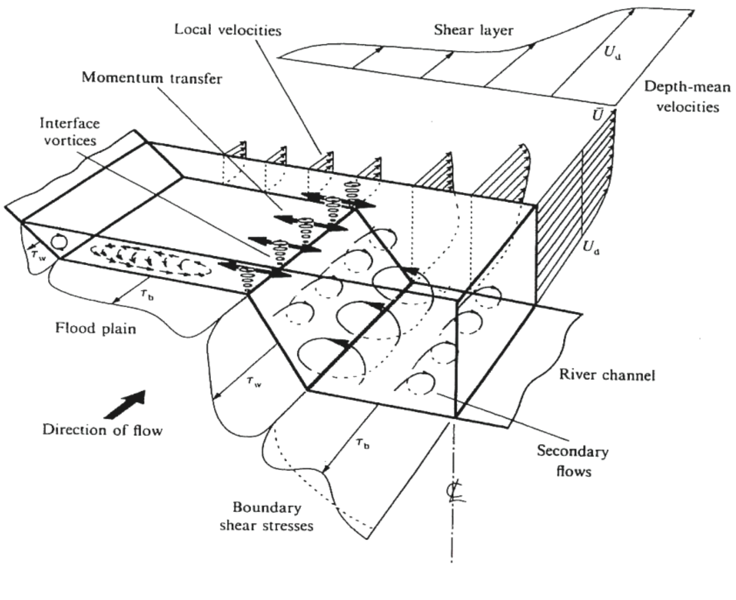

Figure 1: Flow structures in a straight two-stage channel (after Knight and Shiono, 1996)

The flow in and over the vegetation in river channels involves complicated interactions between flow, fluid properties and biophysical properties of vegetation. In general, the vegetation increases the flow resistance, changes the velocity distribution and affects the channel discharge capacity (Yang et al., 2007). Mertens (1989), Naot et al. (1996) and Tsujimito (1999) found that a vortex structure also exists in vegetated compound channels similar to those noted by Sellin (1964) and others in the case of unvegetated compound channels. Yang et al. (2007) noted that the lateral gradient of velocity distribution increases after the floodplain is vegetated and that resistance to flow varies with the vegetation type.

For overbank flow in compound channels, Knight (2006) gave a list of the factors to be taken into consideration when modeling these channels. The list includes: interaction between the main channel and floodplain flows, proportion of flow between sub-areas, the use of hydraulic radius, roughness differences between river and floodplains, significant variation of resistance parameters with depth and flow regime, boundary shear stress distribution, sediment transport and channel sinsousity.

Although, the so-called 1-D, 2-D and 3-D (all are 3-D but with different simplifying assumptions) numerical hydrodynamic models can be used for simulating the water level for a given discharge in natural rivers with compound channels, the UK Department for Environment, Food and Rural Affairs and the Environmental Agency (DEFRA/EA) (2003a) reported that 1-D models are the most effective solution for estimating water levels for a given discharge for the foreseeable future. Furthermore, Yen (2002) noted that the 1-D description of compound channel flow by means of the well known Saint Venant equations continues to be the most efficient tool for a substantial number of fluvial problems. Hence, the modelling discussion in this report is mainly confined to “1-D” models, better described as “hydraulic” models.

4. Roughness Description in 1-D flow

Many of the existing methods for describing roughness are based on the coefficients used in the Chezy and the Manning semi-empirical formulae. Despite their empirical nature and lack of rigorous physics in their developments, they are widely used in practical river engineering studies. The Darcy-Weisbach friction factor is also used to quantify roughness. However, the Manning coefficient, the Chezy coefficient and the Darcy-Weisbach friction factor are related and explanations of the relevant relationships can be found in Henderson (1966), U.S. Army Corps of Engineers (USACE) (1991) and Yen (2002). Chow (1959) noted that the roughness coefficient depends on many factors such as bed form, flow structure, channel irregularity and vegetation. Cowan (1956) developed an equation to aggregate the roughness resulting from a number of contributing factors. The Cowan's equation has the following form

$$n = (n_b + n_1 + n_2 + n_3 + n_4)m \quad (1)$$

where n_b is a base n value for a straight uniform smooth channel, n_1, n_2, n_3, n_4 *and* m are basically adjustment factors for the effects of surface irregularity, variation in shape and size of the channel cross section, obstruction, vegetation and meandering of the channel, respectively. The above equation can be used to determine the Manning roughness for sub-areas in composite and compound channels.

DEFRA/EA (2003b, 2004) adopted the notation of *unit* roughness (roughness due to an identifiable segment of boundary friction per unit length of channel) in computing the channel conveyance. The unit roughness at a point in the channel section can comprise of up to three roughness components (surface material, vegetation and irregularity). These three components are combined to give the total unit roughness n_l at a point according to:

$$n_l = \sqrt{(n_{sur}{}^2 + n_{veg}{}^2 + n_{irr}{}^2)} \quad (2)$$

where n_{sur}, n_{veg} and n_{irr} are the unit roughness values due to surface material, vegetation and irregularity, respectively. These unit roughness values are considered to be associated with a depth of 1 m representative of the river flow depth in the UK. Fisher and Dawson (2003) noted in DEFRA/EA (2003b) that the roughness values calculated based on the Cowan approach (equation 1) under estimate at low flow and over estimate at high flows. However, the roughness values calculated on the basis of the square root of the sum of the squares of the unit roughness values (equation 2) give more priority to the most dominant roughness element and provide good matching with measured values.

5. 1-D methods for Compound Channel Resistance

Conventional 1-D hydraulic methods for compound channel flow resistance can be broadly categorized into the single channel method (SCM) and the divided channel method (DCM) (Cao et al. 2006, Helmiö, 2002). In the case of the SCM, the compound channel is treated as a single channel without taking into full consideration the complex channel-floodplain interaction and the flow structure across the channel. In the case of the DCM, the compound channel is divided into a number of subsections using various assumptions with each sub-section being treated as an independent single channel resulting in a parallel channel system. In practical applications, the DCM is considered to be more widely used than the SCM and it has been incorporated into a number of well established hydraulic modeling software packages (Cao et al., 2006). Knight (1999) found that the SCM and DCM usually underestimate as well as overestimate the discharge. This can be the result of the discontinuity of the overall roughness at the bankfull level resulting in a corresponding discontinuity in the stage discharge relation in some cases (cf. Knight, 1999; Smart, 1992)

Various DCMs, such as Henderson-Lotter, Pavlovskii, and Horton are described in standard hydraulic text books (e.g. Chow, 1959, Henderson, 1966 and French, 1994). Yen (2002) provided a comprehensive review of 17 DCMs. These methods differs in terms of the assumptions made regarding the relationships between the discharge, velocities and forces (shear stresses) between the subsections and the total cross sections. They also differ in the manner in which the channel is divided into distinct subsections. The channel subsection can be obtained using vertical, horizontal and diagonal division rules. Yen (2002) noted that the determination of which DCM is more suitable and whether or not more suitable methods can be derived from fluid mechanics is still an unresolved issue.

Various attempts have made to modify the DCM taking into consideration the knowledge gained about the flow structure in compound channel. The various DCM modifications can be grouped into five categories and a detailed description of these modifications can be found in Knight (2006). Some of these modified DCMs are also described in Helmiö (2002, 2004), Cao et al. (2006) and Werner and Lambert (2007).

Within the New Zealand context, Barnett (2002) developed a modification for the Henderson-Lotter DCM based on perimeter adjustment. This modified method compensates for the usual DCM tendency to overestimate the discharge, producing more accurate responses. It is currently used in the *AULOS* software package.

After a comprehensive literature review about channel conveyance of river channels and consultations with an advisory experts panel, DEFRA (2003a) identified two key approaches for discharge estimation, namely, the energy loss approach (Ervine and Ellis, 1987; Shiono et al., 1999) and the Depth-integration of the Reynolds Averaged Navier-Stokes (RANS) approach (Shiono and Knight, 1990; James and Wark, 1992;

Ervine et al., 2000). The RANS approach has several merits over the energy loss approach. For this reason DEFRA selected the RANS approach for the Conveyance Estimation System (CES) providing guidance to practitioners (DEFRA/EA, 2004). These two approaches are worthy of further investigation with regard to their applicability to New Zealand rivers. However, such investigations are beyond the scope of the present report.

6. Method for estimating the Hydraulic Roughness coefficient

In the simulation of open channel flow using numerical physically-based hydraulic models, the estimation of the values of hydraulic roughness coefficient is paramount. The use of an inadequate set of roughness values would generally produce poor predictions. The estimation of the hydraulic roughness coefficient is a complex non-trivial task. The main difficulty with the estimation of hydraulic roughness is that it cannot be measured directly.

The methods used for estimating the value of the hydraulic roughness can be classified in four broad categories, namely, the a priori approach, the profile fitting approach, the residual flow approach and the combined approach. The first method can be used for both gauged and ungauged sections/reaches while the second and third methods can only be used for gauged sections/reaches where longitudinal stage profiles are available. The fourth category is essentially a combination of the three categories noted above.

6.1 The a priori Approach

As the hydraulic roughness coefficient is a physically meaningful parameter, thus it is possible to estimate its value a priori from the available knowledge of field conditions. The visual estimation method is the most commonly used for estimating the hydraulic roughness (Kidson et al. 2006). This method is based on transfer of information from sections/reaches where the hydraulic roughness coefficient values are known a priori and confirmed previously via stream gauging and hydraulic calculations. In this method, the hydraulic roughness coefficient is estimated by making a photographic image comparison between the section/reach under investigation and sections/reaches with known roughness coefficients and selecting the roughness coefficient for the section/reach which is closest to the site under investigation. Several examples of these photographic images can be found in Chow (1959) and Barnes (1967). Within the New Zealand context, Hicks and Mason (1991) provided a comprehensive set of field photographic images to facilitate the estimation the hydraulic roughness coefficient. USACE (1997) mentioned that “Hicks and Mason presented information for 78 river reaches in New Zealand encompassing a broad range of conditions that are quite representative of conditions found elsewhere in the world. Like Barnes, Hicks and Mason avoided computation of flow resistance in floodplains, although their work does provide some insight as to the contribution of bank vegetation to channel roughness”.

The estimation of the hydraulic roughness by the visual estimation method is basically a manual process which requires a lot of skill, experience and knowledge about the local conditions. It also lacks objectivity in the selection of the most similar section/reach. Tables giving the hydraulic rough coefficient values are also available in many standard hydraulic text book, e.g. Chow (1959), Henderson (1966) and French (1994).

The hydraulic roughness coefficient can also be estimated using semi-empirical equations developed independent of the numerical model relating channel properties to the hydraulic roughness coefficient. However, these equations are not taken into consideration in many of the existing software packages.

In the estimation of the hydraulic roughness coefficient values by the a priori approach, it may be inevitable that these values would require modification to yield the best possible simulations.

In most recent years, the advances being made in remote sensing using airborne Light-Induced Direction and Ranging (LIDAR) have provided new possibilities for the a priori estimate of the roughness coefficient for channel with vegetation. LiDAR provides high resolution topographical and vegetation heights (Mason et al., 2003, French 2003, Bates, 2004).

6.2 The profile fitting approach

This approach, also known as *model calibration,* is based on adjusting the values of roughness coefficients (parameters) and finding the best set of coefficient values yielding the best possible fit to the observed longitudinal profile of stage and discharge. In pure mathematical term, the process model calibration is essentially a non-linear parameter optimization problem.

The estimation of the roughness coefficients may be achieved using manual or automatic optimization methods. Manual optimization is subjective, whereas automatic optimization is objective. There is no guarantee that either approach will produce physically meaningful roughness coefficient values. It is very plausible the estimated coefficients may not be physically meaningful after compensating for deficiencies in geometry and boundary conditions.

6.2.1 Manual Optimization

Manual optimization of parameters involves guessing the values of the roughness coefficients and then, in turn, adjusting these values and observing their effects visually on the longitudinal water surface profile. On the basis of trial and error procedure (i.e. by the discovery of ad hoc rules), the parameters are systematically adjusted and the whole exercise is repeated until satisfactory reproduction of the observed longitudinal water surface profile is obtained based on visual comparison (Khatibi et al., 1997). What constitutes satisfactory reproduction is based on the personal judgment of the user/modeller which can be very subjective.

The use of the manual optimization methods requires considerable experience in terms of familiarity with the model operation and sensitivity. The drawback of the manual optimizations is that they may be quite laborious and time consuming. In the manual optimization methods, the parameters may be adjusted based on a specific objective function (e.g. least squares error function, relative error).

6.2.2 Automatic optimization

The estimation of the roughness coefficient by automatic optimization requires the specification of an estimation criterion to quantify how good are the simulated water surface profiles in replicating the actual profile (i.e. a criterion of goodness of fit). The automatic optimization methods use pre-defined sets of rules to advance the search of the roughness coefficient values which give the optimum value of the objective function. To date there are only few studies dealing with the estimation of the roughness coefficient using automatic optimization and limited to roughness estimation in the bank-channel (see Wiggert et al., 1976, Fread and Smith 1978; Khatibi et al., 1997). However, more recently Nguyen and Fenton (2005) extended the use of automatic optimization to roughness identification in compound channels. The use of automatic optimization involves a large number of repeated runs of the numerical model. In this case, the computational time will be a crucial factor. It is very plausible this may be the inhibiting factor for the widespread use of automatic optimization as many of the available models are computationally time demanding.

In the above limited studies there is no consensus about which objective function to be used. The objective functions used in these studies include the sum of the squares of errors, the sum of absolute errors and the sum of the relative errors. Khatibi et al. (1997) found that estimated roughness coefficient values are affected by the choice of the objective function.

In principle local and global search methods can be used for automatic optimization. The global optimization methods are efficiently oriented to search for the global minimum. However, the identification of roughness has only been carried out using local search methods such as the Newton-Raphson search method.

In estimation of the parameters of complex hydrodynamics models by automatic optimization, it is very likely that they suffer from the same problems associated with parameter identification of complex over-parameterised environmental models. These problems are very well documented (cf. Ibbitt and O'Donnell, 1974). The over-parameterization would result in poor parameter identifiablity - a problem which is referred to by Beven (1993) as equifinality in which for a given model there are many parameter sets providing equivalent simulations for the real system.

6.3 The residual flow approach

In this process, introduced by Barnett (2008) for this study, the observed profiles are fitted exactly by setting them as boundary conditions at stub tributaries set up at each profile measurement point. Balancing residual inflows and outflows are required to maintain the exact level match, and minimization of these (after taking into account reasonable actual tributary flows) provides the criterion of final calibration.

6.4 Combined Approach

In view of the uncertainties associated with both the a priori and profile fitting approaches, it is considered good practice to apply both procedures concurrently, modifying assumptions until there is substantial overlap between the two ranges of values produced. If this can be achieved, the resistance can be regarded as calibrated.

7. Flow resistance of Vegetation

Most of the approaches developed to estimate flow resistance of vegetation are derived from laboratory flume experiments using simulated vegetation. However, some recent studies have used actual plants (Kouwen and Fathi-Moghadam, 2000; Wilson and Horritt, 2002). However, in spite of the substantial research being carried out, the effects of vegetation on flow resistance are still not fully understood (e.g. Tsihrintzis, 2001). There is no universal agreed approach about how to estimate the flow resistance and new studies are continually emerging.

The methods used to estimate the flow resistance of vegetation can be classified into two categories depending on whether the vegetation is submerged or partially submerged.

7.1 Flow resistance of Partially submerged vegetation

In the case where the plant height is of the same order of magnitude or higher than the flow depth, Righetti and Armaninin (2002) noted that the "*equivalent resistance can be evaluated as the combined effects of the hydrodynamic drag*". The majority of models developed to estimate the vegetation flow resistance are based on laboratory experiments treating plants as rigid cylinders. Lin and Shen (1973) using different rigid cylinder setups found that the grouping of the cylinders has significant effects on the flow rate. Furthermore, they noted four factors which could affect the drag. These factors which were previously summarized by Petryk (1969) are 1) the open-channel turbulence; 2) the non-uniformity of the velocity profile; 3) the free surface effects; and 4) the effect of blockage. However, in the case of densely vegetated channels, the first two of these factors can be neglected (Lindner, 1982). The following is a brief literature review of the relevant studies investigating the flow resistance of partially submerged vegetation.

Klaassen and Zwaard (1974)

This paper investigated the determination of the roughness coefficient for partially submerged vegetated floodplains using laboratory experiments on large and small flumes. Two types of vegetation were considered, namely, hedges and orchards. The study found that the value of the Chezy coefficient is dependent on the average spacing of hedges, the number of trees per unit area in orchard and the water level in a floodplain. By assuming the water level to be parallel to the bed and the hedges to be uniformly distributed with spacing *d*, the Chezy coefficient for vegetated floodplains C_f is given by:

$$\frac{1}{C_f^2 h} = \frac{1}{C_g^2 h} + \frac{1}{2gd}\frac{\left(-\mu^2 p^2\right)}{\mu^2 p^2} \quad (3)$$

where h is the water depth, μ is the discharge coefficient, C_g is the Chezy coefficient of grass covered floodplain without other vegetation, g is the acceleration due to gravity and p is the percentage of opening in hedgerow. The product $\mu\, p$ can be calculated using experimental relationships which were provided in the paper. These relationships were only given for water depths up to 2.5m. However, it is not clear how the above equation will perform when the vegetation distribution is not uniform and also under non-uniform flow conditions. There were no clear statements being made regarding the generality and the applicability of the above equations to sites other than those investigated in the paper.

Petryk and Bosmajian (1975)

In this paper, a theoretical analysis of flow through partially submerged (large woody) vegetation was presented using a simple flow model. The theoretical basis of this model is that flow resistance through vegetation is a function of many variables including flow velocity, distribution of vegetation in the vertical and the lateral directions, the roughness of channel boundary and the structural and hydrodynamic properties of the leaves and stems of the plants. Furthermore, the following assumptions were made in the development of the model:

- The velocity is small enough to prevent a large degree of plant bending;
- The vegetation is relatively uniformly distributed in the lateral direction;
- Large variations in average velocity do not occur across the channel;
- The maximum flow depth is less than or equal to the maximum height of vegetation;
- Large variations in flow velocity do not occur over the flow depth.

Petryk and Bosmajian (1975) developed a quantitative model to predict the Manning roughness coefficient as a function of flow depth and vegetation characteristics. In this model, the estimation of the flow resistance was based on the calculation of the drag forces created by the larger plants and trees that constitute much of the resistance on the floodplains. For steady uniform and gradually varied flow conditions and rigid vegetation, they gave the following equation to estimate the equivalent/apparent/composite Manning roughness coefficient n_{eq}

$$n_{eq} = n_v \sqrt{1 + \frac{C_d \sum A_i}{2gAL} n_b^{-2} R^{\frac{4}{3}}} \qquad (4)$$

where n_v is the bed roughness without vegetation, A_i is the projected plant area in the upstream direction, C_d is the drag coefficient of vegetation, A is the cross-sectional flow area and L is the reach length. The above equation was obtained by summing the forces in the longitudinal direction due to pressure, shear and plant drag.

In the above equation, the term $\frac{C_d \sum A_i}{AL}$ represents the vegetation characteristics as a multiplication of the drag coefficient and vegetation density. Flippin-Dudley et al. (1998) designed a field device to measure the vegetation density. Righetti and Armani (2002) reported that the estimation of the drag coefficient C_d in the above equation is the most uncertain parameter.

Freeman et al. (2000) presented the following discussion about the limitations of the above equation

"The channel velocity must be small enough to prevent bending or distortion of the vegetation, and large variations in velocity cannot occur across the channel. Vegetation such as grasses and shrubs are then excluded. Vegetation must also be distributed relatively uniformly in the lateral direction. Finally, according to Petryk and Bosmajian, the flow depth must be less than or equal to the maximum vegetation height. During flooding, the velocities over the floodplains can be relatively high and large degrees of bending and distortion of vegetation often occur. Vegetation types and densities can also vary widely across a floodplain, and water depths often submerge vegetation. However, when tree trunks dominate sections of a floodplain, this method can be used to predict the total resistance coefficient, n"

Fathi-Moghdam and Kouwen (1997) and Kouwen and Fathi-Moghdam (2000)

In these papers, the authors showed the assumption of rigid vegetation commonly used for vegetation on floodplains leads to large errors in the estimation of roughness and it is paramount to take into consideration the flexibility of the foliage.

Kouwen and Fathi-Moghdam (2000) developed a physically based model for calculating the roughness coefficient using experiments carried out using coniferous tree in water flumes and in air on a moving truck. According to this model the friction factor f is given by

$$f = 4.06\left(\frac{V}{\sqrt{\frac{\xi E}{\rho}}}\right)^{-0.46}\left(\frac{h}{h_g}\right) \qquad (5)$$

where V (m/s) is the flow velocity, E (N/m^2)is the tree modulus of elasticity, ξ is a factor accounting for deformation (dimensionless), ρ (kg/m^3) is the density of water, h (m) is the depth of flow and h_g (m) average height of vegetation canopy. The above equation was derived using four coniferous tree species in which the tree height varied between 2 to 4 m. Furthermore, Kouwen and Fathi-Moghdam (2000) noted that the use of the above method for non-coniferous trees is anticipated to be more accurate than those methods which do not account for the vegetation flexibility. The advantage of this method is that it generalises the vegetation properties and it is applicable to different plant types. However, its main disadvantage is the difficulty in estimating the vegetation properties, although the physical basis of the properties suggest that direct laboratory measurement should be possible.

Freeman et al. (2000)

In this report, the authors noted that previous research studies on the estimation of flow resistance of vegetation mainly focused on vegetation such as grasses, agricultural crops, and on the rigid blockage of cylindrical tree trunks. They also reported that there has been a limited number of studies dealing with the flow resistance effects of submerged or partially submerged plants and shrubs. They argued that flexible stems and varying shapes of plant leaf mass complicate the physical understanding of this resistance. As a result, they conducted experiments on large and small flumes to study the effects of ground cover plants, small trees and shrubs on flow resistance. This study involved more than 220 experiments with 20 different plant species. The results indicated that the hydraulic roughness in vegetated channels depends on the stiffness of the plants growing in the channel, the depth, the velocity, the hydraulic radius, the plant density and the frontal area of the plant obstructing the flow. For submerged flow conditions the Manning roughness coefficient is given by:

$$n_{eq} = 0.183\left(\frac{EA_s}{\rho A_i V_*^2}\right)\left(\frac{H}{h}\right)^{0.243}(MA_i)\left(\frac{\nu}{V_* R}\right)^{0.115}\left(\frac{1}{V^*}\right)(R)^{2/3}S^{1/2} \quad (6)$$

where

E = Modulus of plant stiffness (N/m^2)

A_s = Total cross-sectional area of all of the stem(s) of an individual plant, measured at $H_p/4$ (m²)

A_i = Frontal area of an individual plant blocking flow (m²)

ρ = Fluid density (kg/m^3)

V_* = Shear velocity (m/s)

H_p = average undeflected plant height

h = flow depth (m)

ν = Fluid kinematic viscosity m²/s

R = hydraulic radius (m)

S = bed or energy slope

M = number of plants per m^2

In the above equation, the estimation of the stiffness modulus E is very important. Freeman et al. (2000) gave the following empirical equation for calculating E as a function of the average un-deflected plant height H_p and the stem diameter D_s measured at $H_p/4$:

$$E_s = 7.648\times10^6\left(\frac{H_p}{D_S}\right) + 2.174\times10^4\left(\frac{H_p}{D_S}\right)^2 + 1.809\times10^3\left(\frac{H_p}{D_S}\right)^3 \qquad (7)$$

The stiffness modulus can also be estimated from measured values of similar plants. However, actual field measurements of E are recommended where possible. The above method is also applicable to multiple plants where the average plant characteristics are calculated and used in equation (6) to estimate the corresponding Manning roughness coefficient.

7.2 Flow resistance over Submerged vegetation

A typical example of submerged flow is the flow in grass lined channel. One of the earliest methods used for estimating the flow resistance of submerged grass is the n-VR retardance curve approach where n is the Manning roughness and VR is the product of average velocity and hydraulic radius (USDA handbook, 1954). These empirical curves show that the value of n decreases as the product VR increases. Wu et al. (1999) noted that the decrease in the value of n is the result of increased plant bending and submergence as VR increases. However, the difficulty of using these curves is that they are specific to a particular type of grass and channel configuration (Wu et al., 1999).

Kowuen and Unny (1973) developed a more theoretically based approach for determining the roughness coefficient as a function of the bio-mechanical properties of grass (e.g. vegetation stiffness) and the strength of the flow. Kouwen (1992) showed that this approach could satisfactorily produce the empirical USDA n-VR curves. Based on this approach Kouwen and Li (1980) in experiments with flow over flexible plastic strips, showed that the vegetation roughness height (k) is given by:

$$k = 0.14h_g\left[\frac{\left(\frac{MEI}{\tau}\right)^{0.25}}{h_g}\right]^{1.59} \qquad (8)$$

where h_g (m) is the vegetation height, MEI (N/m^2) is vegetation stiffness and τ (N/m^2) is the local boundary shear stress. Kouwen (1988) found that MEI is related to the grass vegetation height by the following equation

$$MEI = \begin{cases} 319\,h_g^{\;3.3} & \text{for growing grass} \\ 25.4\,h_g^{\;2.26} & \text{for dormant grass} \end{cases} \qquad (9)$$

Once the vegetation height is determined the Darcy-Weisbach friction factor (roughness coefficient) is found using a semi-logarithmic resistance relation which has a similar form to the physically-based Colebrook-White equation for rough turbulent flow (Kouwen and Li, 1980). However, the coefficient of the semi-logarithmic resistance relation varies depending on the ratio of the boundary shear stress to a critical shear stress. Mason et al. (2003) used equations (8) and (9) in the development of a 2-D hydraulic model for river flood inundation. The advantage of this method is that it generalises the vegetation properties and this is applicable to different types of plants. However, its main disadvantage is the difficulty in estimating the vegetation properties.

Using laboratory experiments in which plants were modelled as rigid cylinders of diameter d_v with spacing s_v, Thompson and Robinson (1976) found that the wake velocity u_w is dependent on both vegetation diameter and spacing according to the following equations:

$$\frac{u_w}{u} = 0.48\left(\frac{s_v}{d_v}\right)^{0.14} \quad \text{for } 4 \le \left(\frac{s_v}{d_v}\right) \le 20 \qquad (10)$$

$$\frac{u_w}{u} = 0.7\left(\frac{s_v}{d_v}\right)^{0.08} \quad \text{for } 20 \le \left(\frac{s_v}{d_v}\right) \le 100 \qquad (11)$$

where u is the approaching velocity. The main disadvantage of this method is that it is only valid for non-flexible vegetation.

Freeman et al . (2000) gave the following equation which is similar to equation (4) for calculating the Manning roughness for partially submerged flow:

$$n_{eq} = 3.478\times10^{-5}\left(\frac{E_s A_s}{\rho A_i V_*^2}\right)^{0.15}\left(MA^*_i\right)\left(\frac{\nu}{V_* R}\right)^{-0.622}\left(\frac{1}{V^*}\right)\left(R\right)^{2/3} S^{1/2} \qquad (12)$$

The above equations generalizes the vegetation and also applicable to multiple plants situation.

7.3 Experience from Overseas

7.3.1 Australian Experience Brisbane City Council in Australia (2007)

(http://www.brisbane.qld.gov.au/bccwr/lib117/ncd_appendixc_part3.pdf)

In determining the channel roughness, the Brisbane Council uses the procedure developed by Cowan (1956). In this procedure, the Manning roughness coefficient is obtained by summing the resistance due to a number of factors and then multiplying the sum by a further factor to take into consideration the effects of meandering.

In this report, tables and photographs are given to help in the a priori selection of appropriate values for the Manning roughness coefficient.

7.3.2 US Experience

U.S. Army Corps of Engineers (USACE) (1991) noted that in natural channels a distinction should be made between the main channel and the floodplain in estimating the flow resistance. In the main channel, the friction forces stem from sediment grains and bed forms while in the floodplains friction forces stem from vegetation and perhaps, structures. USACE (1991) outlined four methods which can be used for estimating the Manning roughness, namely,

(i) Estimation based on experience which was noted as the best guide

(ii) Estimation based on observed data

(iii) Estimation based on the data of similar reaches

(iv) Estimation based on published guidelines

7.3.3 UK Experience

DEFRA/EA (2004) developed a software package (Roughness Advisor (RA)) for estimating the local hydraulic resistance due to surface material, vegetation or irregularities. The roughness values are obtained from the information or the knowledge of the reach of interest e.g. channel description, photographs, grid co-ordinates. DEFRA/EA (2004) noted that "*If a roughness description is available, the user can navigate through the different roughness components and select the roughness values. If a site photograph is available, this can be used to identify the surface cover by comparison to the RA photographs. If the grid reference is known, this can be used to obtain expected vegetation morpho-types. In the absence of any survey data or channel description, the RA provides advice using the national data set obtained through the national survey of river habitats".* Thus, the approached adopted in the UK is not that different from the USA.

7.4 Summary and Conclusions

There is only a limited number of analytical equations which can be used for the estimation of the flow resistance of vegetation. Some of these equations lack generality in terms of their applicability to vegetation of different properties.

Most of these equations are derived from laboratory flume experiments and hence have many limitations when used in practical applications. These limitations can arise from experimental setup as well as violation of the basic assumptions. Thus, in practical applications these equations should be used under conditions within their range of applicability. These limitation arise because experiments are usually conducted under uniform flow conditions in prismatic single channels. They also arise due to the use of simulated vegetation as well as a limited range of tree species and sizes in these experiments.

The stiffness and the flexibility-based vegetation roughness estimation methods (see equations 5, 7, 8 & 12) (Fathi-Moghdam and Kouwen, 1997; Kouwen and Fathi-Moghdam, 2000; Kouwen and Lin 1980; Freeman et al. 2000) are very promising due to their generalization of vegetation properties. This is essentially advantageous given the heterogeneity of plants in natural rivers. These methods are also applicable to flexible vegetation. Thus, these methods should be further investigated with regard to their applicability to New Zealand rivers. However, in the present study equations (5) and (8) are selected to be incorporated in the *AULOS* software package for the determination of the hydraulic resistance for tall and short vegetation, respectively. They are mainly chosen instead of equations (7) and (12) of Freeman et al. (2000) due to their simplicity. In spite of theoretical elegance of the flexibility methods, it is very difficult to know how they perform when used in practical applications. As far as the author is aware, there are no comprehensive studies dealing with the evaluation the performance of the flexibility methods using actual field data.

8. Opanuku Case Study

This Section provides a summary of the results of the original (2007) Opanuku case study. That study was completed in February 2008, but was then still lacking records of an adequate flood event for field verification of the calibration obtained using the flood of 1 October 2006. Partial verification was achieved using the minor flood of 16-17 August 2007, but this was not large enough to reach significant areas of riparian vegetation. A more significant flood event was recorded on 24 August 2008, providing the opportunity to expand and consolidate the original study results. The resulting updated material is presented in later Sections.

The original model was obtained by incorporating equations (5) and (8) into the *AULOS* software package, henceforth, known in this report as the modified version. The computer coding of these equations into *AULOS* was performed by Hydra Software for the client (Barnett & MacMurray Ltd) following a series of discussions. The implementation of these equations into *AULOS* requires the definition of a switch to enable the model to distinguish between tall and short vegetation. This switch is based on the parameter h_g. Similar to Mason et al (2003), the vegetation is considered as short if $h_g < 1.2\ m$ otherwise it is considered as tall. Also, the modified *AULOS* friction factors are converted into the Manning roughness using standard relations between the Manning equation and the Darcy-Strickler equation for rough turbulent flow. In this preliminary implementation of the short vegetation model, the original semi logarithmic relation of Kouwen and Li (1980) is not used. For simplicity, the parameter *k* is interpreted as the Strickler *k* for rough turbulent flow instead of the Kouwen and Li (1980) semi-logarithmic relation.

The original Opanuku study reach covered the chainage 4.706 to 4.839. The flow event chosen for the study was the October 2006 event. The files containing the original calibrated model using the unmodified version of *AULOS* were provided by Barnett & MacMurray Ltd. The relevant data including the cross-section, boundary and initial conditions was contained these files. However, the boundary at the branch Inflow1 0.000 was set to the error flow from the calibrated Opastudy run instead of the level hydrograph at the Vintage gauge. The main reason for this is to test the sensitivity to riparian resistance with extended model boundaries to provide buffering effect. The name given to these files is “Exam2”. The results of the calibrated model were checked priori to their subsequent use in the modified version of *AULOS* files. The original model layout is shown in Figure 2. Further, details about Exam2 modelling experiment can be found in Barnett (2008).

The objective of this was to test the fidelity of the modified version of *AULOS* by

- Testing the performance of the modified *AULOS* software package in simulating the water levels at Opanuku 4.706, measured immediately downstream of the junction by comparison with the Exam2 results.
- Testing the performance of the model lateral overflows from Opanuku 4.706, measured at the weir at Overland 0.030 by comparison with the Exam2 results

Comparison of the values of the relative roughness in the areas covered by tall vegetation with those obtained from the unmodified version of the software package (Exam 2). After each model run, the modified version of *AULOS* prints the values of the relative roughness at different time periods and for the different cross-sections in a temporary debug file.

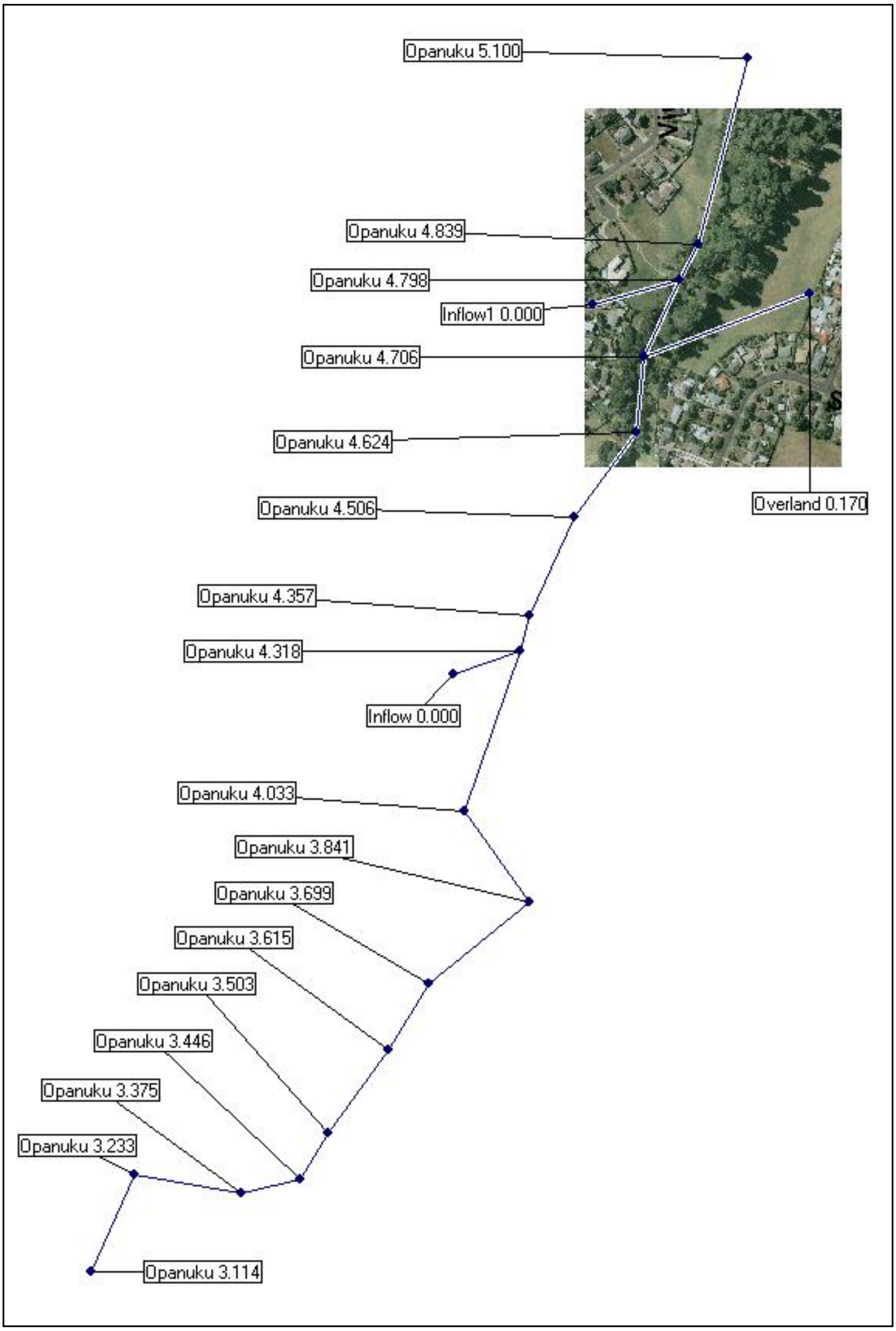

Figure 2: The original (2007) Opanuku model setup

8.1 Model Setup in the Modifed *AULOS*

The hydraulic model in the modified *AULOS* software package for the Opanaku required the specifications of various variables which included:

- The spatial extent of tall vegetation in the floodplain across the cross-section for the reach (chainage 4.706 to 4.83): This was determined using the LIDAR image of the Opanaku river.
- The global Manning roughness coefficient: The value of this coefficient was taken as 0.045 similar to the calibrated model obtained using the unmodified version of *AULOS*.
- The relative roughness in the floodplains outside the study reach as well as in the reminder of the floodplain reaching areas not covered by tall vegetation in the study reach: The value of this relative roughness was taken as 10, as for those of the calibrated model obtained using the unmodified version of *AULOS*.
- The stem wave speed which can be defined from equation (5) as $\sqrt{\frac{\xi E}{\rho}}$. The term ξE, which is known as the vegetation index, is unique for a particular tree species. The vegetation index is determined through lab experiments involving the measurements of the resonant frequency, mass and length of a tree specimen. As far as the author is aware there are no published values for the vegetation index for the New Zealand tree species. However, limited studies carried in Canada showed the value of the vegetation index can vary between 2.07 N/m^2 (Cedar) to 4.54 N/m^2 (Austrian pine) (Kouwen and Fathi-Moghadam, 2000). Accordingly, the value of the stem wave speed can vary between 0.045 m/s (Cedar) to 0.067 m/s (Austrian pine). In the present work, the value of the stem wave speed is taken as 0.05 m/s which is can be regarded an average value deduced from the limited known values of the vegetation index reported by the Canadian studies.
- The average height of vegetation in the Canopy: This was assigned a value of 6 m based on a crude estimate during a visit to the site. This preliminary study only considers tall vegetation which dominates the floodplains just outside the main channel in the study reach.

8.2 Model Results of the Modified *AULOS*

Figure 3 shows a comparison between the simulated water levels at Opanuku 4.706 obtained by a priori literature-based estimation of riparian resistance in the modified version of *AULOS* (measured immediately downstream of the junction) with those calibrated from the Exam2 modelling experiment using the unmodified version of

AULOS. Examination of the figure shows that the results of these two versions are almost indistinguishable.

Examination of the temporary debug file at cross section 4.706 shows that the corresponding a priori value setting of the relative roughness near the peak water level in the areas covered by tall vegetation is generally less than 2. In the unmodified version of *AULOS*, the calibrated relative roughness for these areas is around 10. At moment, it is not clear what is the exact cause of such a difference in the relative roughness value between the two versions. One possibility is that the tall vegetation model is not suitable for this area. It is worth noting that a values of relative roughness of 10 in the modified version can be obtained by increasing the value of the stem wave speed by considerable amount e.g. 0.5 m/s Barnett (2008) which is significantly beyond the upper limit of published values (0.067 m/s). However, in the present study this is considered as physically unrealistic. Further studies beyond the scope of this study should be aimed at explaining this difference.

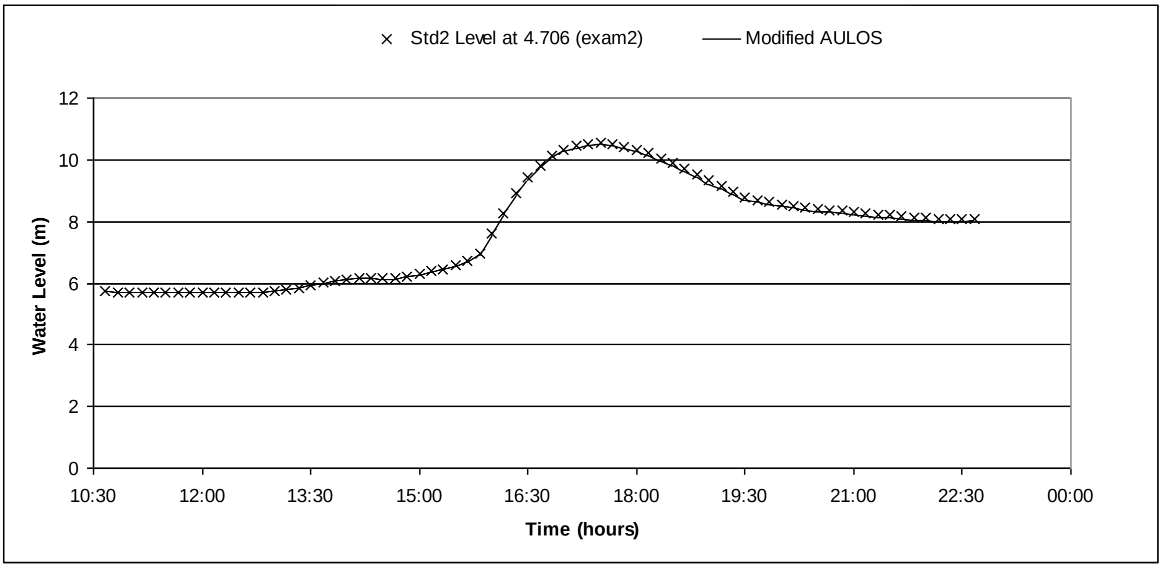

Figure 3. Simulated water levels at 4.706 for the October 2006 event.

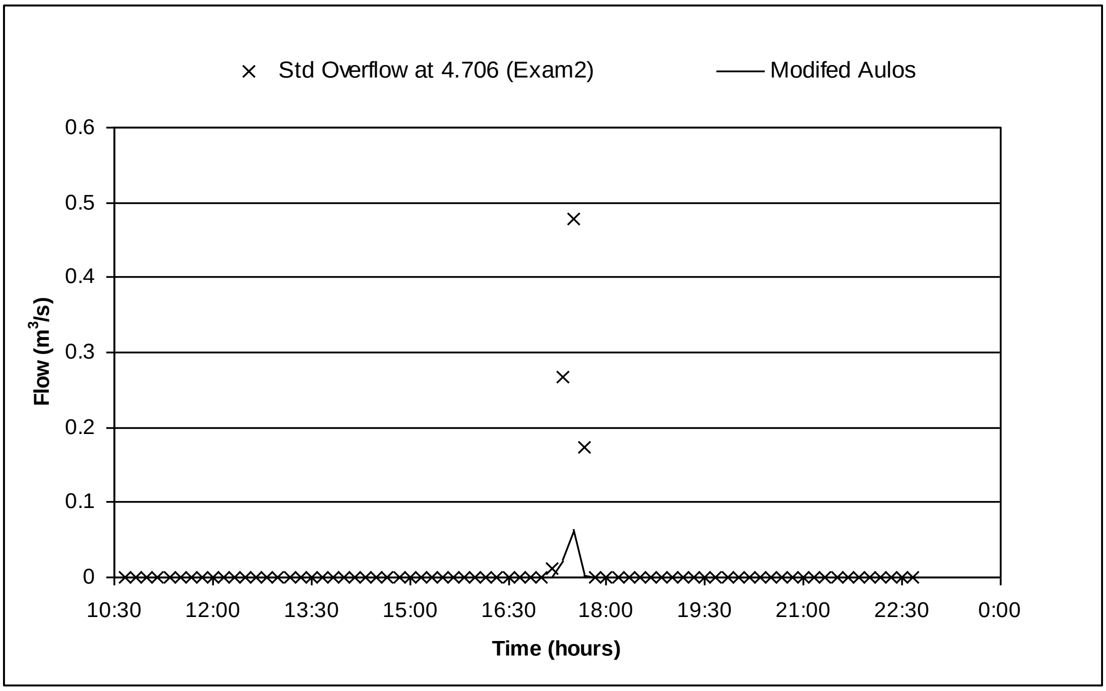

Figure 4. Simulated lateral overflows from Opanuku 4.706, measured at the weir at Overland 0.030 for the October 2006 event

Figure 4 shows a comparison of the simulated lateral overflows from Opanuku 4.706, obtained by a priori riparian resistance in the modified version of *AULOS* with those obtained from Exam2 modelling calibration using the unmodified version of *AULOS*. Examination of the figure reveals that there are significant differences between the results obtained using the two versions, reflecting the effect of the reduced riparian resistance estimated a priori from the literature.

9. Field Data

With assistance from Auckland Regional Council staff, the ARC data archives were searched with the original intention of finding a short-list of a few sites with adequate data to support the required model evaluation.

Requirements for sites were:

a. The site must include a gauging station or flow measuring device with known performance.

b. At least two level recorders were required on the same channel to provide a field measurement of slope throughout at least one calibration and one verification event.

c. A reasonable density of rain gauge cover was needed to support hydrological checking of flow records.

d. Surveyed cross-sections were required at frequent intervals (no more than 100m).

e. High resolution recent aerial photography of the site vicinity for visual assessment of vegetation cover.

f. Lidar survey to support automated digital techniques of terrain data assessment.

g. Most importantly, local riparian vegetation issues relevant to the study objectives.

Unfortunately, of the many sites accessible by the ARC database, not one in the Auckland Region was found to meet all of these requirements. This included all sites monitored by central government groups such as NIWA and all sites run by the territorial authorities. The main causes for rejection were failure to meet criteria a, b, d or g, suggesting hydrological thinking had been dominant in planning for field survey. Given a fixed survey budget, this tends to prefer to cover a wider range of catchments with one gauging station per catchment, rather than monitoring a smaller number of catchments with full instrumentation directly measuring hydraulic gradients as well as tracking flows.

One site, the Opanuku Stream at Vintage Reserve, was initially thought to meet all requirements, and work started on analysis at this site. However on closer inspection, criterion b was not fully met because the new level recorder at Border Road was found to have malfunctioned initially, so only one event (that of 1-2 October 2006) had been captured there with a hydrographic record of acceptable quality. Because this site otherwise matched the criteria well (in particular with respect to a proposed intensive riparian planting programme in the vicinity), and because there were no suitable alternative sites, it was agreed to begin work using that site in the hope that the required second (verification) event would occur while the study was in progress.

No such event occurred before the original project termination date of 30 June 2007, but as the calibration based on the October 2006 event had by that time been delayed by various factors, the project was extended by mutual agreement. On 16-17 August 2007, a flood was recorded which reached the riparian vegetation, so this was initially adopted as the verification event even though it was significantly smaller than the October 2006 event.

9.1 National Survey Data

An extensive study of national survey data collected by the Water Resources Survey, formerly of the Ministry of Works and Development and more latterly transferred to DSIR management, was published by Hicks and Mason in 1991 as "Roughness Characteristics of New Zealand Rivers". As was accurately noted by the reviewers (Jowett and Thompson (1992)) "(Manning) *n* increases in value with flow at only 5 or 6 sites as the water level encroaches on the vegetated berms. This book will assist by drawing attention to the need to adjust *n* for these effects."

In the present context, the most interesting of the sites showing an increase in Manning n with flow is the Ngongotaha at SH5 Bridge (Hicks and Mason p.154), as the stream is of comparable size to several significant Auckland streams and has dense riparian vegetation. From inspection of the supplied photographs, much of this vegetation is native, although willows also feature. At low flows the Manning n is around 0.045, but this doubles to 0.090 in the largest flow rated of 27.7 cumecs.

Bearing in mind the ratio of unobstructed channel area to vegetated area shown in the plotted cross-sections, this suggests a relative roughness of the order of 10 in the vegetated areas.

Of the Auckland sites covered, Orere at Bridge (p. 54) and Hotea at Gubbs (p. 174) both show decreases of Manning n with increasing flow, but the photographs show riparian vegetation as mainly pasture in both cases, rather than dense shrubs or trees. The Kaipara at Waimauku (p. 234) has rather more mixed riparian vegetation, and sure enough the Manning n tends to remain approximately constant with increasing flow.

9.2 Evaluation of Opanuku Dataset

As already discussed in the introduction to Section 9 above, only one event was initially available for calibration of this stream model, and data for the second verification event came available during September 2007.

9.2.1 Cross-Section Data

This was provided by the client with a satisfactory longitudinal density between Border Road and the Vintage Reserve, and again downstream of Henderson Park, but data between these reaches was sparse. For example, there were 18 sections available between Opanuku chainage 2859 and 4839, an average spacing of 116m, but then a 140m gap to 4979m, a 233m gap to 5212m and a 202m gap to 5414m.

Further inspection of the latter three sections revealed that none were trustworthy, as the section at 4979m was a direct copy of that at 4798m, while those at 5212m and 5414m were identical. The suppliers of the cross-sections, Waitakere City, then advised (K. Fan Email dated 20 August 2007) that the section at 4979m should be deleted. This left a 373m gap to the section at 5212m, so it was then clear that detailed modelling could not continue downstream of the section at 4839m (=4.839km). Further investigation of the duplicated section data downstream was therefore discontinued.

Since the key Vintage Reserve gauging site was only one cross-section upstream of this last usable section, a strategy for artificially extending the model downstream was required, and this was essentially approached by projecting the section at 4.839km downstream at a gradient equal to the average slope of the upstream channel reach. This is discussed further in Section 17.

9.2.2 Aerial Photographs

Aerial photographic coverage scaled at 1.325 pixels/m was supplied by Waitakere City. This was georeferenced in NZMG coordinates by given corner coordinates on an inscribed rectangle.

9.2.3 Lidar Data

Excellent Lidar coverage of the area was provided by the client, although this was recorded in NZTM map coordinates whereas all data (aerial photographs, cross-sections) supplied by Waitakere City Council was in NZMG coordinates. Because the Lidar data was already in digital form, it proved easier to harmonise the various supplied datasets by writing software code to transform the raw Lidar data to NZMG, rather than converting several miscellaneous NZMG data files into NZTM coordinates.

All data coordinates were therefore managed in NZMG coordinates so as to make direct overlay mapping possible. The transformation from NZTM to NZMG was calibrated against coordinate transfers available from the LINZ web site, and a horizontal accuracy of +/-1cm was obtained for the four corner points on the perimeter of the area of interest.

9.2.4 Comparison of Lidar-Based and Surveyed Cross-sections

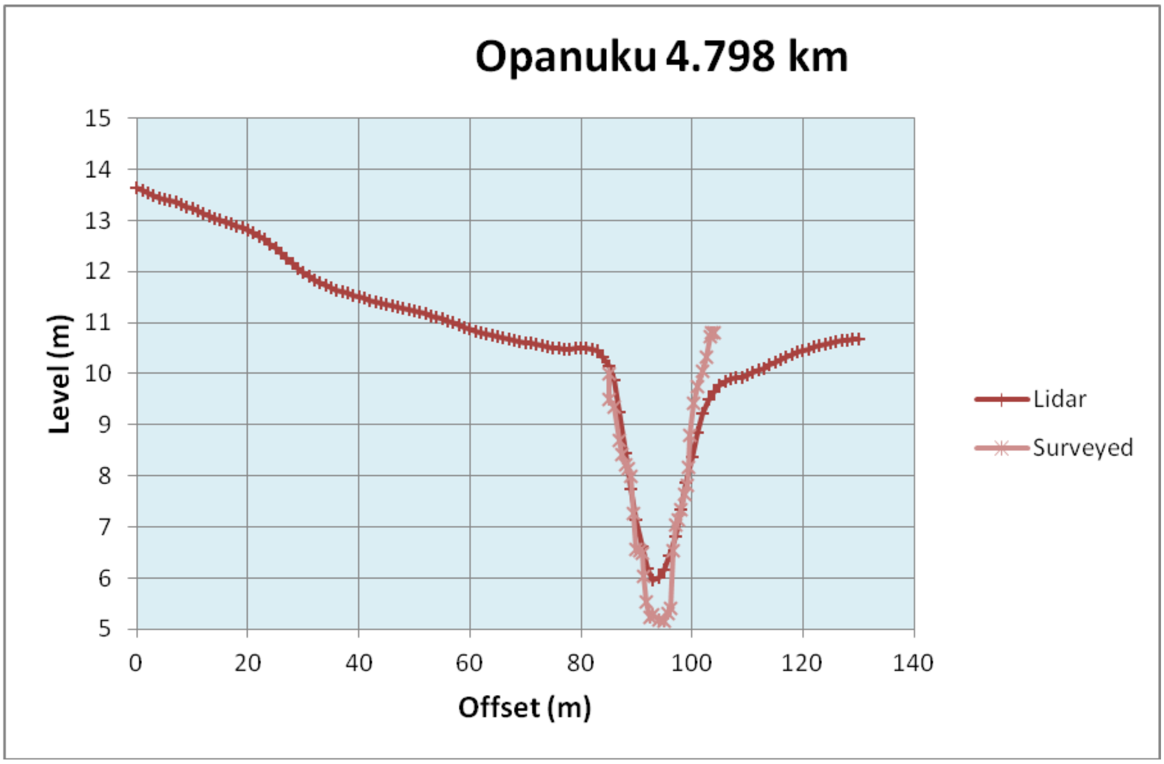

Figure 5. Surveyed and Lidar-based Cross-sections at the Vintage Reserve Gauging Site

The reach adjacent to the Vintage Reserve gauging site was originally selected for intensive study (see also Figure 2 in Section 8). In this reach, Lidar-based cross-sections were derived and compared with the surveyed cross-sections. Figure 5 shows the result at the Vintage Reserve gauging site.

This was typical of the results found at all sections compared, with the surveyed cross-sections approximately 1m deeper than the Lidar-based sections. This was not a matter of datum error in either survey, as except for the low-flow part of the channel, level discrepancies were fairly well distributed about a mean of roughly zero.

Similar results have been found in studies for other clients, so that the Lidar seems to systematically underestimate depths in low flow channels. This is consistent with the known inability of standard Lidar to penetrate water, so the error is readily explained by the presence of water in the channel bottom at the time the Lidar survey was flown, giving a reading from the water surface rather than the channel bottom. There may also be a shading effect in incised channels, within which oblique Lidar pulses would be unable to reach the channel bottom, giving instead a reading from the channel side.

It was difficult to place the surveyed cross-sections on the Lidar map, because only one set of coordinates was provided for the location of each cross-section.

The Lidar cross-section was drawn approximately perpendicular to the stream axis through this point, but without information about the surveyed cross-section orientation and the lateral offset along the section at which the location was specified, all that could be done was to align the channel sides by eye in the two surveys as shown in Figure 5.

This no doubt contributed to the discrepancies visible in the ground levels outside the channel, so it is recommended that in future at least two points are georeferenced in each surveyed cross-section to provide both the orientation and lateral location of the surveyed section.

Meanwhile, it was obvious that the lack of cross-section data downstream of 4.839km could not readily be made up using Lidar data, at least for the low flow part of the channel. Similarly, infill of cross-sections at closer spacing than that surveyed could be done for the low flow channel only by hydraulic interpolation, as otherwise a sudden rise of the order of a metre in channel invert would be conveyed to the channel model, destroying any chance of improved model profiling.

9.2.5 Gauging Site Suitability

During the analysis of the model data, it became clear that the Opanuku Stream would overflow at the right bank at flows at or above the peak reached during the October 2006 storm. This means that any gauging above that peak will sample only the flow remaining in the stream, with an unknown additional flow bypassing through Henderson Park. Of course, both the bypass flow and the main stream flow can be estimated by hydraulic modelling, but the whole point of such gauging sites is to provide independent flow measurements against which hydraulic models can be evaluated.

For any kind of time series analysis, use of a gauged flow which is short of the total stream flow by an unknown amount is highly undesirable, as this will convert to a dangerous underestimate of all flows of return period greater than the overflow event – in this case all return periods greater than about two years.

The monitored site at Border Road has no such problems, as any lateral overflows will be constrained by a very significant road embankment. Further, the riparian management programme appears to impact directly on riparian vegetation around the Vintage Reserve gauging site, meaning that changes in the rating will inevitably accompany riparian vegetation changes. No changes on a similar scale appear to be planned in the vicinity of the Border Road crossing, and indeed a relatively steep reach immediately downstream appears likely to reduce the influence of vegetation on the flow/level rating applying there.

Changing of the primary rating site from Vintage Reserve to Border Road therefore makes good sense, although level recording at both sites should be retained if riparian resistance studies are to continue.

9.2.6 Rain Gauge Coverage

Rain gauge density in the area was good, with one recording site (Power NZ) immediately adjacent to the Vintage Reserve and another (Candia Road) available in the main stream catchment upstream of Border Road.

Figure 6 shows the general location of the chosen test area on a reach of the Opanuku Stream in West Auckland, relating the gauging sites to the catchment and reach subcatchment boundaries.

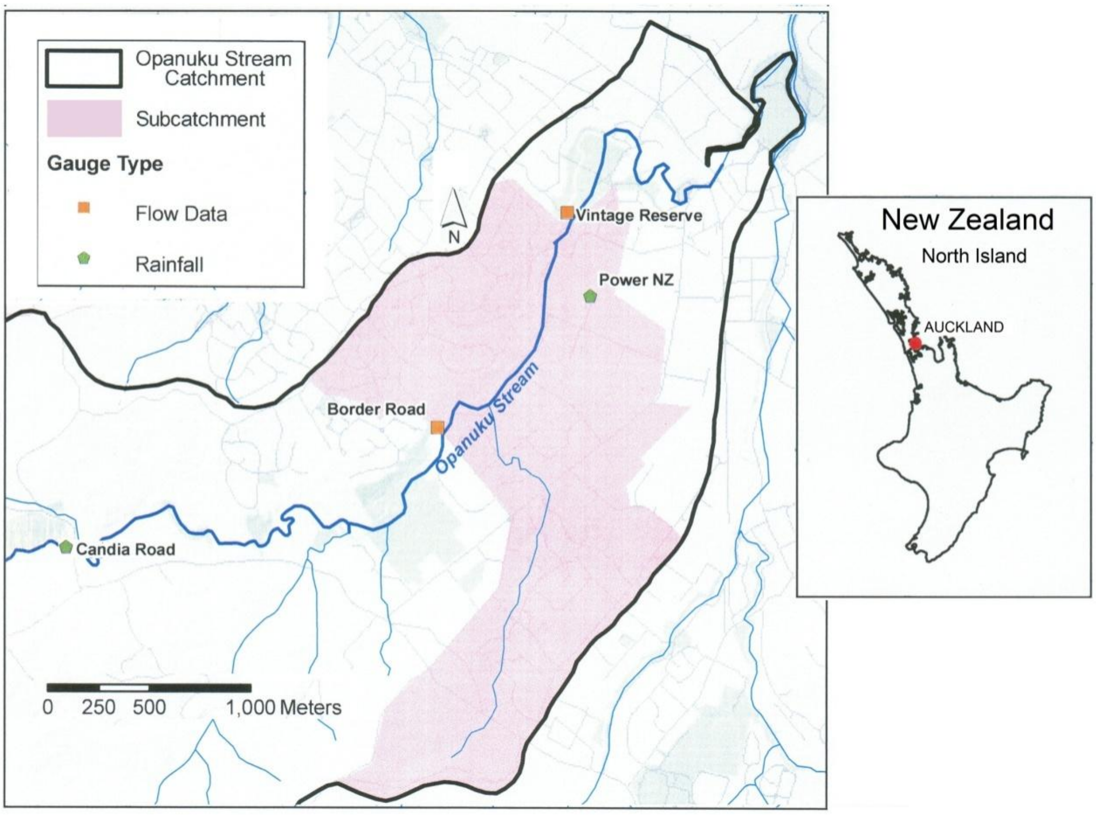

Figure 6. Location diagram, showing position of recording water level gauges and rain gauges.

10. Vegetation Resistance Models

As set out in Section 7, two vegetation models have been adopted for further evaluation. Short and tall vegetation have been found to offer quite different resistance characteristics under progressive inundation, so a separate model for each type is recommended.

Both use vegetation height as a major parameter, and the distinction between “short” and “tall” vegetation seems to occur at heights of around 1m, as woody structures need to supplant leafy structures to support plants above this height. A height of 1.2m has therefore been adopted as the switch between models, as almost all examples in the literature appeared either to fall below or rise above this figure by a clear margin.

10.1 Resistance Computation

According to Shamseldin (Section 7.1) the flow resistance of tall vegetation is given by

$$f = 4.06\left(\frac{V}{\sqrt{\frac{\xi E}{\rho}}}\right)^{-0.46}\left(\frac{h}{h_g}\right)$$

See equation (5)

and the flow resistance of short vegetation is given by

$$k = 0.14h_g\left[\frac{\left(\frac{MEI}{\tau}\right)^{0.25}}{h_g}\right]^{1.59}$$

See equation (8)

The variables are defined in Section 7. For computational purposes, the variables in the right hand side of these equations fall into two groups: those supplied by the flow solution, and those supplied directly by the modeller. The computation of vegetation resistance is essentially the evaluation of local bed shear in a subchannel, so that the total resistance to flow can be accumulated numerically across the whole channel. An example is shown in Figure 7.

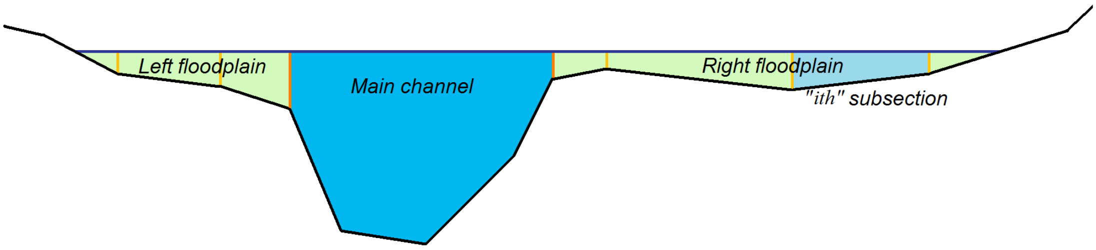

Figure 7: Typical channel cross-section.

The channel is conceptually divided into a main channel, in which there is typically permanent flow, and a left and right floodplain (looking downstream), in which there is flow only during flood events. The vegetation under investigation is terrestrial rather than aquatic, so will be supposed to occupy an arbitrary subsection of the floodplain. This subsection is extracted and shown in more detail in Figure 8.

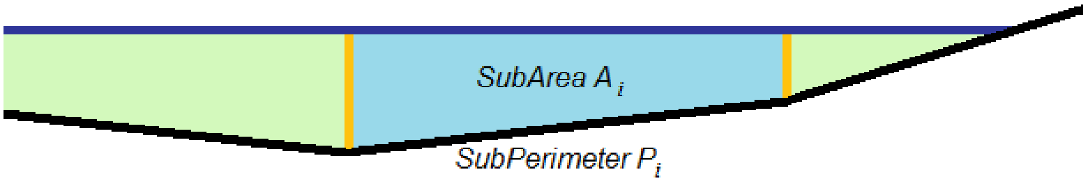

Figure 8: The "ith" subsection in the floodplain

In this subsection, the depth *h* in Equation (1) is not constant, but can be represented by the hydraulic radius

$$R_i = A_i / P_i$$

where A_i and P_i are respectively the area and perimeter of the *ith* subsection as shown in Figure 8. Similarly, the representative velocity *V* can be obtained from $V_i = Q_i / A_i$, where Q_i is the flow through the subsection.

10.1.1 Classical Conveyance Modelling

Conveyance modelling separates the geometrical properties of the cross-section from the velocity in the solution for section discharge. In other words, conveyance is a function of the channel stage or water level alone, but discharge may vary significantly through a channel of a given conveyance, directly corresponding with a variation in velocity for a given water level depending on the gradient applying. If the water level and gradient can be assumed constant over the whole cross-section, the discharge may then be distributed over the subsections in direct proportion to the distribution of conveyance.

Expressing this mathematically, the Manning, Chézy, Strickler and Darcy-Weisbach descriptions all depend (Henderson, 1966) on a relationship

$$\tau_0 = a\rho v^2 \qquad (13)$$

where τ_0 is the shear stress at the bed, ρ is the density (= γ/g where γ is the specific weight and g the acceleration of gravity), v is the velocity and a is a dimensionless coefficient which is effectively found empirically by calibration. This relationship derives from dimensional analysis, and represents a general finding that the drag force is proportional to the square of the velocity in a wide range of cases. The difference between the Manning, Chézy, Strickler and Darcy-Weisbach descriptions is then essentially found in differing approaches to the evaluation of a, with the common basis that all of these approaches exclude a velocity influence (at least in the fully rough turbulent range of current interest).

According to the textbook approach (e.g. Henderson, 1966) the shear force does external work on a flow element, allowing a balance to be found between the shear and the flow-work term through either end of a reach. Under steady flow conditions, this means

$$\tau_0 P\Delta x = -\gamma A\Delta H$$

Therefore, using $$S_f = -\Delta H/\Delta x \qquad R = A/P$$

$$\tau_0 = \gamma R S_f \qquad (14)$$

Here, H is the energy head, and the gradient of this with respect to channel distance x (the energy gradient or "friction slope") is supposed to be constant over the whole cross-section. While the reach length need not be infinitesimal, it is implied in this analysis that the reach length is small enough for τ_0, wetted perimeter P and area A to be reasonably constant, in other words, flow is locally prismatic. This is consistent, because the same implied restriction applies to Equation (13), as otherwise no meaning could be attached to the value of v.

Thus, finally, using Equation (13) to eliminate τ_0,

$$v = \sqrt{\frac{g}{a} R S_f}$$

Thus, using $Q = vA$, $$Q = A\sqrt{\frac{g}{a} R S_f}$$

This can be rewritten $$Q = K S_f^{1/2}$$

The advantage of this rearrangement is that the coefficient K is entirely a function of the geometrical properties of the cross-section. It is also directly proportional to the discharge Q, and therefore expresses the capability of the section to convey flow under a given friction slope – hence it is called the section "conveyance". This classical formula does not depend on the resistance formulation beyond Equation (13).

Clearly $$K = A\sqrt{\frac{gR}{a}}$$

and conveyance has the dimensions of discharge, bearing in mind that *a* is dimensionless for all of the Manning, Chézy, Strickler and Darcy-Weisbach formulations of resistance.

For all these formulations, it is equally permissible to assume that S_f is constant across the section, so that because the total section discharge is the sum of the subsection discharges, the distribution of the subsection discharges will follow the distribution of the subsection conveyances. Therefore, the mathematical definition of conveyance applies as much to the *ith* subsection as to the whole section, provided that the conveyance for the whole section is obtained from the sum of the conveyances of the subsections.

10.1.2 Switching Formulations

Chézy Formulation

This simply introduces the Chézy *C*, defined as

$$C = \sqrt{\frac{g}{a}}$$

Therefore $$K = CA\sqrt{R}$$

Manning Formulation

The Chézy *C* is made dependent on *R* by the formula

$$C = \frac{MR^{1/6}}{n}$$

where M is a dimensioned constant coefficient = 1.000 $m^{1/3} s^{-1}$ and *n* is the "Manning n", a dimensionless roughness parameter.

Therefore $$K = \frac{MAR^{2/3}}{n}$$

Strickler Formulation

Strickler related the Chézy *C* to the size *k* of the bed roughness material. Originally this related to experiments with uniform sized granular material, so that *k* had a direct physical interpretation as the grain diameter.

More recently, however, k is understood as an “equivalent grain size”, which is simply the uniform grain size which if coated on a bed would give the same Chézy C as that observed (under fully rough flow conditions). This allows k to be used in expressions such as Equation (8) where no granular material is involved.

Essentially, the Strickler formulation gives $$C \propto \left(\frac{R}{k}\right)^{1/6}$$

Taking into account the Manning formulation, this means $$n \propto k^{1/6}$$

Since n is dimensionless, the constant of proportionality must depend on the dimensions of k. For example, Ackers (1958) gave the relationship for k measured in mm as

$$n = 0.012k^{1/6} \qquad (15)$$

The expression for conveyance then follows by substituting for n in the Manning formulation.

Darcy-Weisbach Formulation

The Darcy pipe flow equation can be written in present terminology as

$$S_f = \frac{f}{D}\frac{v^2}{2g}$$

where D is the pipe diameter.

It follows from the definition of $R = A/P$ that $R = D/4$, so $a = f/8$ and

$$C = \sqrt{\frac{8g}{f}}$$

Williamson (1951) found experimentally that f could be linked to k/R in pipes from small diameters up to very large diameters (~6m) by the single equation

$$f = 0.113\left(\frac{k}{R}\right)^{1/3} \qquad (16)$$

It follows from this that $$n = \sqrt{\frac{0.113M^2}{8g}}\,k^{1/6} \qquad (17)$$

Again, the constant of proportionality must depend on the dimensions of k, because the numerical values of both M and g depend on the units used. Working through the calculation using g = 9.81 m s^{-2}, this gives

$$n = 0.0119994k^{1/6}$$

for k measured in mm. This shows that for applications, the empirical relationships (5) and (6) give practically identical results. However, both of these relationships were obtained for granular materials, and it is something of a leap to transfer these relationships to vegetation, by applying them to the f and k as expressed in Equations (5) and (8) respectively. The most realistic hope is that the proportionalities will continue to apply, even if the coefficients have somewhat different values.

10.1.3 Expanded Conveyance Modelling

The objective is to incorporate subsections using classical conveyance models and subsections covered with vegetation into a unified conveyance model for the whole section. Further, some vegetated subsections will be supposed to follow the tall vegetation description of Equation (5) and others the short vegetation description of Equation (8).

To avoid overcomplicating the objectives, each vegetated subsection will be assumed to be covered by either tall vegetation or short vegetation (not some mixture), and to be characterised by a single value of h_g, the average height of vegetation canopy. Bearing in mind that there is a break in height between typical grasses and typical trees, it could be that the distinction between tall and short vegetation may be drawn solely on average height, saving the need to add a tall/short switch to the data description. In other words, h_g below some value (assumed to be 1.2m) could be taken to invoke Equation (8), while larger values of h_g would invoke Equation (5).

The conveyance computation currently available (from the HYDRA Software (2012) package *AULOS*) is based on the Manning formula. More precisely, in the "*ith*" subsection (see Figure 8) a reference Manning n for the whole section (n_s) is locally converted to a subsection Manning n by multiplying by a relative resistance factor rr_i. This has the considerable advantage of allowing the simultaneous adjustment of the whole section resistance by modifying the section n_s to satisfy calibration criteria, without altering the relative conveyance contribution of each subsection.

Since the Manning formula is the basis of the existing treatment, and the various classical resistance formulations can readily be switched as discussed in subsection 10.1.2, the Manning formula is proposed to be the basis of the expanded conveyance modelling.

10.1.4 Tall Vegetation

Using Equation (16) to substitute for f in Equation (5) gives,

$$0.113\left(\frac{k}{R_i}\right)^{1/3} = \frac{4.06\left(\frac{\xi E}{\rho}\right)^{0.23}}{V^{0.46}}\frac{R_i}{h_g}$$

Rearranging,

$$k^{1/6} = \sqrt{\frac{4.06R_i}{0.113h_g}\left(\frac{\xi E}{\rho}\right)^{0.115}}\frac{R_i^{1/6}}{V^{0.23}}$$

This equation has the problem that as *V* decreases to zero, *k* increases without limit, and therefore so does Manning *n* from Equation (7). This is unphysical, because *k* is an equivalent grain size, which should not depend on *V* when *V* is small. Clearly, the inverse dependence on *V* reflects an effective decrease in equivalent grain size as *V* increases, corresponding with a bending down of the vegetation under the drag forces. However as the vegetation straightens there will be a minimum applicable *V* at which no deflection is detectable, and below this *V* the vegetation height and hence *k* will remain constant.

V cannot be guaranteed to remain above this minimum value. This is because unsteady flow simulations typically start from one known solution to determine the next solution a short time step later, and the easiest way to provide the first known solution (the initial condition) is to specify a static solution in which *V=0*.

It is reasonable to assume from the definitions that the maximum value of *k* is linearly related to h_g, and the simplest linear relationship is $k_{max} = h_g$. Then the minimum applicable *V* is given by

$$\left|V_i\right|_{\min}^{0.23} = \sqrt{\frac{4.06}{0.113}\left(\frac{\xi E}{\rho}\right)^{0.115}}\left(\frac{R_i}{h_g}\right)^{2/3} \qquad (18)$$

Note the relationship is taken to be reversible, so for reverse flow the magnitude of *V* will apply.

There is also a natural limit on *k* set by the effective depth, *R*, as only that part of the equivalent grain size which is submerged can be effective in creating drag.

Therefore $k \leq R$.

The proposed rules for computation of the equivalent grain size *k* of tall vegetation in the "*ith*" subsection are therefore

1. Obtain the minimum applicable V_i from Equation (18), using R_i from the previous time step.

2. Take V_i from the previous time step:

If $|V_i| > |V_i|_{min}$

then $$k^{1/6} = \frac{|V_i|_{min}^{0.23}}{|V_i|^{0.23}} h_g^{1/6}$$

else $$k^{1/6} = h_g^{1/6}$$

3. If $k > R_i$ then $$k^{1/6} = R_i^{1/6}$$

10.1.5 Short Vegetation

The procedure is similar to that of tall vegetation. Equation (8) can be written

$$k^{1/6} = C_s^{1/6} \tau_0^{-0.06625} \quad \text{where} \quad C_s = 0.14 h_g^{-0.59} MEI^{0.3975}$$

Using Equation (14) to evaluate τ_0 from the previous time step again gives k increasing without limit in the static case $V = 0$, as this case also sets $S_f = 0$. As before, a minimum applicable value can be deduced from $k_{max} = h_g$, this time for S_f, given by

$$|S_f|_{min}^{0.06625} = \left(\frac{C_s}{h_g}\right)^{1/6} \frac{1}{(\gamma R_i)^{0.06625}} \tag{19}$$

The proposed rules for the computation of the equivalent grain size k of short vegetation in the "*ith*" subsection are therefore

1. Obtain the minimum applicable S_f from Equation (19), using R_i from the previous time step.
2. Take S_f from the previous time step (note this friction slope is the same for all subsections under the rules for computing conveyances)

If $|S_f| > |S_f|_{min}$

then $$k^{1/6} = \frac{|S_f|_{min}^{0.06625}}{|S_f|^{0.06625}} h_g^{1/6}$$

else $$k^{1/6} = h_g^{1/6}$$

3. If $k > R_i$ then $$k^{1/6} = R_i^{1/6}$$

10.1.6 Conversion of k to Relative Resistance

For both tall and short vegetation, a value of *k* is now available for a subsection. This can be converted to the relative resistance rr_i for the "*ith*" subsection by using $n = rr_i n_s$ and equation (17):

$$rr_i = \sqrt{\frac{0.113M^2}{8g}}\frac{k^{1/6}}{n_s}$$

The standard computational method can now be applied to obtain the conveyance through each subsection, whether each rr_i is specified directly in the classical approach or computed at each time step for vegetation.

10.2 Model Implementation

10.2.1 Harmonisation with Grain Roughness

The previous subsection of this report showed how vegetative parameters would be converted to grain roughness *k*. This invites an extension of the logic to permit *k* values to be input directly if the software user wishes to work with a grain roughness resistance formulation.

Accordingly, the neutral word "size" has been chosen to head a column of roughness length settings for each floodplain subsection, with the meaning of the word switchable between Grain Size and Vegetation Length. Both will be entered in metres to avoid confusion of units, but 4 decimal places will be allowed to take the dimension down to tenths of millimetres. For very smooth surfaces, 4 decimal places are needed for the equivalent sand roughness even if the units are millimetres, so this would be dealt with by a future option to use size units of mm.

As previously explained, grain roughness can be included in the standard conveyance model, as it has no dependence on velocity, so the first stage of the computational method extension would be a once-only conversion from grain size to relative roughness for each floodplain subsection at the beginning of model run-time. The model will thereafter run with no logical difference from the existing relative roughness computations.

It would be necessary to ensure that relative roughness and "size" are not both specified for a given floodplain subsection, as these are almost certain to give conflicting results. As soon as a valid "size" is entered therefore, the corresponding relative roughness should be disabled. Conversely, entry of an invalid size value should re-enable the corresponding relative roughness. A size of zero is obviously invalid, so this can be taken as a standard signal that the relative roughness model then applies at the given subsection.

10.2.2 Specification of Vegetation Model

The average canopy height h_g can be seen as the "size" parameter for the vegetation, and can therefore be given one value per floodplain subsection under the proposed layout. Since floodplain subsections can be defined to any resolution (at least down to the 1cm imposed by the practicalities of the chosen input format), in principle any horizontal distribution of canopy heights can be accommodated.

For short vegetation, MEI is a function of h_g and can therefore be computed as soon as h_g is available. However for tall vegetation, three other factors ξ, E and ρ feature, so facilities are required to specify these in the model. On consulting the internet, the stiffness modulus E of wood seems to be quoted in a wide range of units, from dynes/cm^2 to MPa to GPa, and ρ may also take numerical values of around 1 or around 1000 if this is the density of water. Even assuming ξ is a dimensionless constant of Order 1 chosen at the beginning by the user, suggesting an initial default value for each of these three parameters seems likely to cause dimensional confusion and hence substandard model quality assurance.

Bearing in mind that the three parameters always appear together in the same relationship $\sqrt{(\xi E/\rho)}$, and that this takes the form of a wave velocity, it is proposed to call this "stem wave speed" and require the user to enter this in m/s, consistent with standard velocity units in river hydraulics. On consideration of various figures quoted in the literature, it appears (Section 8.1) that a default value of 0.05 m/s is reasonably representative of this stem wave speed. This will be used initially, but this is subject to refinement if more extensive laboratory results come available, particularly for indigenous plant species.

It is proposed to allow this stem wave speed to be specified once only per cross-section, and NOT once per floodplain subsection, but this is open to discussion.

10.2.3 Catering for Velocity Dependence

For vegetation models, because of the variation of velocity through a section in any time varying computation, the relative roughness distribution across all floodplain subsections will have to be recomputed at every time step. This is less computationally elegant than the conveyance approach, and carries some computational instability risk if the guiding functions have sudden turning points. However, on close inspection the functional behaviour seems benign enough to support the local linearization required for the use of classical linear matrix solutions. This is therefore proposed as the initial approach.

10.2.4 Data Entry: General Values

With the advent of automatic data extraction from Lidar terrain data, sections with subsections numbering in the hundreds are becoming common. This makes individual entry of values for each subsection tedious. Further, in practice, there is usually not sufficient information to support the individual setting of parameters for each floodplain subsection. Indeed, if observed water levels are to be used for calibration, there are considerable advantages in allowing a uniform value of “size” to be specified for each section, or each reach comprising a number of sections, or even globally for the whole model.

On the other hand, certain limited parts of the section typically still require individual setting. This applies to the low flow channel in particular, where low flow data is available to support a localised roughness which is not typical of the section under flood conditions.

The data entry task is therefore likely to represent a combination of many entries of some kind of general berm roughness with a few special entries where local information is available. It is proposed to introduce user-specified “general” values of the “size” parameter for the vegetation canopy height, and these will be used as the initial default on every subsection. If these initial entries are subsequently edited, they will then be “special” by the very fact they are different from the “general” values.

Such “special” values can therefore be automatically detected and left unchanged by any modification of the “general” value.

10.2.5 Implementation: Tall Vegetation

The Chézy *C* is linked (Section 10.1.2) with the Darcy-Weisbach *f* in Equation (5) by

$$C = \sqrt{\frac{8g}{f}}$$

The Manning formulation expresses *C* as

$$C = \frac{M R^{1/6}}{n}$$

where M is a dimensioned constant coefficient = 1.000 $m^{1/3}\ s^{-1}$, *R* is the hydraulic radius and *n* is the “Manning n”, a dimensionless roughness parameter.

Therefore $$n = \sqrt{\frac{f}{8g}} M R^{1/6}$$

$$= \sqrt{\frac{4.06}{8g}} \left(\frac{\sqrt{\frac{\xi E}{\rho}}}{V} \right)^{0.23} \left(\frac{h}{h_g} \right)^{0.5} MR^{1/6} \qquad \text{using Equation (5).}$$

Here, we can substitute the subsection hydraulic radius R_i as representative of the depth h as the depth itself may be varying considerably over the subsection (see Figure 8). Also the local value of R is R_i.

Thus
$$\frac{n}{MR_i^{2/3}} = \sqrt{\frac{4.06}{8gh_g}} \left(\frac{\sqrt{\frac{\xi E}{\rho}}}{V} \right)^{0.23}$$

Now V is the local velocity, that is, the velocity of flow passing through the subsection. This local V can be expressed as

$$V = \frac{MR_i^{2/3} S_f^{1/2}}{n}$$

where S_f is the local friction slope, which according to conveyance theory is also the friction slope for the whole cross-section. Substituting,

$$\left(\frac{n}{MR_i^{2/3}} \right)^{0.77} = \sqrt{\frac{4.06}{8gh_g}} \left(\frac{\xi E}{\rho |S_f|} \right)^{0.115}$$

Therefore, finally,
$$n = MR_i^{2/3} \left(\sqrt{\frac{4.06}{8gh_g}} \left(\frac{\xi E}{\rho |S_f|} \right)^{0.115} \right)^{1/0.77}$$

(20)

This equation still has the problem that it fails as $S_f \rightarrow o$, corresponding with the failure of the original Equation (5) as $V \rightarrow o$, so a minimum value of S_f must be set for applications.

A Manning n of 1.00 is generally considered an upper extreme for practical problems, and for tall vegetation, the hydraulic radius R_i is typically less than h_g. Therefore a friction slope which attains an extreme Manning n even when $R_i = h_g$ can reasonably be considered a practical minimum. Equation (10) can be rewritten

$$n^{0.77} = \sqrt{\frac{4.06}{8g}} \left(\frac{\xi E}{\rho |S_f|} \right)^{0.115} \left(\frac{R_i}{h_g} \right)^{0.5} M^{0.77} R_i^{\left(1/6 - 0.46/3\right)}$$

The exponent of the final term in R_i is therefore only 0.0133..., and even for extreme values of R_i in the range 0.01 – 100m, $R_i^{0.0133...}$ can be taken as having the numerical value of 1.00 within an accuracy of 6%.

Therefore, the minimum S_f is defined by taking n = 1, $R_i = h_g$ and remembering that M has the numerical value of 1.00. Therefore

$$\left|S_f\right|_{\min} = \frac{\xi E}{\rho}\left(\frac{4.06}{8g}\right)^{1/0.23} \qquad (21)$$

For the suggested default value of stem wave speed of 0.05m/s (see Section 8.1), this gives a value for minimum friction slope of 6.39x10^{-9}. This is an extremely small value, so even though somewhat arbitrary, it is clearly below normal values of friction slope, except for quasi-static cases where the accurate application of Equation (20) is not of central importance.

Therefore, for practical purposes the value derived in Equation (21) is suitable for general use.

Substituting (21) back into (20), we have

$$n = MR_i^{2/3}\left[\left(\frac{\left|S_f\right|_{\min}}{\left|S_f\right|}\right)^{0.115}\sqrt{\frac{1}{h_g}}\right]^{1/0.77}$$

Bearing in mind that by definition $rr_i = n/n_s$, where rr_i is relative roughness for the *ith* subsection and n_s is the standard Manning n value for the whole section, we get

$$rr_i = \left(\frac{\left|S_f\right|_{\min}}{\left|S_f\right|}\right)^{0.1493506}\frac{h_g^{-0.6493506}}{n_s}R_i^{2/3} \qquad (22)$$

10.2.6 Coding Parameters

For software coding purposes, it is computationally efficient to calculate time invariant parameters once only at the beginning of a run, leaving only time varying parameters to be recomputed each time step, and then preferably as simply as possible.

In this case, two time invariant parameters, *paramin* and *sizetorr* were used to expedite the computation of Equation (22), bearing in mind that the time varying model solution renewed S_f and R_i at every time step. These coding parameters were defined by:

$$paramin = \left|S_f\right|_{\min} \qquad \text{(as per Equation (21))}$$

$$sizetorr = \frac{h_g^{-0.6493506}}{n_s}$$

10.2.7 Implementation: Short Vegetation

Equation (8) describes the resistance in terms of the Strickler grain size *k*, in which case it is appropriate to relate this to the Manning n by the Williamson relationship (Section 10.1.2)

$$n = \sqrt{\frac{0.113M^2}{8g}}\, k^{1/6} = 0.0379454 k^{1/6}$$

The coefficient differs from Equation (15) as *k* is now in metres. Also the shear τ can be expressed by

$$\tau = \rho g R_i S_f$$

with definitions as in the previous section.

The term MEI is defined by the model developers as a function of h_g alone, which for dormant vegetation is

$$MEI = 25.4 h_g^{2.26}$$

Therefore Equation (8) can be rewritten using ρ = 1000 kg/m^3, g = 9.81 m/s^2

$$k^{1/6} = 0.14^{1/6}\left(\frac{25.4}{\rho g R_i\left|S_f\right|}\right)^{\frac{1.59x0.25}{6}} h_g^{\frac{1.0-1.59+2.26x1.59x0.25}{6}}$$

$$= 0.4856351\left(\frac{h_g}{R_i\left|S_f\right|}\right)^{0.06625} h_g^{-0.0148583}$$

Bearing in mind that h_g < 1.2m, the conventional limiting height for short vegetation, this can be represented with sufficient accuracy as

$$k^{1/6} = 0.5\left(\frac{h_g}{R_i\left|S_f\right|}\right)^{0.06625} \qquad (23)$$

This relationship is exact at h_g = 0.14059m, and (in view of the approximations inherent in the estimation of h_g) adequately accurate at all other reasonable values of h_g.

Again the problem arises of failure of the expression as $S_f \rightarrow o$. However in this case the physical interpretation of k as a roughness element size suggests the maximum value of k can be no larger than h_g. Accordingly, the minimum applicable value of S_f is defined by

$$\left|S_f\right|_{\min} = \frac{h_g}{R_i}\left(0.5 h_g^{-1/6}\right)^{1/0.06625} \qquad (24)$$

Here, h_g/R_i is understood to have a maximum value of 1.00, as vegetation above the water surface cannot have any effect on drag resistance.

Therefore $$k^{1/6} = \left(\frac{\left|S_f\right|_{\min}}{\left|S_f\right|}\right)^{0.06625} h_g^{1/6} \qquad (25)$$

And finally, remembering $rr_i = n/n_s$

$$rr_i = \frac{0.0379454}{n_s}\left(\frac{\left|S_f\right|_{\min}}{\left|S_f\right|}\right)^{0.06625} h_g^{1/6}$$

10.2.8 Coding Parameters

Since for any channel subsection a choice must be made between the tall and short vegetation models, the coding parameters *paramin* and *sizetorr* are available for use with either model.

For short vegetation

$$paramin = \left(0.5 h_g^{-1/6}\right)^{1/0.06625} \qquad sizetorr = \frac{0.0379454}{n_s} h_g^{1/6}$$

11. Initial Model Definition

11.1 Model Structure

Conceptually, it is fairly obvious that changes in riparian vegetation must have some effects on the conveyance of flow through a stream channel, with denser or larger vegetation causing more resistance than sparser or smaller vegetation. The purpose of this study was to establish whether this hydraulic sensitivity to riparian vegetation could be quantified reliably enough for planning decisions on riparian planting to be made on an objective rather than an arbitrary basis.

The flow in a stream at any given time is subject to many influences which are not caused by riparian vegetation, such as recent precipitation in the catchment. The aim of the model design was therefore to provide test conditions quarantined as far as possible from external interference, so as to allow controlled modelling experiments to be carried out which would isolate the effects of alternative descriptions of riparian vegetative resistance. At the same time, for the purposes of this study it was desirable to use field data rather than laboratory measurements so that the results could be extended immediately to other field situations where planning decisions are required.

According to standard hydraulic theory, a change in conditions (say bed resistance) in a channel reach will modify flow both upstream and downstream, but the upstream effects (either backwater or drawdown) diminish rapidly with distance. Therefore, it can be expected that, on a river of appreciable slope, modifications to the reach near the Vintage Reserve gauge at chainage Opanuku 4.798 (see Figure 2) should cause minor (if not negligible) effects on the flow conditions at Border Road, some 1.7km upstream.

Similarly, although the supplied cross-section data is inadequate downstream of the Vintage Reserve, the boundary errors associated with an extension of local cross-section characteristics downstream should not penetrate more than a few hundred metres upstream towards the Vintage Reserve.

11.2 Boundary Location

Accordingly, the strategy adopted was to set the model upstream boundary at Border Road (Opanuku chainage 3.114km), and the downstream boundary at the end of a uniform reach based on an extension of the most downstream local measured cross-section at chainage 4.839km. The length and slope of that reach was established by trial and error, such that conditions at the Vintage Reserve could be calibrated to available flow measurements.

Refer to Figure 2 for the original model layout. This shows the controlled intensive test area within the aerial photographic background, with the extended model boundaries set at some distance from the test area to provide a buffering effect.

Because level measurements from the Vintage Reserve gauge exceeded the overflow crest level of the right bank upstream in the available calibration event of 1 October 2006, an overland flow discharge pathway was required at this point. Drowning of the resulting weir could be ruled out as the valley cross-section expanded downstream, so a simple constant downstream boundary level (at position marked Overland 0.170) could safely be set below weir crest level without any fear of influencing flows in the area of interest.

In predicting the responses of the study area to riparian planting, the level hydrographs measured at the Vintage Reserve gauge in a single event could not be used directly, as these should change in response to changes in the resistance assumed for the adjacent reach. However, they are initially essential for calibration of the existing resistance, and were included by attaching the hydrographs (at position marked Inflow1 0.000 in Figure 2) to a stub tributary linked to the main stream. Given adequate conveyance of the stub, this should ensure that levels at the stream junction closely follow the recorded data. The laws of hydraulics require such level changes to be accompanied by inflows or outflows along the stub, to compensate for any deficiencies or excesses respectively in the balance of stream inflows into the junction (at the Vintage Reserve gauging position, marked Opanuku 4.798) less outflows from the junction.

Junction outflows are largely a response of the downstream reach to the imposed levels, allowing adjustment of the downstream boundary conditions to match reality, as stub inflows can physically correspond only with runoff from the Opanuku Stream catchment between Border Road and the Vintage Reserve. Such inferred catchment outflows can be assessed by comparison with hydrological estimates based on observed precipitation.

Since lateral overflows were not observed (except possibly at an insignificant level), stub outflows are hardly realistic, except for very minor surges which may penetrate up drains as short term reverse flows.

Once catchment runoff hydrographs have been calibrated, they can be transferred to a representative inflow point further upstream (marked Inflow 0.000 in Figure 2), leaving any residual stub flows through the point Inflow1 0.000 as a measure of overall model flow balance error.

11.3 Original Rating Curve

Rating information relates measured flows to levels at a gauging station. Some scatter in the measurements is to be expected, as the soft bottom/bank produces some variation, and there are seasonal and long term vegetation effects and a hysteresis for rising and falling water levels. The rating curve supplied by the Auckland Regional Council in May 2007 was fitted to flow data measured from dates 21/7/99 to 11/7/05. This curve is plotted in Figure 9.

An initial model estimate of resistance could be obtained by fitting steady flows to the rating curve, and the curve could then be extrapolated, for instance to a 100 year flood, by applying increased flows through the upstream model boundary at Border Road.

11.4 The 100 Year Flood Peak

According to the 2006 GHD report, Table 22, the 100 year ARI flood peak flow for two alternative land development scenarios would be 234.3 and 234.7 cumecs at Border Road Bridge, and totals of 234.9 and 235.4 cumecs combining flows past the Vintage Reserve gauge and the Henderson Park overflows.

For present purposes these differences are not significant, so the 100 year flood peak has been modelled by a steady flow of 235 cumecs imposed as an upstream boundary at the Border Road bridge. Lateral flow boundaries were set to zero and the downstream boundary for the Opanuku Stream modelled reach was drawn down to levels where no upstream influence could apply (see description in Section 15.1).

Similarly, the downstream boundary for the Overland flow path through Henderson Park was drawn down to a level where control rested entirely with the upstream lateral weir formed by the right bank of the Opanuku Stream at the overflow point near chainage Opanuku 4.706km – refer to Figure 2.

The resulting flow split was 128.6 cumecs past the Vintage Reserve gauge and 106.4 cumecs through Henderson Park. This is somewhat more than the 88-89 cumecs “Henderson Overflow” predicted by the GHD report, but as can be seen from Figure 9, the modelled flow and level at the Vintage Reserve Gauge is reasonably consistent with extrapolation of the existing rating curve.

There must also be some question about both models raised by the lack of cross-section data immediately downstream of chainage 4.839km – GHD may have used the spurious cross-section at 4.979km (see subsection 9.2.1) while the current model methodology of projecting downstream the cross-section at 4.839km is also exposed to considerable uncertainty at flows so far above the calibrated model range.

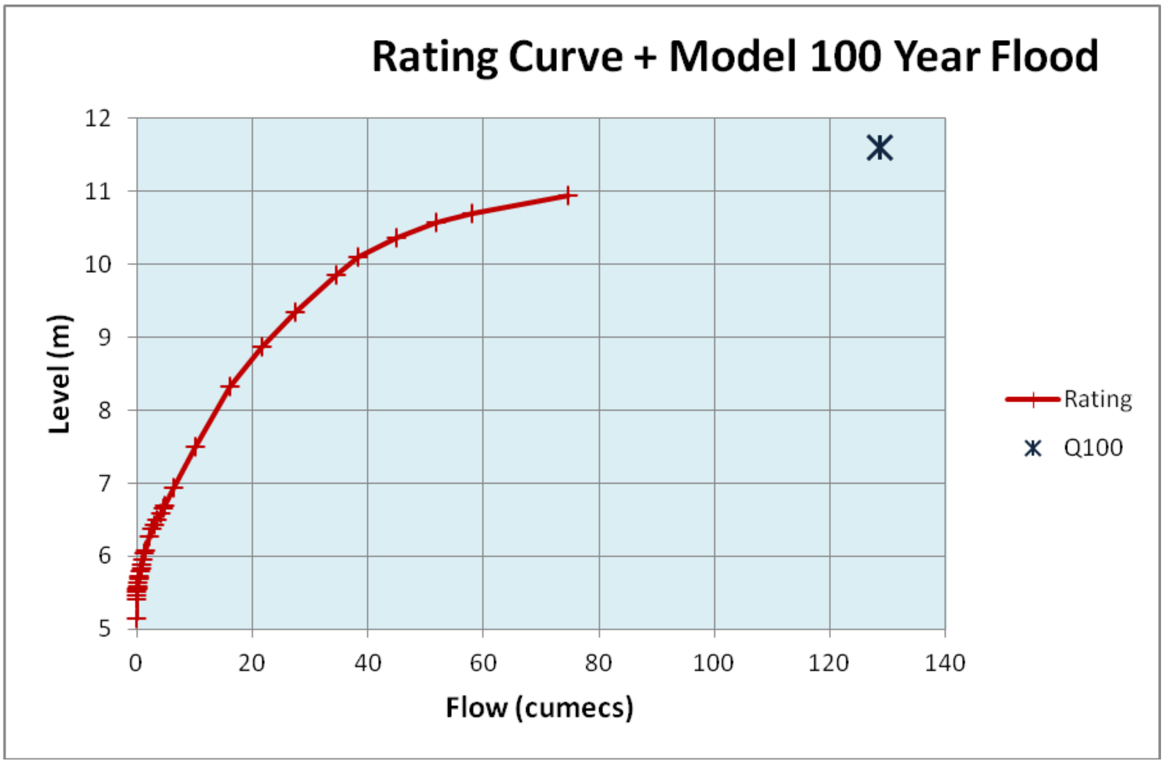

Figure 9: Modelled 100 Year Flood at Vintage Reserve Gauge cf. Rating Curve

Greater certainty about the predicted flow split at return periods of the order of 100 years must therefore await improved cross-section data, as well as upgrading of other field survey as already discussed.

12. Comparison with Hydrological Models

12.1 Residual Flow Models

As explained in Section 11.2, catchment runoff hydrographs can be inferred from purely hydraulic models, by establishing the residual between upstream inflow hydrographs and downstream outflow hydrographs for a channel reach. This residual is generated at the downstream end as the amount of lateral flow required to maintain a mass balance in the model reach, taking into account changes in reach volume corresponding with measured level changes.

Both upstream and downstream discharges are affected by changes in model resistance settings even though the boundary level variations are fixed by measurement, as a given level gradient through a given cross-section can discharge more flow at low resistance than at high resistance. However the *difference* between cumulative inflows and outflows is approximately fixed, as the reach volume under a given level gradient at any time is only weakly dependent on resistance.

Taking these factors into account, it turns out that the cumulative residual flow is highly sensitive to the resistance setting, with residual hydrograph volumes increasing significantly for relatively small increases in resistance.

In the original 2008 report, the main test of calibration accuracy was a comparison with the cumulative catchment runoff. While this provided the primary test that runoff should not exceed precipitation, the implied assumption that precipitation was instantly transformed into stream inflow was cruder than necessary, as some transmission delay across the catchment can reasonably be expected. Diversion of part of the precipitation to long term storage or evapotranspiration is also conventional hydrology.

12.2 Hycemos-U Modelling

An attempt was therefore made to calibrate the inferred residual flow hydrographs against a hydrological model. Hycemos-U was used as the hydrological modeling package, as this is a physically based model relying on kinematic wave propagation over an “open book” model, in which the two side sloping faces can each be calibrated separately from the central collecting “gutter” (Barnett et al, 1992).

The results were reported by Barnett and Hellberg (2011). Figures 10 and 11 illustrate the greatly increased sensitivity of the residual flow test to quite small resistance changes, as against the more conventional approach of comparison with the (1999-2005) rating curve.

Further, the calibrated cumulative runoff curve for the Manning n = 0.042 compares quite closely with the “Power NZ Runoff” obtained using a Hycemos-U model. This had a catchment area of 2.71 km2, of which 65% was a “fast response” hillslope, corresponding to typical Runoff Coefficient values used in standard Rational Method modelling of industrial, commercial, shopping areas and town house developments.

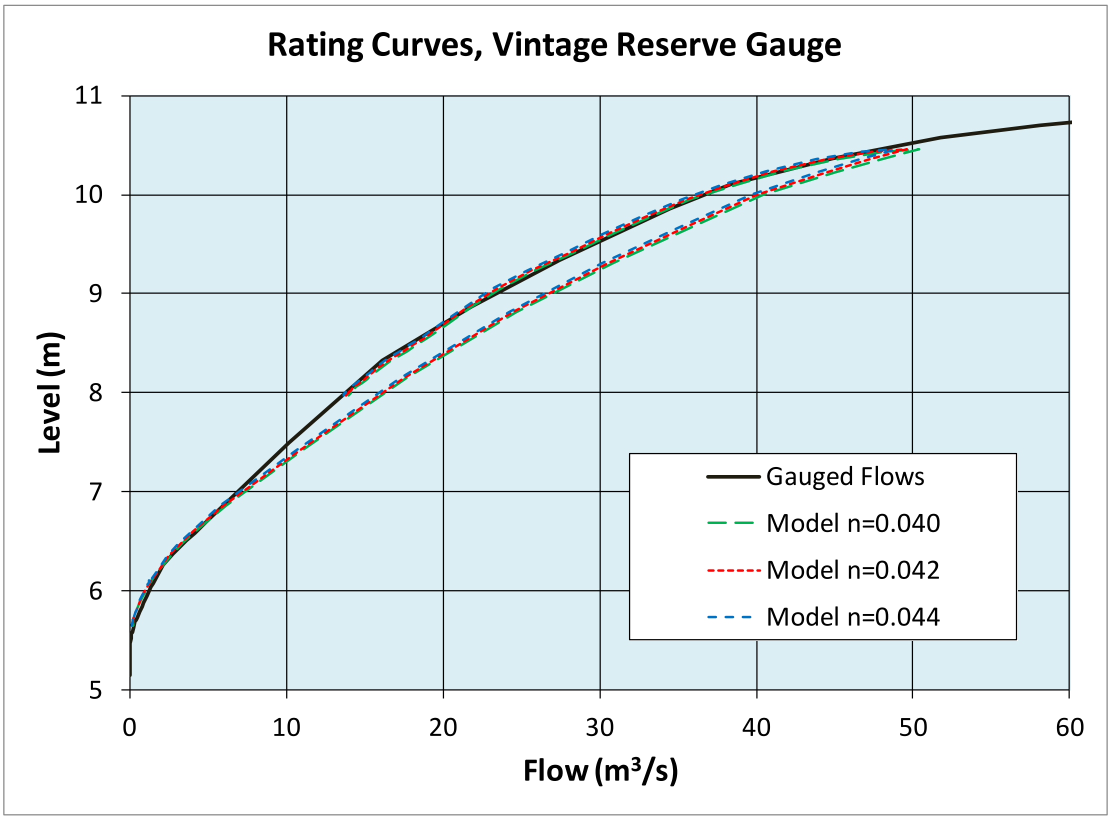

Figure 10. Calibration Using Rating Curves

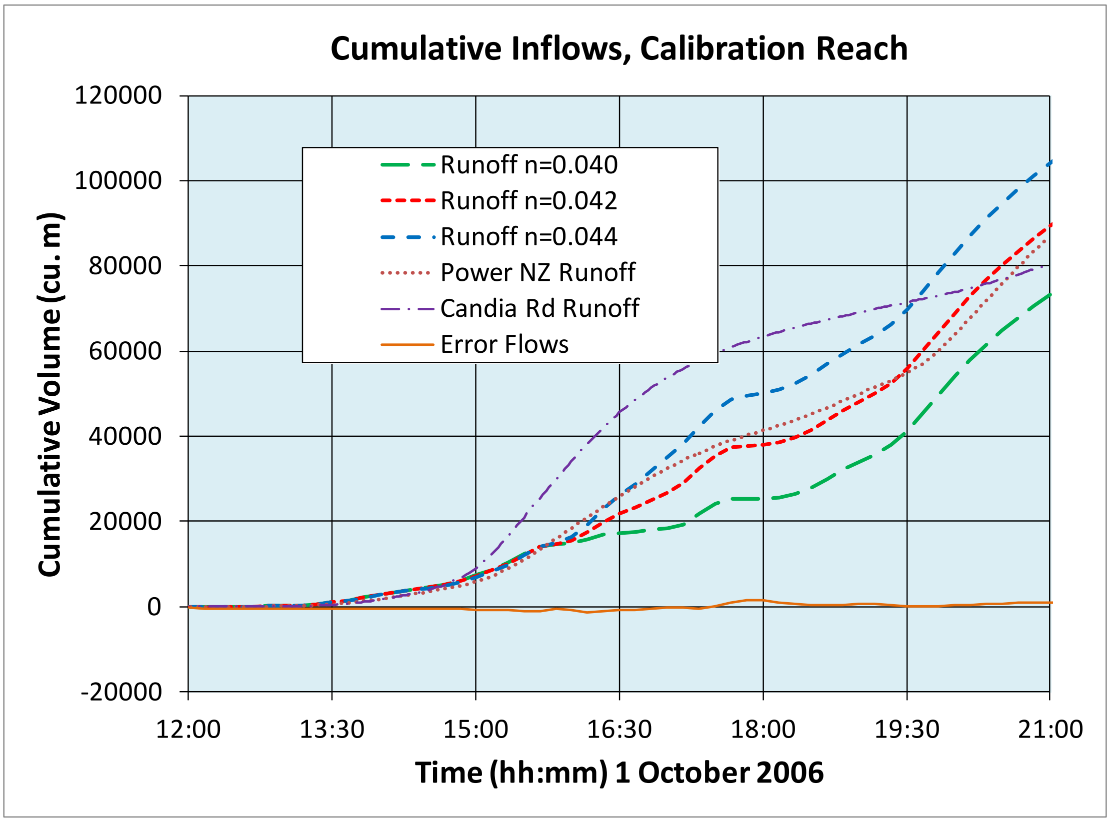

Figure 11. Calibration Using Residual Flows

The fast response hillslope was defined with a Manning n of 0.020, an upslope length of 0.2 km, and a gradient of 0.002. A further 30% of the catchment area was set up as a "slow response" hillslope, with a Manning n of 0.200 and the same upslope length and slope as the fast response hillslope.

Finally, the gutter was given the very high Manning n of 1.000 and a gradient of 0.0005 to mimic the relatively slow response of the residual flow hydrograph to rainfall inputs, even though the gutter area was 500m upslope x 20m wide. The balance of the catchment area was not modelled, corresponding with a loss allowance of just under 5%.

As can be seen from Figure 11, the match of the Hycemos-U runoff based on the local Power NZ rain gauge with the "Runoff n=0.042" curve was quite good.

However the runoff obtained by applying the rainfall measured at the neighbouring Candia Rd gauge to the same Hycemos model matched only in final cumulative output, suggesting that rainfall intensity over the test catchment can have high spatial and temporal variability, even within a single storm event. This clearly imposes limitations on the match which can be expected between runoff from hydrological modeling based on sparse rainfall records and that measured directly by hydraulic analysis based on intensive flow records where the runoff concentrates into a stream.

13. 2008 Verification Event

13.1 Verification: Events of 16-17 August 2007 and 24 August 2008

No verification event was available at the time of commissioning of the 2007 study. However a small storm event occurred just after the original calibration was completed, so the study was delayed to enable a verification exercise to proceed as the data became available. This was included in the original study report (Barnett, 2008), which was presented in February 2008.

Subsequently a far more satisfactory verification event occurred on 24 August 2008, and this offers a range of flows slightly exceeding those in the initial October 2006 calibration event, therefore testing cross-section resistance settings up to at least the same level. Accordingly in this report this has now superseded the August 2007 event for verification purposes.

13.2 Review of Lateral Overflow Model

In the original model, the peak calibration levels overtopped the Lidar ground levels at the right bank near chainage 4.706, and an overland flow path was accordingly specified as shown in Figure 2. The predicted overtopping was only marginal in the October 2006 measurements, but should have been significant according to the higher measured levels during the peak of the August 2008 flood. However no reports of overland flooding in this area are recorded during the floods of either 2006 or 2008, even though both peaked in daylight hours,

The resulting lateral overflow discharge complicated the model, as additional inferred catchment runoff was required to make up the water spilled. Since the Lidar record appears to give crest levels which are too low, the right bank model crest level was raised by 0.5m in the lowest area, at which level the remaining model peak level overflows in the verification event are of such small scale that they may well not have been noticed.

This difference in bank height could be explained by a sharp bank crest formed by slumping and erosion on the stream side, as the averaging effect of the Lidar processing would then give a lower level corresponding with adjacent spot levels below the channel edge. Some support for this explanation is provided by Figure 5, although the sections plotted there are a little further downstream at the gauging site.

13.3 Expansion of Intensive Model Coverage

On recent review of the project, the available photographic data on vegetation changes is too sparse to support concentration on the intended intensive study area, so the resistance testing area has been expanded to cover the whole reach between the level recorders at Border Creek and Vintage Reserve. The revised test reach model coverage is shown in Figure 12.

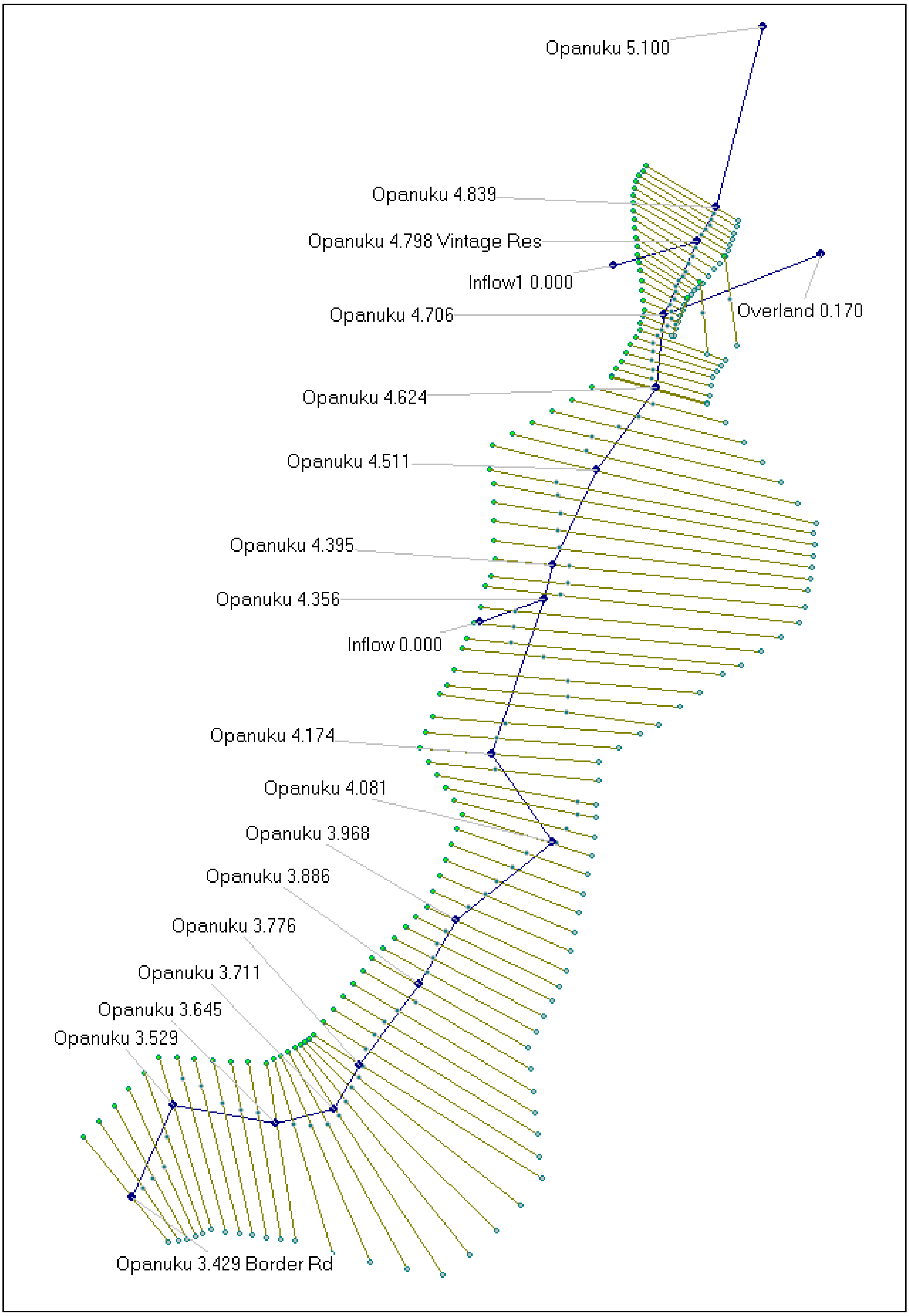

Figure 12: Final Model Layout

Note however that the cross-sections (brown lines) are less closely spaced in the remaining part of the reach compared with the original test reach from Opanuku 4.624 to Opanuku 4.839.

Also, use of the standard channel chainages could not be continued, as these apparently relate to measurements along the low flow channel, which takes several sharp turns within a more gradually curved floodplain. For modelling purposes, the distance between cross-sections must be measured perpendicular to the cross-sections if accurate volume balances are to be maintained. This distance is significantly less than the surveyed chainage differences where the low flow channel is oblique to the cross-sections, which are set up to describe the floodplain to cover high flow events as well as low flows.

As a result, it was necessary to modify the river chainages outside the original test area, where the low flow channel was approximately straight. The standard and revised chainages are given in Table 1, and the changes can also be assessed by comparing Figures 2 and 10.

Table 1

Standard chainages vs revised model chainages

Standard Chainage (km)	Revised chainage (km)
3.114	3.429
3.233	3.529
3.375	3.645
3.446	3.711
3.503	3.776
3.615	3.886
3.699	3.968
3.841	4.081
4.033	4.174
4.318	4.356
4.357	4.395
4.506	4.511
4.624	4.624

Downstream from chainage 4.624 the chainages are as in the original model. Note this reduces the length of the reach from Border Road to Vintage Reserve (chainage 4.798) by 315m to 1.369 km, and the slope between ends accordingly increases.

The cross-sections were derived by merging the data from the Lidar survey with that from the cross-section survey. With reference to Figure 5, the cross-section survey was preferred for the low flow channel, as the Lidar readings are unlikely to be accurate where water was covering the bed during the Lidar measurements. Because cross-sections were required at closer spacing than the available survey, low flow sections were interpolated where necessary using the AULOSInterp hydraulic interpolation routine. Outside the low flow channel, sections were extracted from the Lidar terrain model using the *AULOS* editor.

The overland flow branch was retained in the updated model as shown in Figure 10. This was to allow bank overflows at higher flows, although these were reached only marginally in the verification event, as discussed in Section 13.2.

The stub tributaries Inflow1 and Inflow are retained from the previous model, and in the same positions.

13.4 Review of Rating Curve

Although the 2008 verification event was of a comparable peak height to the 2006 calibration event, there was considerable difficulty in producing a fit with the previous model settings, as any residual flow which fitted the 2008 peak seemed to have an excessively high recession flow, which could not be supplied by credible catchment runoff estimates. The problem was traced to differences between the shape of the 2006 and 2008 curves, as recorded at the Vintage Reserve gauge. These shapes are plotted in Figure 13.

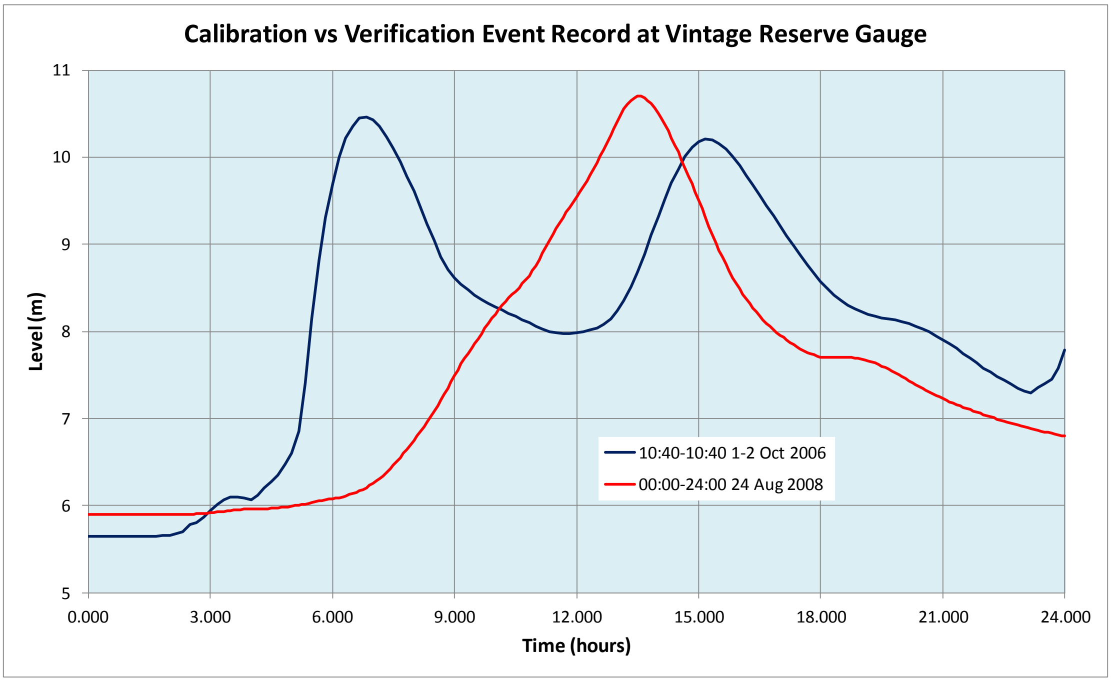

Figure 13. Comparison of Calibration and Verification Events over 24 hours

The first major difference is the multi-peaked nature of the calibration storm as successive bursts of rain crossed the catchment. To avoid the complications of calibrating several peaks, the calibration analysis was terminated at 10:40 pm on 1 October, 12 hours from the nominal start point of the analysis.

After several explanations were considered, the most likely related to the rating curve between levels 6.5m and 8m, as this range is not reached on the truncated recession of the calibration event. This range is traversed by the rising limb, but very rapidly, meaning that acceleration terms can be expected to move the actual stage/discharge curve well to the right of the mean rating curve, increasing the discharge for a given level.

In contrast the single-peaked verification event passes through this range relatively slowly in both rising and recession limbs, so the corresponding actual stage/discharge curves can be expected to lie much closer to the mean rating curve. If the mean rating curve is actually to the left of that originally supplied (see Figure 9), then the downstream outflows will be less than those obtained from the level recorder via the original rating, reducing the residual inflows required to make up the flow shortfall from upstream.

The investigation of this possibility is described in the next Section.

14. Re-evaluation of Rating Data

Fortunately, considerably more ratings had been performed at the Vintage Reserve site since the original study commenced in May 2007, and the additional data was supplied by Auckland Council.

This data consisted of a summary of the gaugings undertaken at the site since July 1999, as well as a series of rating curves fitted from time to time as the data accumulated. This data is presented in Figure 14, together with an extra curve (in black) marked “Composite”.

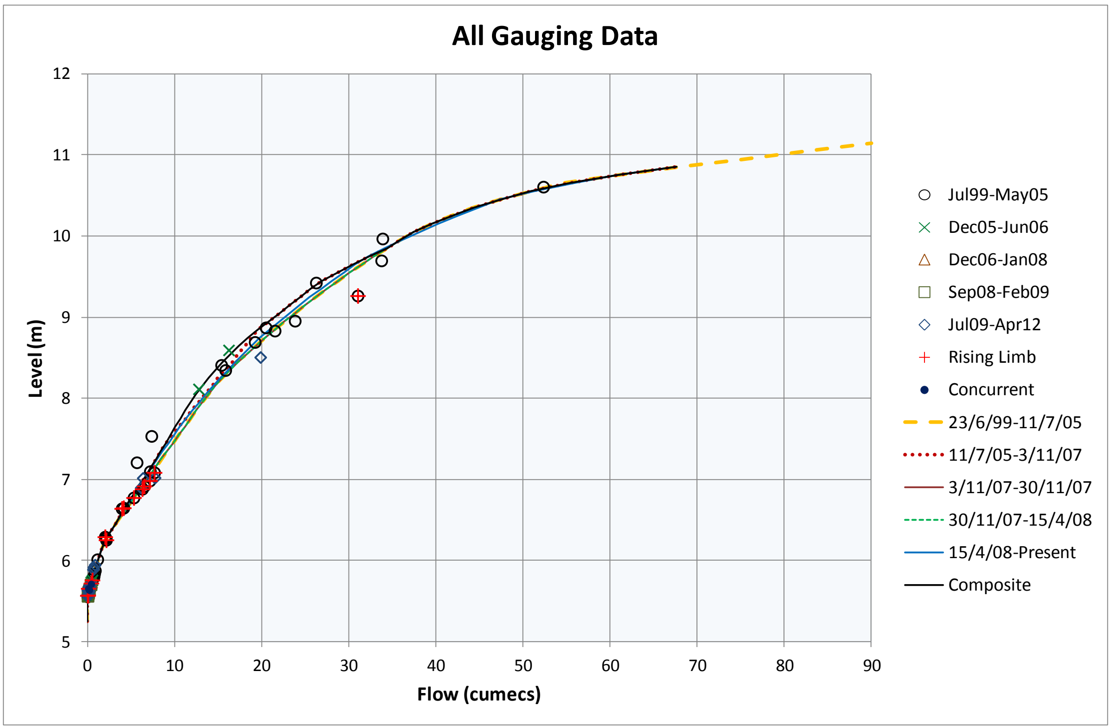

Figure 14. Gauging Data with various Rating Curves.

The general layout divides the plotted points into groups of interest. The circles are the original data, gauged up to May 2005, and the corresponding original rating curve is marked with a long-dashed line. This is also the curve plotted in Figure 9. The following three groups of points were gauged near the time of the calibration and verification events (1 October 2006 and 24 August 2008 respectively), so those marked with the cross were just before the calibration event, those marked with the triangle were between calibration and verification, and those marked with a square were just after the verification. Finally, those marked with a diamond are relatively recent.

In addition to the selection by time, those gaugings performed during rising flow were marked by a red plus sign, and those gaugings nearest before and after the calibration and verification events are marked with a bullet point labelled “Concurrent”.

The rating curves in addition to the original and “Composite” curves were supplied by Council, and are identified by the Council descriptions.

For the levels above 7m, most of the gaugings appear to be marked by the original circles, with the outlier furthest to the right of the curves measured during a rising flow as might be expected. However the gaugings between 7m and 9m levels appear to support a rating to the left of the original curve, especially those just before the calibration event marked with crosses and those earlier gaugings between 7m and 8m. Only the recent diamond gauging supports a move to the right below 20 cumecs, and this is well after both the calibration and verification events.

The area of concern is the range of levels between 6.5m and 8m, which could be called the “Minor Flood” range. An enlargement of Figure 12 in this area is plotted as Figure 15.

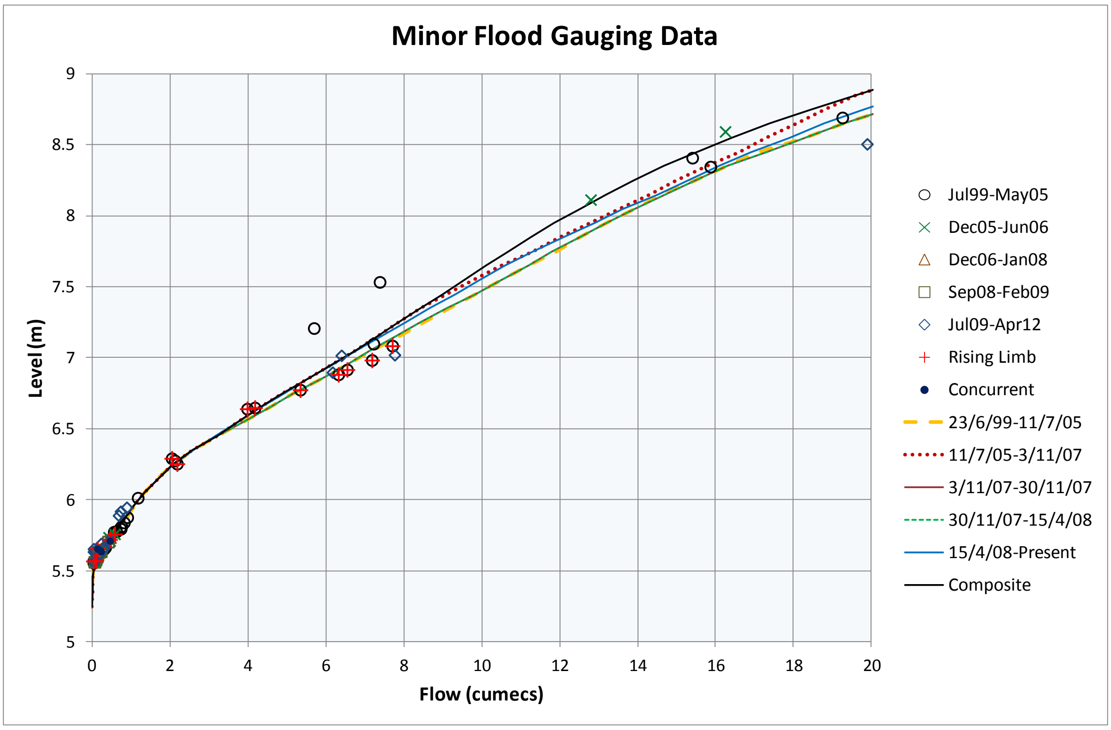

Figure 15. Gauging Data with various Rating Curves – Minor Flood Range

Council staff had already concluded that an adjustment was necessary in the period 11/7/05-3/11/07, which of course includes the calibration event. Figure 14 shows this involved a move to the left of the (red dotted) rating curve in the range from 20-35 cumecs, and from this Figure that general move left extends down to about 3.5 cumecs. However, for some reason this move left is decreased between about 8 and 20 cumecs, even though the only new gaugings (marked with crosses) are from exactly this period, and fall well to the left of the Council adopted curve (red dotted line).

On closer examination of the tabulated curve points, a clear break in gradient occurs at the curve flows 8.43 cumecs and 19.6 cumecs, so a cubic spline was fitted between these points to preserve continuity of gradient. This gave the black line, which is a better fit to the new gaugings from the period as well as giving a smoother connection to lower and higher parts of the Council adopted rating for the calibration period. Therefore that red dotted rating was modified by the cubic spline from 8.43-19.6

cumecs, and the modified rating was adopted as the “Composite” rating for study calibration.

The tabulated Composite rating was then significantly to the left of the original rating throughout the range up to about 35 cumecs, and the resulting smaller downstream outflows reduced the need for continuing balancing inflows, particularly during the long recession limb.

This provided hope that the noted calibration difficulties could now be overcome successfully.

15. Calibration

15.1 Calibration: Event of 1 October 2006

At the time of undertaking the initial calibration, full data from only one event of any size could be provided to the consultants, as the gauging site at Border Road was not fully functioning for earlier events. The supplied event occurred during 1-2 October 2006, even though this had been exceeded in peak level at least five times since August 2001. However, since the Border Road site was the crucial upstream boundary of the model, earlier data from larger events was only of minor value.

The October 2006 event was multi-peaked, but the first and highest peak passed through in the 12 hours from 10:40 – 22:40 on 1 October (see Figure 13), so only this period was selected for modelling.

Because observed data was available only at two gauging sites, there was little basis on which to calibrate longitudinal variation of model parameters. Therefore, the calibration was simplified to three whole-model parameters:

1. Low flow channel Manning n.
2. Riparian Manning n (expressed as the relative roughness, the ratio to the low flow value)
3. Downstream channel boundary conveyance. This could be varied in many ways, but the parameter chosen was channel slope, with cross-section fixed to create a uniform channel of cross-section as measured at Chainage 4.839km and length 150m (i.e. reaching to Chainage 4.989km - note the balance of the distance to the downstream Chainage 5.100 marked on Figure 2 is required to accommodate the transition from the uniform channel through an overfall to a known level boundary condition as required by the information structure of the computational model).

15.2 Calibration Criteria

The Manning n values were calibrated to give as close as possible a match to the rating curve established by flow gauging at the Vintage Reserve. Clearly, matching the lower part of the rating curve was dominated by the low flow channel Manning n, as the Riparian values would come into play only at higher flows.

The downstream channel boundary conveyance was calibrated mainly by matching stub inflows with hydrological catchment model runoff, both in terms of instantaneous flows and cumulative flows. Flatter downstream slopes gave unphysical negative catchment runoff, while steeper downstream slopes gave cumulative flows equally unrealistically exceeding cumulative runoff of 100% of the recorded precipitation.

In the absence of cross-section survey data in the vicinity, the 150m uniform reach downstream was set to a slope of 0.0024 for calibration and verification. This is plausible, being comparable with the 3.281m fall (see Figure 21 below) over the 1.369 km from Border Road to Vintage Reserve.

The significance of these descisions is discussed in more detail under the sensitivity analysis of Section 17.

15.3 Final Calibration

The level hydrographs as observed at Border Road and Vintage Reserve during the event of 1 October 2006 are shown in Figure 16. When the difference in height of the two stations is removed (3.372m based on the initial low flow levels), the Vintage Reserve hydrograph generally lags the upstream Border Road hydrograph as would be expected, but a small event reaches Vintage Reserve at around 13:30 before any significant change is observed at Border Road. The peaks are similar in height, but the hydrograph recession at Vintage Reserve is clearly flatter than that at Border Road.

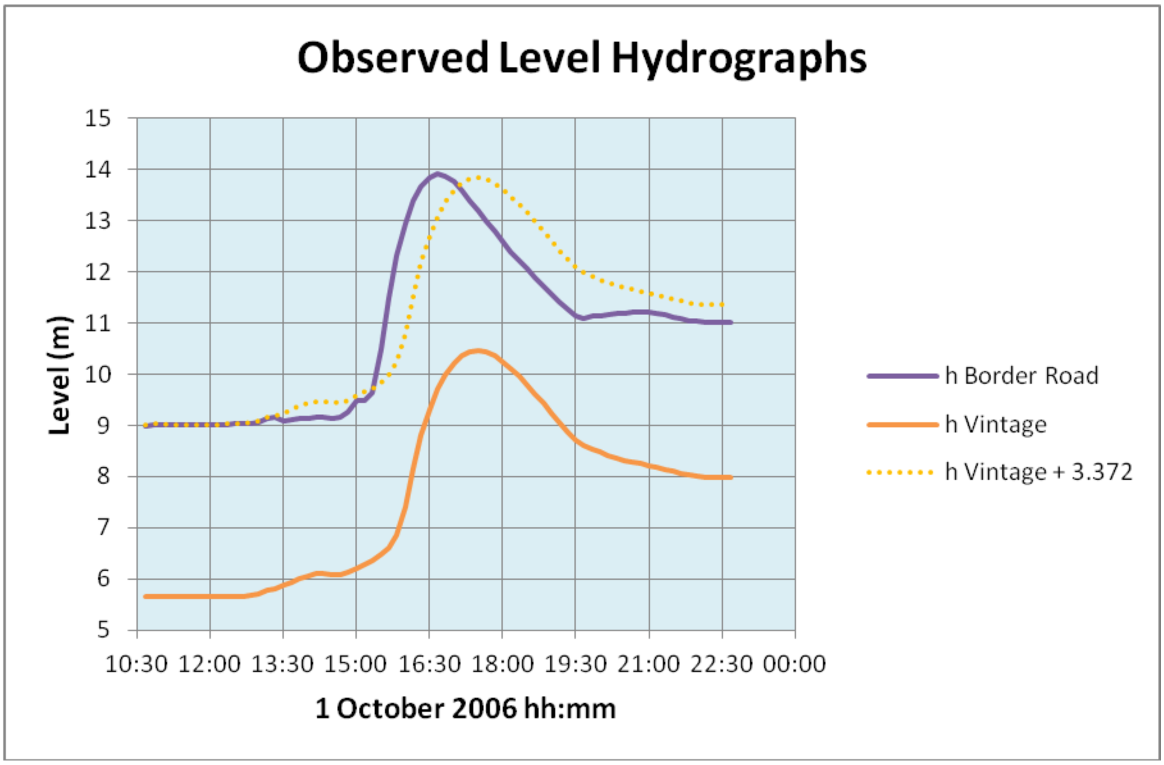

Figure 16: Observed Level Hydrographs for 1 October 2006 Event

All this supports a suggestion of significant local catchment inflow occurring between the two gauging sites, and indeed Waitakere City Council advised (K. Fan, Email of 30 August 2007) that there is a local contributing catchment of 271 ha.

Rain gauge records are available from within this catchment at the Power NZ site, with adjacent records from the Candia Road site further upstream. These locations and the local contributing catchment are shown in Figure 6.

15.3.1 Calibration Against Rating Curve

Figure 17 shows the calibration of the model flows on 1 October 2006 at Vintage Reserve compared with the rating curve supplied by the client. Note the model flows are taken just downstream of the junction with the stub conveying the measured level hydrograph to the solution, so effectively the model curve shows the calibrated flows corresponding with the levels actually recorded.

The major difference is the model produces a “loop rating” rather than a single rating curve. This is a well known outcome of hydraulic theory, see standard texts such as Henderson (1966).

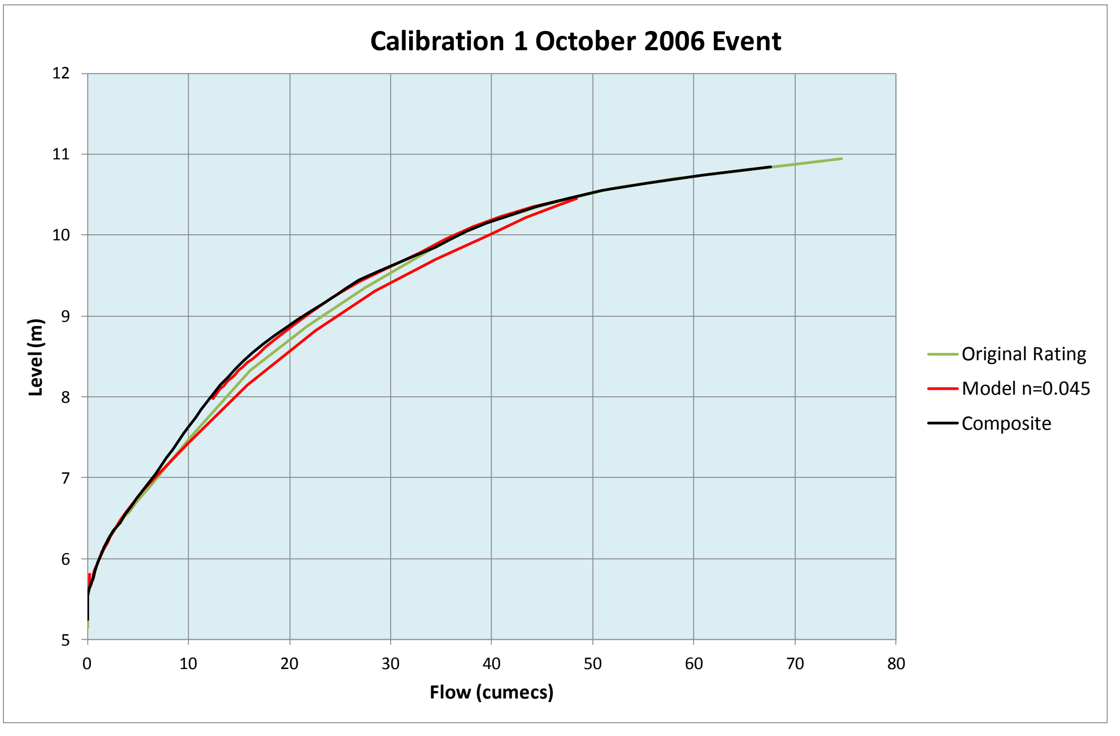

Figure 17: Model Flow Calibration against Levels Recorded at Vintage Reserve Gauge

The low levels correspond with the pre-event low flows, and the calibrated flows begin slightly low, then quickly exceed rated flows up to the peak, as is consistent with the hydraulic gradient exceeding the low flow slope during the rising flood limb. At peak the rating is almost exact, then the calibrated flows track the rating curve back down the recession limb, with flows running slightly below the rating through the period of rapid recession during which the hydraulic gradient can be expected to fall below the low flow slope.

The calibration presented in Figure 17 was obtained for all flows throughout the flood event using a Low flow channel Manning n of 0.045 and a Riparian relative roughness of 10.0, comparable with field measurement figures for the Ngongotaha Stream – see Section 9.1.

Of course, the rating curve is itself a mean curve drawn through a scatter of field gauging results. Some bias of the rating curve towards recession is likely, as there would be a tendency to undertake more gaugings during the falling limb of the hydrograph for logistical reasons - it takes time for a gauging crew to respond to a callout.

15.3.2 Comparison of Flow Hydrographs

It is helpful to plot all relevant flow hydrographs on a single graph to allow comparisons of timing and orders of magnitude, as shown in Figure 18.

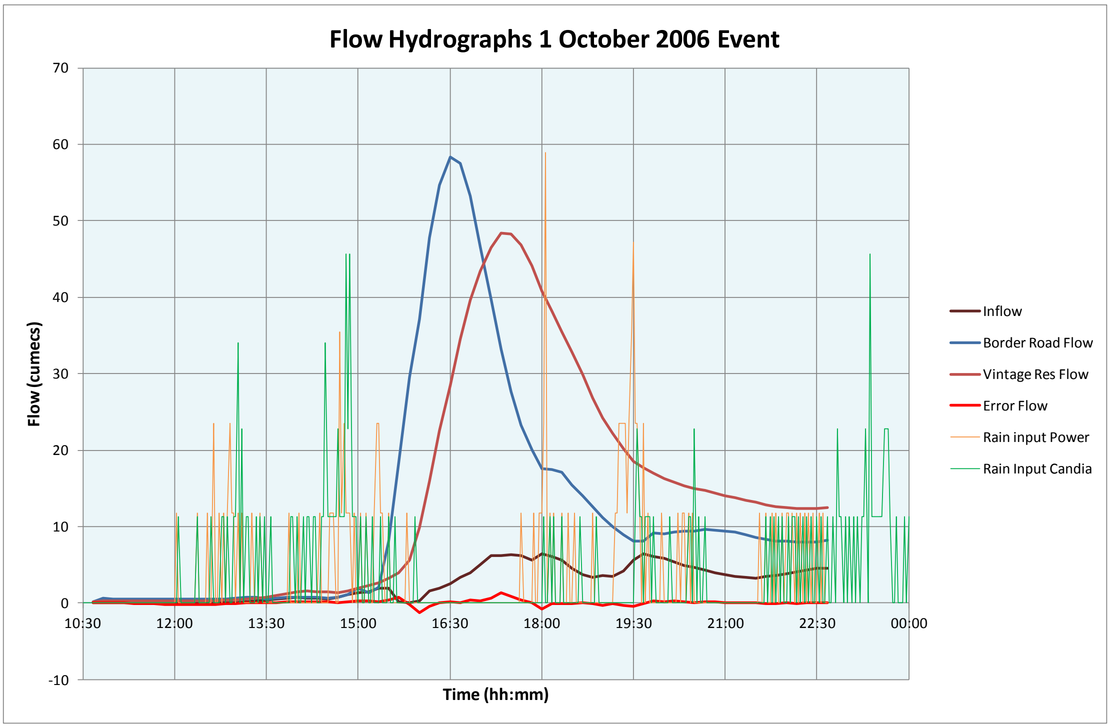

Figure 18: Comparison of Flow Hydrographs

Of prime interest is the difference between the hydrographs at Border Road and Vintage Reserve. There is obvious attenuation of the flood peak. This illustrates that using the flow hydrograph derived solely based on the levels and rating curve at Vintage Reserve to represent the inflow hydrograph at Border Road would produce significant underestimation (20%) of the flood peak of the inflow hydrograph. This is the same order of error as using the rainfall depth for a 20 year event when designing for a 100 year event, so comparable errors could then be expected from the use of techniques such as Flood Frequency Analysis. This would not be improved by neglect of the intervening local inflow, as without this, the difference between peak flows would actually *increase*!

The “hydrographs” marked as Rain input are actually derived from rainfall intensities at the Power NZ and Candia Road continuous rain gauges, multiplied by the catchment area of 271ha (see Section 15.3 above) supplying the model between the end points of Border Road and Vintage Reserve. These inputs are distributed over the catchment, so various hydrological processes will delay and reduce the amount of these inputs appearing as stream inflows.

The plotted “Inflow” is the flow balance required at point Inflow1 0.000 to maintain the observed level hydrograph at Vintage Reserve, and transferred to the point Inflow 0.000 as described in Section 11.2. Because moving the “Inflow” upstream to a more representative entry point means that the required balancing flows no longer arrive exactly as required, a residual flow balance is still required at point Inflow1, and this is plotted as “Error Flow”.

Some experimentation was used to minimise this error flow, and obviously a lead time is likely to be helpful to compensate for the travel time downstream by 480m, so the hydrograph from Vintage Reserve was advanced by 10 minutes, corresponding with an average wave velocity of 0.8m/s.

The actual wave velocity will vary considerably during the course of the flood, so more advanced methods of phase shift could be tried, but the plotted Error flows are sufficiently small (particularly compared with the total streamflows at Border Road and Vintage Reserve) that more sophisticated adjustments were judged to be of low priority.

Comparison of the “Inflow” curve with the two Rain input curves shows a plausible cause/effect timing relationship, in that “Inflows” increase after a suitable delay following precipitation in the catchment. Further, as would be expected, the relationship is more closely linked to the local Power NZ site records than the Candia Road records further upstream, because the response to the first rainfall period (say 12:00 – 16:00) is weaker than the response to the second (say 17:30 – 20:30). At Candia Road the second rainfall period is comparatively minor, while at Power NZ this second period is dominant, consistent with the balancing inflows found to be required by using the model.

15.3.3 Cumulative Inflows

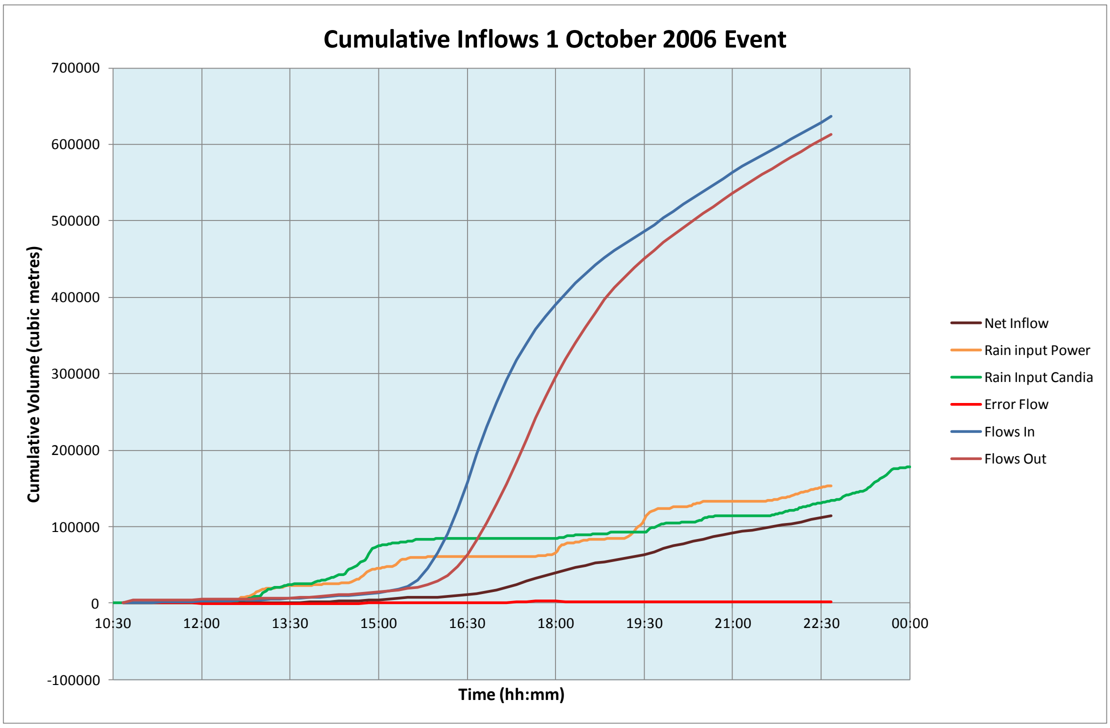

Figure 19: Cumulative Inflows Corresponding to Figure 16

Cumulative inflow plots offer a different perspective on the same data. Figure 19 shows first that the Error Flows are essentially noise, with mean flow approximately zero. This is especially in comparison with the Flows In (Border Road + catchment Inflows) and Flows Out (Vintage Reserve), so the vertical difference between these two lines at any time indicates the current volume in the model.

The other three lines are the basis for a comparison of considerable importance. The spiky nature of the rain input records is now smoothed, showing substantial differences between the event as recorded at Power NZ and as recorded at Candia Road, both in timing and intensity of bursts. This illustrates the difficulty of setting up rainfall/runoff models, even if the precipitation gauges are relatively close together as in this case.

Comparison of both of these curves with the Net Inflow curve adds the necessary upper bound to the Net Inflow calibration, as it is clear that a Net Inflow accounting for more than 100% of the event precipitation is equally as unphysical as a negative Net Inflow. The result plotted shows flows accumulating at approximately 55%-65% of the cumulative precipitation recorded at Power NZ, and was therefore adopted, as this is typical of runoff coefficients recommended for mixed residential/industrial areas by authorities such as the New Zealand Building Code Clause E1.

As described in Section 12, a rainfall-runoff model was then tried, based on a “fast response” component of 65% of the catchment area and a “slow response” component of 30% of the catchment area, with the balance being a connecting channel and an allowance for losses. The model was left with the same settings as those used to obtain the fit shown in Figure 11, although since that work the model of the study reach had been modified by slight shortening of the reach between Border Road and the Vintage Reserve and the inclusion of Lidar terrain data over the full reach as described in Section 13.3.

The resulting match is shown in Figure 20.

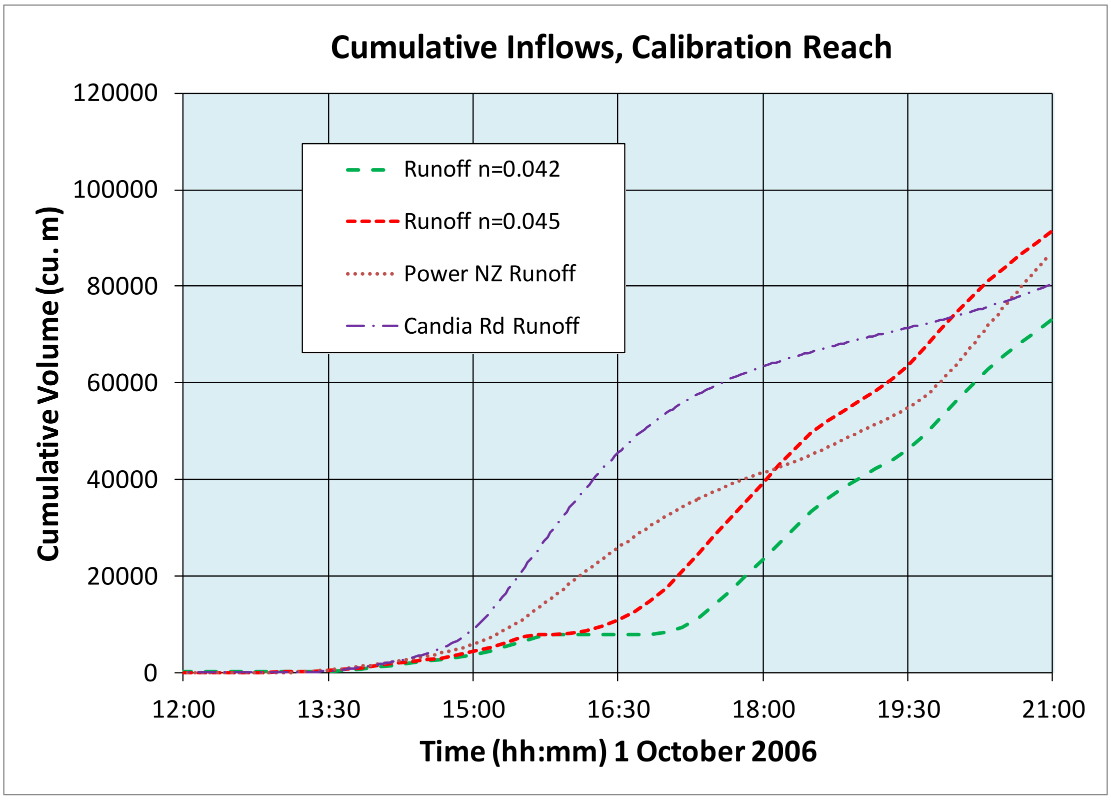

Figure 20. Recalibration of Resistance for Revised Model Cf. Figure 11.

Note the runoff estimates associated with the Power NZ and Candia Rd rain gauges are unchanged, as the rainfall/runoff model retains the previous settings. However the previous best match at n=0.042 is no longer acceptable, as the mean slope of the reach has been increased. A value of 0.044-0.045 is indicated, with the higher value preferred in the light of the inferred crossing of the dashed red and dotted brown lines just off the right of the plot.

Although the change from 0.042 to 0.045 in Manning n is around 7%, this is an encouraging demonstration of the fact that the value obtained is relatively insensitive to quite significant changes in the definition of the channel reach.

16. Verification

16.1 Verification: Event of 24 August 2008

Figures 21, 22, 23, 24 and 25 are the equivalents for the Verification Event of Figures 16, 17, 18, 19 and 20 respectively, with all model parameters set to the same values except for the Manning n, since there were known significant changes to the riparian vegetation between events. Instead of n=0.045, a value of n=0.040 was found to be required to provide the match, as demonstrated by these result plots.

Comparing Figures 21 and 16, the events are rather different. Apart from the differences discussed in Section 13.4, there is a small difference in the initial gradient, although this is likely to correspond with the significantly larger initial flow rather than some fundamental change in bed slope. Also the peak level does not attenuate, presumably because the rate of rise is much slower, so the reach storage has less effect and the initial runoff has more chance to contribute to the downstream flow.

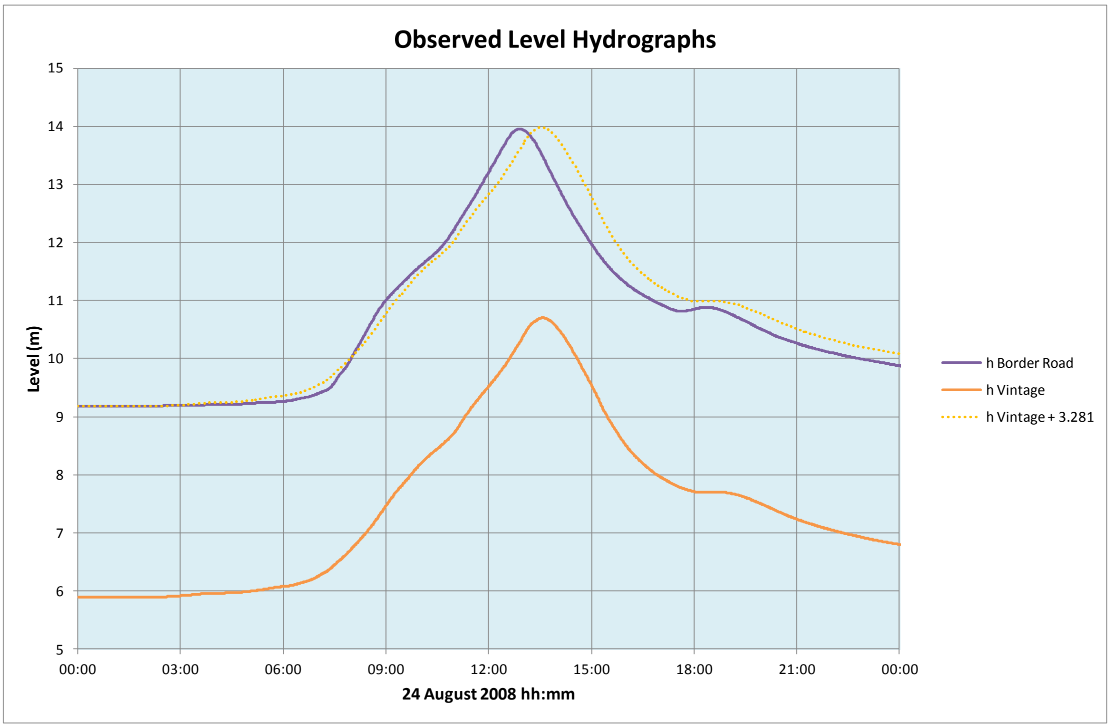

Figure 21: Observed Level Hydrographs for 24 August 2008 Event

Figure 22 shows much less loop in the rating curve than Figure 17, as would be expected from a more gradual event, and the fit to the rating curve is good at low flows. However the peak is now to the right of the composite curve, corresponding with the significantly lower resistance value. As the rating curve is merely an average drawn through the gauging data, this data has been added to the plot, clarifying that the model values are not inconsistent with known gaugings, especially on the recession.

A decrease in resistance is compatible with the verification event occurring in late winter as compared with the spring season for the calibration event, regardless of the riparian planting programmes which intervened.

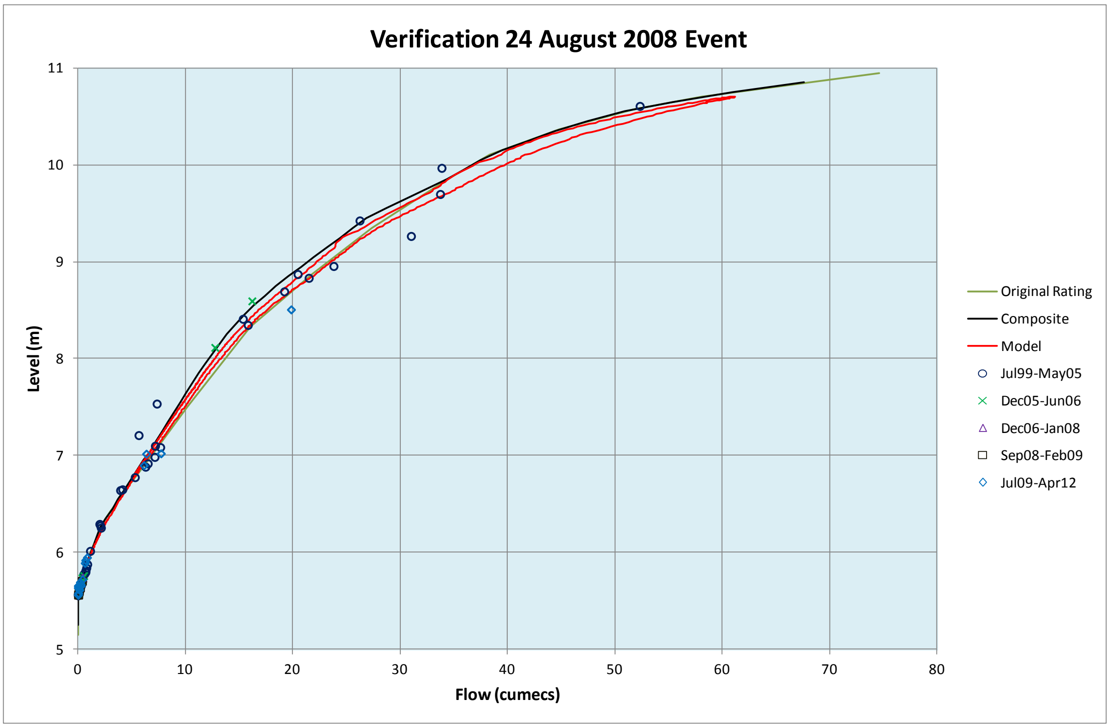

Figure 22: Model Flow Rating against Levels Recorded at Vintage Reserve Gauge

A comparison of Figures 23 and 18 indicates there is still significant attenuation of the flow peak, but a “bump” on the recession curve at about 20 cumecs seems to relate to the intense burst of rain recorded by the Power site just before 15:00 hours.

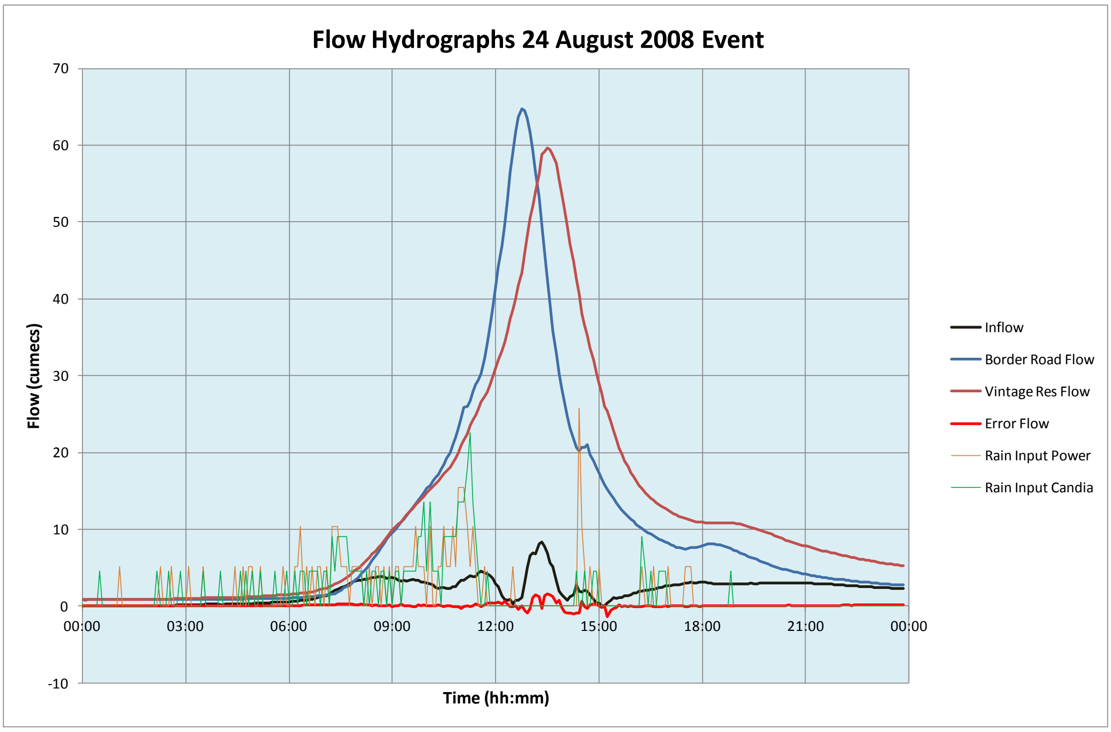

Figure 23: Comparison of Flow Hydrographs

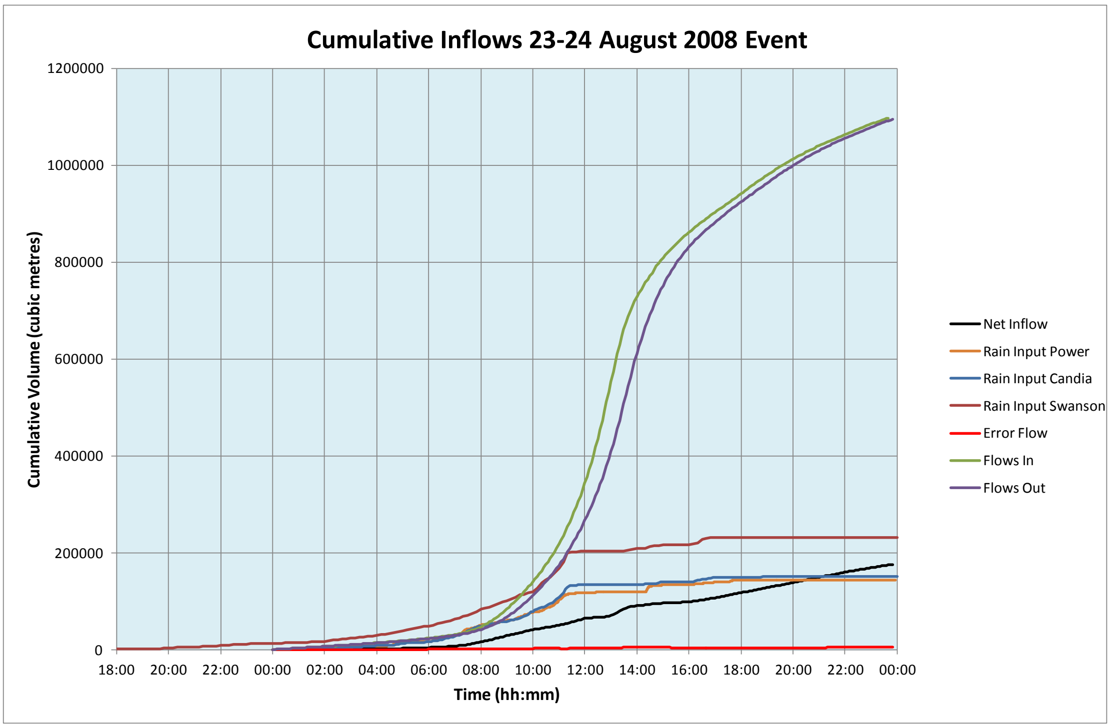

Figure 24: Cumulative Inflows Corresponding to Figure 19

Figures 24 and 25 convey similar views.

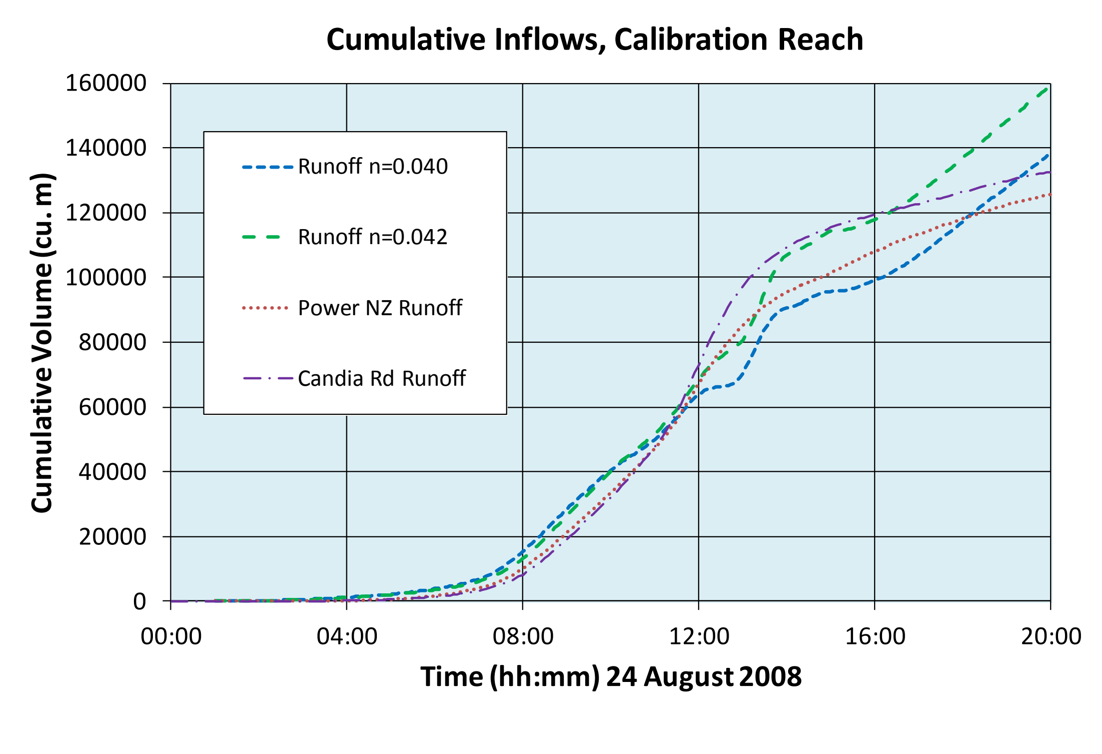

Figure 25. Resistance Calibration for Verification Event

By comparison with Figure 19, the Flows In and Flows Out curves in Figure 24 draw much closer together at the end of the record, but this merely reflects the fact that the volume left in the system is much smaller this time because the event ended at lower levels.

This time, the rainfall precipitation patterns are quite similar between the Power and Candia Rd sites, but the Net Inflow curve now crosses the rainfall input lines from both sites.

The rainfall/runoff model was re-run with the same settings as before, but now of course with the rainfall inputs recorded during the verification event. Figure 25 shows a better match than Figure 20 to the runoff inferred from residual flows, but even the curve with n=0.040 starts to over-run at the end, as would be expected because this is also the curve plotted in Figure 24. By comparison with the curve with n=0.042, this suggests that the resistance should be lowered even further, but this runs counter to the gauging evidence of Figure 22.

It is possible that the Power and Candia sites both missed some heavy precipitation on the catchment, such as that recorded at another adjacent rainfall recorder, labelled Swanson, but on balance the evidence suggests that a significant reduction in resistance has occurred between the calibration and verification events.

In summary, then, the Verification indicates that both events can be modelled using model parameters which are all fixed except for the resistance. This shows a significant decrease between October 2006 and August 2008, but some of the change in riparian vegetation may be seasonal rather than the direct result of intervening riparian planting programmes.

17. Sensitivity Analysis

17.1 Model Test Setup

This study requires tests for hydraulic sensitivity to riparian resistance. As explained in Section 9, the strategy is to provide a controlled intensive test area, with the extended model boundaries set at some distance to provide a buffering effect. This means that a level boundary or rated flow control cannot be used directly on the main channel at the Vintage Reserve gauge site, as changes in levels and hence the rating at this site are precisely the expected result of changes in riparian resistance.

However, lateral inflows at the site can be expected to be virtually independent of riparian resistance, so the level boundary can be replaced by a flow boundary. For this purpose, the calibrated flow solution at the stub boundary Inflow1 0.000 (see Figure 12) can directly replace the calibration event level boundary. Because the solution technique uses a linear matrix, the model should return the original level boundary exactly, at least within the precision limits of rounding to three decimal places of the boundary input units (metres for level and cumecs for flow).

Although the Border Road boundary is remote from the test area, the level boundary there was also reviewed for consistency of treatment. However the flow boundary must be specified at every time step to reproduce the identical matrix solution, and the required work to produce this was judged to be unjustified by any significant quality improvement.

The calibration event was then re-run with the switched boundary at Inflow1 0.000, giving the “Exam2” standard model event.

For quality assurance, the boundary levels computed at Vintage Reserve (Inflow1 0.000) are compared with the original level boundaries in Figure 26. The differences are never more than a few millimetres, too small to be resolved by the plot.

17.1.1 Further Analysis of Error Flow

The inflow boundaries are derived in two stages. First, there is zero inflow through the stub tributary named Inflow, and the observed level boundary applied to the stub tributary Inflow1 at the Vintage Reserve gauge draws in a residual inflow hydrograph. Second, this hydrograph is then transferred (advanced in time by ten minutes) to Inflow as a flow boundary. Although the residual flow is now being supplied to the model, the change in inflow point and the time advance together modify the solution, so the hydrograph at Inflow1 is not exactly zero as applied to Inflow in the first stage. The resulting flow hydrograph at Inflow1 (the so-called “Error Flow” in Figure 23, for example) is that now required computationally to exactly preserve the observed levels.

The properties of this “Error Flow” are usefully illustrated by the standard numerical technique (Anon., 1961) of successive differencing of the residual flow hydrograph supplied at the point Inflow 0.000. This technique removes smooth variations in an input data series, isolating sudden jumps in gradient.

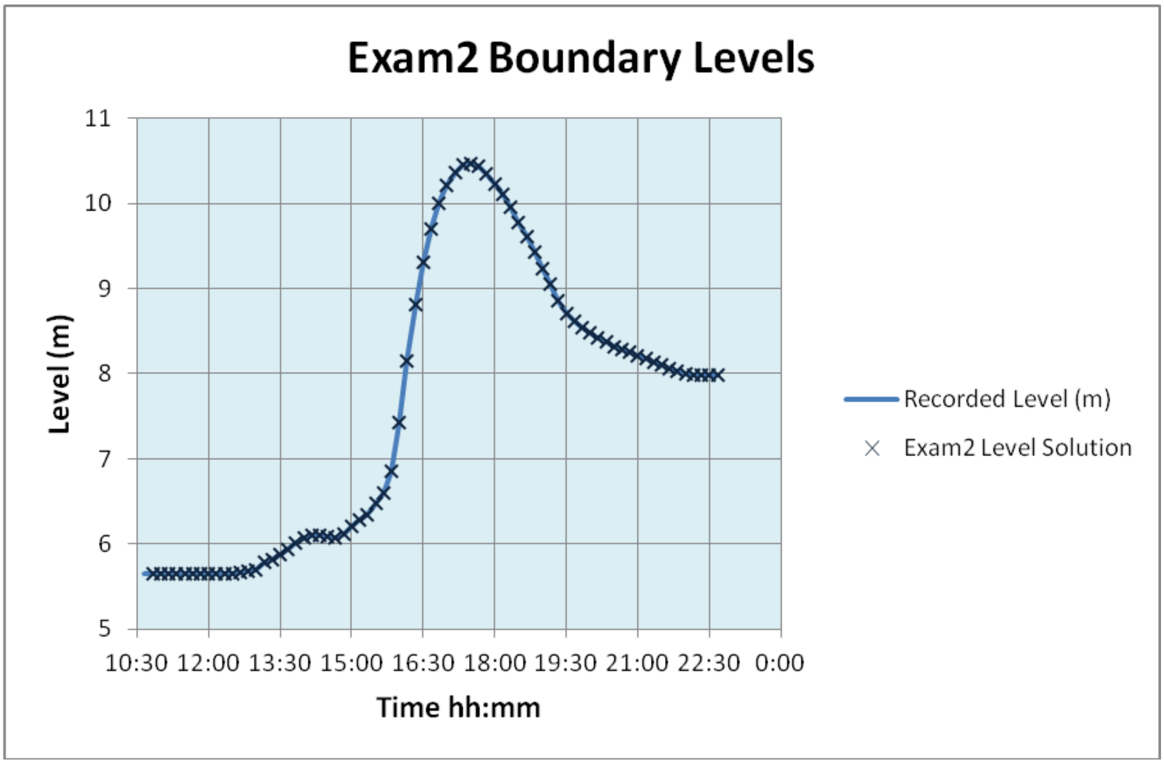

Figure 26: Comparison of Recorded Boundary and Exam2 Solution at Vintage Reserve

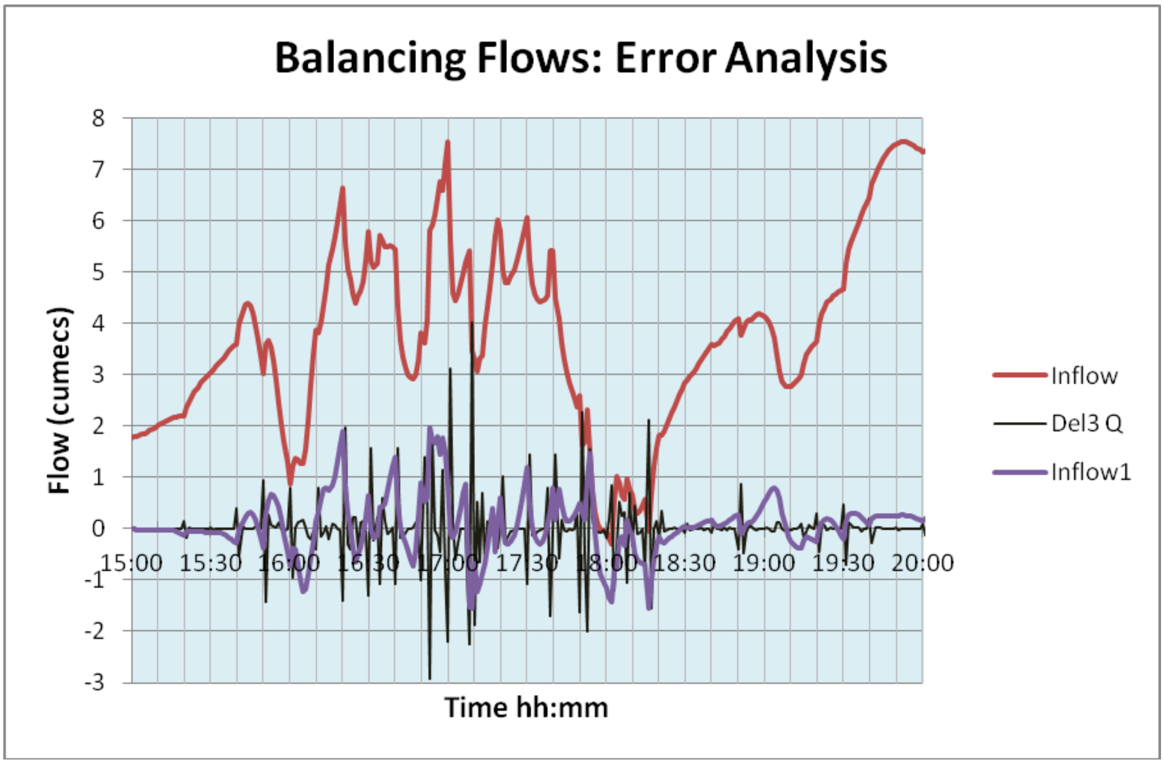

Figure 27: Analysis of Flow Balances During Calibration Flood Peak

The results are presented in Figure 27. “Inflow” is the inferred residual flow hydrograph required to match the level boundary, and “Del 3 Q” is the third difference of the Inflow data series. Prominent in this plot is the association of most spikes with the 10 minute grid lines, indicating the effect (strongest at peak flows) of sudden changes in gradient from linear interpolation of the recorded level hydrograph as supplied at 10 minute intervals.

This suggests that smoothing of the level hydrograph would remove much of “Inflow1” which is the direct result of the interaction between the computational solution engine and the transfer of the balancing inflow from the Vintage Reserve upstream to mid-catchment.

As a result, the verification event modelling used gauge level records at a resolution of 1 minute intervals, removing most of the erratic behaviour from this source.

17.2 Calibration Sensitivity

17.2.1 Sensitivity to Manning n

The effect of varying the Low Flow Manning n is shown in Figure 28. This is the lower left-hand corner of Figure 22, with the red line marking the response to the fitted model as before. In addition to the Manning n of 0.040, this model used the calibration values of 10 for the relative (riparian) resistance and 0.0024 for the downstream slope.

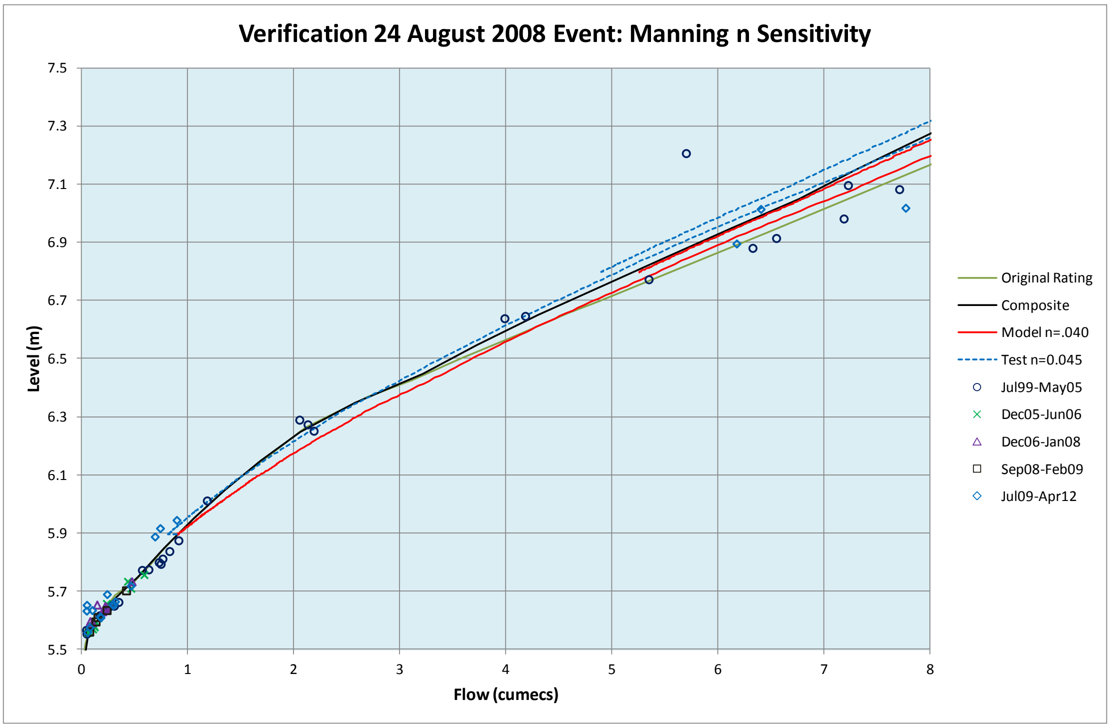

Figure 28: Model Response to Variation of Manning n.

The extra curve (dashed blue line) shows the sensitivity of the model results to a change in Manning n back to 0.045, the value giving the best fit for the calibration event.

The initial conditions are taken to be the same, fitting the “composite” curve, but the increase in the base Manning n immediately reduces the model flow, shifting the curve substantially to the left even at low flows. Clearly the flows are too low, being mainly to the left of the composite curve even in rising flows.

In contrast, use of the same Manning n in the Calibration event (Figure 17) produces rising flows to the right of the green original rating curve in the same flow range. At higher flows the pattern does not change, so these are not plotted in this case.

17.2.2 Sensitivity to Riparian Resistance

The effect of varying the relative (riparian) resistance value is shown in Figure 29. This reproduces Figure 28, but this time with the dashed blue curve showing the model response to Riparian Resistance value of 8.0 instead of the calibrated 10.0. As would be expected, there is little difference at low flows because the water is not passing through the vegetation. As the water level rises, the riparian resistance has more effect, but clearly the model is not very sensitive to a 20% variation in this value.

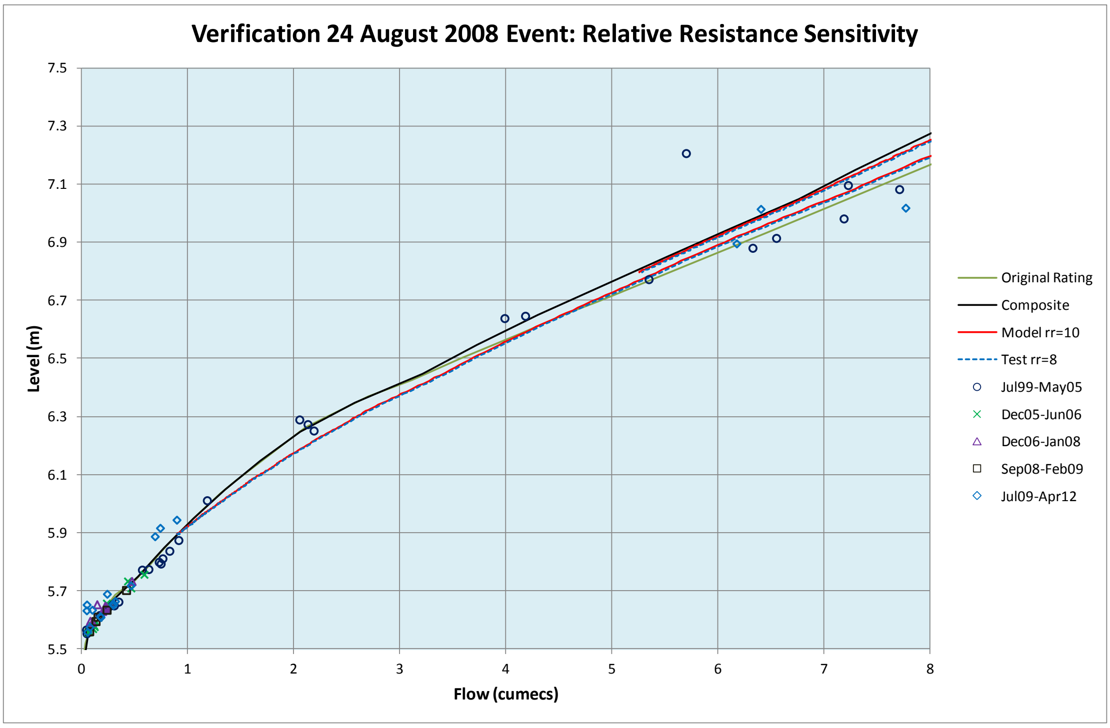

Figure 29: Model Response to Variation of Riparian Resistance Setting.

17.2.3 Sensitivity to Downstream Slope

The effect of varying the slope to the downstream boundary is shown in Figure 30, this time with the dashed blue curve showing the model response to a decrease in the assumed runout slope below the calibrated value. This used the average reach slope of about S=0.0024.

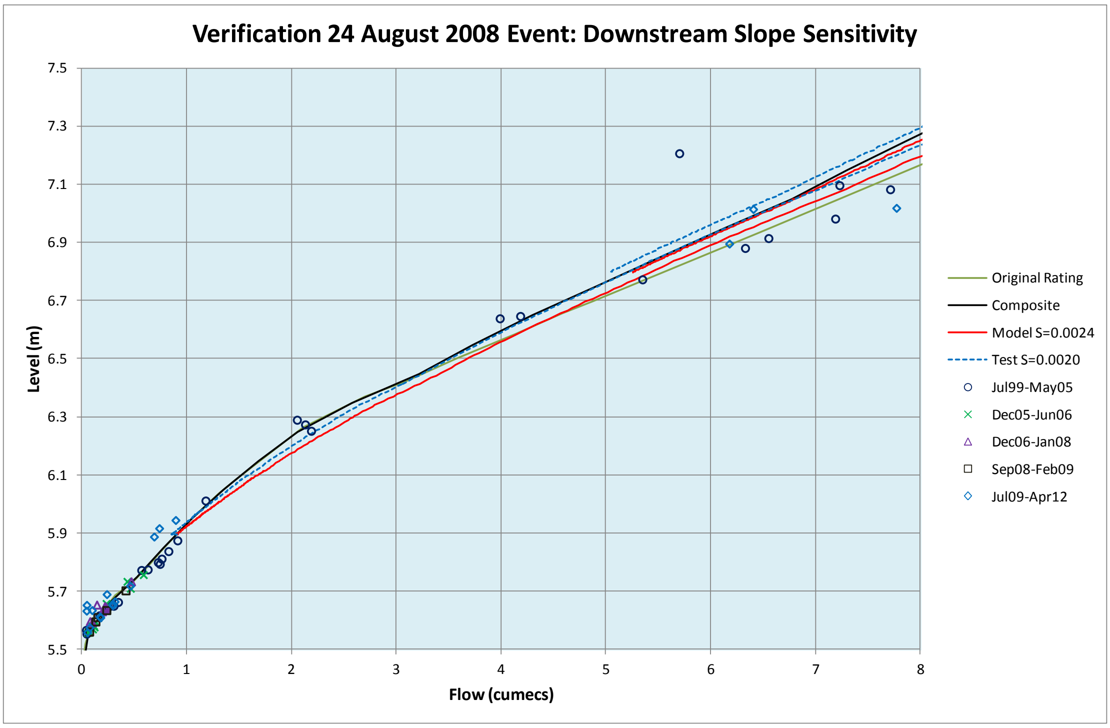

Figure 30: Model Response to Variation of Downstream Runout Slope.

The effect is muted at low flows, because in this range the short reach to the last surveyed cross-section at Opanuku 4.839 is still dominant in setting the backwater profile. This supports the choice of low flow Manning n, as demonstrated by Figure 28. As the flow rises, the runout slope starts to have some effect, with increasing slope producing more flow at a given level.

However the three Figures 28, 29 and 30 show that the base Manning n is the main factor controlling calibration, as the relative resistance formulation for the riparian vegetation implies that the riparian resistance also rises as the low flow Manning n is increased.

18. Dependence on Modelling Platform

While the above results are interesting, they would not be useful if they could not be repeated by other independent researchers using different modelling platforms.

The present results were obtained using the *AULOS* hydraulic modelling software developed by HYDRA Software Ltd. Specifically, the energy solution was applied, using the “Compound” hydraulic radius option at all sections with the “Floodplain” correction switched off. No eddy losses were applied at any point. The low flow Manning n was applied only to the low flow channel (effectively that below the terrain as surveyed by Lidar), and the stated relative resistance factors were applied at all higher points.

The energy solution is an unsteady Bernoulli-type formulation, and the “Compound” hydraulic radius invokes classic conveyance theory as described in Section 10.1.1. The interpretation of the Manning n values therefore strictly relates only to this theory.

However, for flow residuals to be applied, the first requirement of the hydraulic analysis is to interpolate a water surface between the water levels measured at the upstream and downstream ends of the reach at consecutive time intervals. Given that the mean water surface gradient is continually defined in this way, the time variation of volumes within the reach should not be heavily dependent on the model used, whether this is energy, 1D momentum, 2D momentum, or even some simpler kind of spatial interpolation.

The second hydraulic modelling requirement is the relation between steady flow and resistance for the upstream and downstream control points, where the levels are recorded. Thirdly, at the downstream end the model is required to translate timewise rates of change at the fixed measuring point into water surface slopes and acceleration terms during the rising and falling limbs of the hydrograph, so that a looped rating can be related to the stage/discharge gauging points measured from time to time.

Preferably, this should be done by carrying the solution far enough downstream that a backwater curve will reach the same level at the Vintage Reserve regardless of the boundary level chosen downstream (e.g. a fixed tide level). Unfortunately, in this case the reliable surveyed cross-sections did not extend more than 41m downstream of the boundary gauging site, so a channel extension had to be schematized further downstream to provide sufficient runout length.

Once found to be satisfactory, the same unsteady flow correction procedure should be assumed to apply to the upstream boundary as well, although the only check of the accuracy of this theoretical assumption is finally the ability of the calibrated residual flow hydrographs to match those predicted by rainfall/runoff modelling, at least in cumulative volume.

The key requirement of the chosen hydraulic model is the ability to maintain accurate mass balances, as residual flows are relatively small compared with main stream flows. This means that mass balance errors of the order of say 10% will produce false residuals totally dominating the actual lateral flow contributions, on which the whole method is based.

18.1 On the Dimensionality of Models

References to the dimensionality of models as “1D” or “2D” continue to cause confusion. The problem essentially derives from attempts to classify models of fractional dimensions, or fractals, using only integer numbers of dimensions (see Abbott and Larsen (1985)). With respect to the surveyed terrain (including the perimeters of pipes and channels), both “1D” and “2D” models are fully three-dimensional. This can be demonstrated by the ability of both to compute a volume, for example that of a pond, which undoubtedly involves three spatial dimensions. In fact, a pond volume can even be computed using a “0D” model such as a depth contour map, because “1D” and “2D” conventionally refer only to horizontal dimensions, and a contour map uses a vertical projection of the three-dimensional terrain surface.

The conventional “1D” and “2D” refer specifically not to the model itself, but to the method of analysis of the model. “Analysis” is defined by the Concise Oxford Dictionary as “Resolution into simple elements”, and 1D analysis uses a projection of the three-dimensional terrain surface similar to a contour map, but the projection is now horizontal instead of vertical, resolving the terrain into vertical slices instead of horizontal slices. Computation of the pond volume can now take into account longitudinal variations in water level between slices, but in the case where the pond surface is horizontal, the volumes computed by 0D and 1D analysis will be the same if the projections are both made to the same resolution. 2D analysis adds a second horizontal projection of the three-dimensional terrain surface, usually lateral (orthogonal to the first longitudinal projection) to enable a momentum vector equation to be resolved into two orthogonal scalar components. These two projections intersect to form slabs (seen vertically), so the pond volume computed by a 2D analysis can now take into account variations in water level between adjacent slabs laterally as well as longitudinally. However in the case where the pond surface is horizontal, the volume computed by 2D analysis will match those computed by 0D and 1D analysis.

Therefore the fractal dimensionality of the pond volume computation depends on the dimensionality of the pond surface level, with the dimensionality of the “2D” volume exceeding that of the “1D” volume, which in turn exceeds that of the “0D” volume, as the slope of the pond surface becomes significant in the lateral and longitudinal directions respectively.

18.1.1 Isotropic 2D Grids

So far, the dimensionality of the “2D” solution makes it a superset of the “1D” solution, which is in turn a superset of the “0D” solution, as might be deduced from the conventional terminology. At worst, they all give exactly the same volume where both the lateral and longitudinal pond surface slopes are insignificant. However this assumes that the main directions of surface slope are known, so that “longitudinal” and “lateral” are meaningful terms. In situations such as harbours where the water surface gradients are defined not by ground slopes but by tides or tidelike waves (tsunamis, storm surges), level gradients in a considerable range of directions may be experienced over time at a single point (Barnett (1985), Barnett (1998)). In such conditions, the terms “longitudinal” and “lateral” are interchangeable, and it becomes important that the grid directions are also interchangeable. Such grids are called “isotropic” (although strictly this should mean that the analysis should be capable of producing identical answers for any rotation of the grid, rather than only a 90, 180 or 270 degree rotation as supported by most “2D” schemes).

Clearly a 2D grid distorted along a channel cannot satisfy this isotropic requirement, which is why conventional 2D grids are usually square. It follows that the resolution in longitudinal and lateral directions must now be the same. However in cases where flow mainly occurs through an elongated channel, this is a significant disadvantage. For example, a 600mm diameter circular pipe has a significant drainage capacity, yet the lateral velocity gradient must resolve variation from zero to maximum over 300mm, while the longitudinal velocity gradient may be almost zero over lengths of 30m or more. It is beyond current practical computational capacity to refine a 2D square grid indefinitely (Vojinovic and Abbot (2012)), down to say 30mm x 30mm to resolve the lateral gradient , so the usual practice is to compromise between a longitudinal grid of 30m and a lateral grid of 30mm by applying a square grid of about 1m.

Compared with a “1D” solution, this drastically degrades the solution – for example a computation of the volume contained in a length of 600mm pipe using a 1m square grid would be crude in the extreme, so in this case the dimensionality of the “1D” solution exceeds that of the “2D” solution. Remembering that there would then be no “2D” capability for resolution of lateral variations of water level, in this case the “1D” solution is a superset of the “2D” solution, as it is still able to recognise lateral variations of terrain perimeter level while the isotropic “2D” model cannot.

In summary, “2D” solutions are supersets of “1D” solutions *only* where the “2D” grids can be distorted to match elongated hydraulic features. Isotropic “2D” analysis becomes substandard compared with “1D’ analysis as soon as it is applied to elongated channels, in which the physical longitudinal length scales may exceed the lateral length scales by a factor of 1000 or more.

18.2 *AULOS* Mass Balances

The mass balance accuracy of *AULOS* was investigated for the verification event of 24 August 2008. Figure 29 shows the depth contours for the test reach at 0000 and 1300 hours respectively on that date.

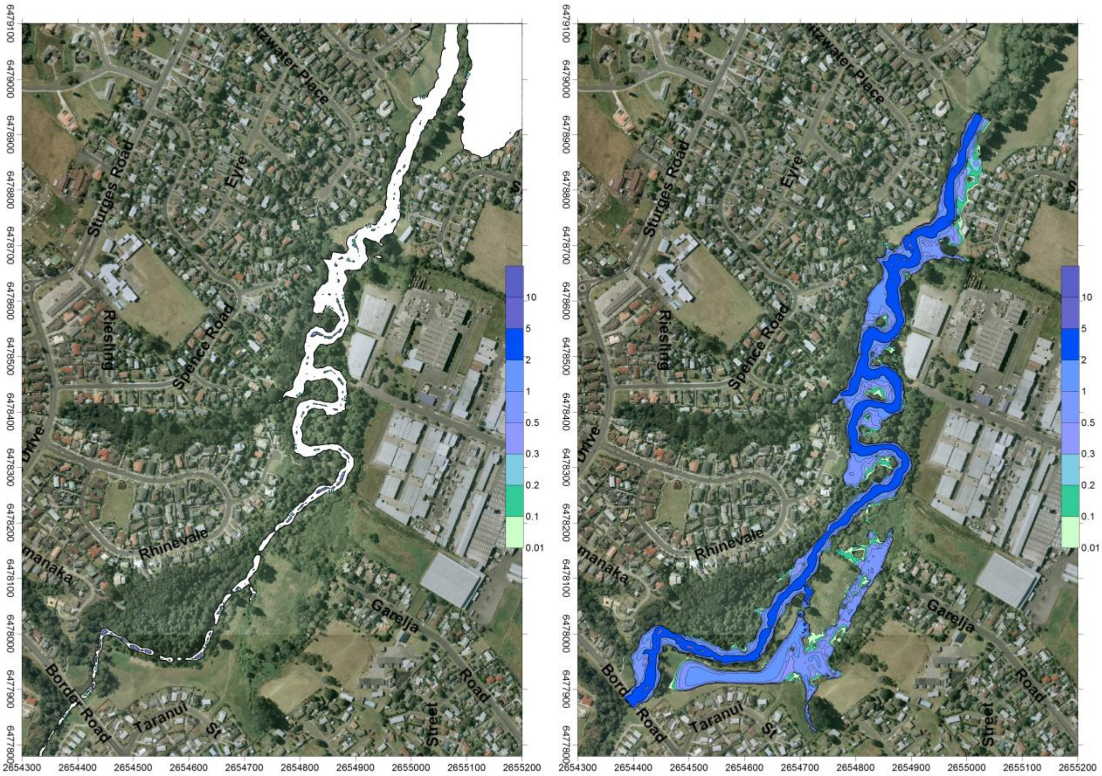

Figure 29. Flow Depth Contours of Verification Event at 0000 (left) and 1300 (right) on 24 August 2008.

The depth contours are based on a 1m x 1m grid, and are relative to a terrain model derived at the same resolution from the Lidar survey.

NZ Map Grid coordinates are provided for location.

Note that no georeferenced sections are available for the channel below the Lidar survey limits (see Section 9.2.4). Therefore because the low flow levels at 0000 hours (before the flood) are in many cases below the Lidar-based terrain, the aerial photograph background has been blanked below the 10m terrain contour in the left-hand contour plot, as otherwise the low flow contour remnants would be almost invisible.

The mass balance errors for the Verification run Opa08X are summarized in Table 2. As water density is assumed constant, the various masses are scaled into volumes in cubic metres. The tabulated volumes are, from left to right the “1D slices”, computed by accumulating the volumes under the model water surface along the channel, the “Net Inflow” which is the difference between the inflows and outflows accumulated from 00:00 to the given time, the “Gross Inflow” which is the cumulative upstream inflow at Border Road, and the “2D Grid”, which accumulates the volumes measured vertically on the 1mx1m grid used to prepare the flood maps in Figure 31.

The “Net inflow” volume is given an initial value equal to the “1D slices” volume, but (in the absence of georeferenced sections for the low flow channel) the initial 2D grid error shown in the left-hand plot in Figure 31 also needs correction. As shown in Figure 21, the modelled flood gradually increased from a steady low flow between 00:00 and about 07:00, reaching a level which should cover the terrain-based version of the low flow channel by about 08:00. Therefore at that time the "2D Grid" model was corrected to a value equal to the "1D slices" volume, and the same correction carried through the remainder of the event.

The flood peaked at around 13:00 hours, so that time was chosen for the test mass balance report.

Table 2

Volume Balance Errors, Run Opa08X. Note the asterisk * denotes values reset at the initial correction point.

24/8/2008	1D Slices	Net Inflow	Gross Inflow	1D Slices	Gross	2D Grid	Grid
Time (hrs)	Volume m^3	Volume m^3	Volume m^3	% Error	% Error	Volume m^3	% Error
00:00	4433	4433*	0	0	0	-	-
08:00	10312	10294	31622	0.18	0.06	10312*	0
13:00	149220	148807	482083	0.28	0.09	149651	-0.29

Table 2 shows that at peak flood, the mass balance error between "1D Slices" and "Net Inflow" was 0.28% in terms of the 1D slices, or 0.09% in terms of the Gross Inflow Volume. The mass error of gridding the solution into a 2D horizontal 1m x 1m grid was -0.29% in terms of the 1D Slices.

Note this solution was named Opa08Xhalfmin.rpt, which ran with 30 second time steps. The 24-hour simulation took 1.5 seconds to run, using an HP 8530p Elitebook with a 2 Core CPU T9600 @ 2.80GHz and 4.0 GB of RAM. The Operating System was Windows 7. If a 2D solution is used, run times will be orders of magnitude longer than this for no discernable advantage if lateral water surface slopes are insignificant.

18.3 Meaning of "Manning n"

The Manning n is normally understood to relate to the Manning equation as discussed in Section 10.1.2, but this applies to a simple undivided cross-section in a uniform flow. In such cases, the acceleration terms in the St Venant equation and the velocity head gradient in the Bernoulli equation both disappear, so that any Manning n calibration should give the same result if the hydraulic radius is used. This is the ratio of the section area, which scales the downstream weight force generated by the slope, and the wetted perimeter, which scales the resistance force generated by bed and wall shear.

In non-uniform flow, the velocity varies along the channel, so that the St Venant equation and Bernoulli equation will no longer calibrate with the same value of Manning n. Usually the St Venant equation will require a *higher* value of Manning n to match a given slope, such as that measured between the gauges at Border Road and the Vintage Reserve.

A “resistance radius” is an alternative to the hydraulic radius, and this effectively replaces the wetted perimeter with the surface width in computation of the Manning formula, removing any allowance for wall shear from calculations. The use of 2D solutions requires a similar approximation, so in both cases calibration to the same water surface gradient will obviously require a *higher* Manning n value than that obtained using the hydraulic radius. The differences will diminish on laterally flat surfaces, and in the idealized “wide rectangular” channel the walls are insignificant so the “resistance radius” and “hydraulic radius” values will approach each other.

With 2D modelling, the available grid sizes are limited to a practical minimum (see Section 18.1), and present practice typically uses 1m x 1m grids or larger. Bearing in mind that a channel starts to look “blocky” if the flow path is less than about ten grids wide, it is not possible to resolve a small low flow channel such as the Opanuku without “blockiness” starting to obstruct flow, particularly when the channel axis is oblique to the model grid lines.

Calibration of a channel with such problems is then likely to require a *lower* Manning n than that obtained using the hydraulic radius, as a form of wall shear is reintroduced by “blockiness” providing a kind of substitute to wall roughness.

In channels of only one or two grids in width, the “blockiness” may become more important than resistance in retarding channel flow, in which case 2D models may even calibrate to a reduced Manning n compared with models using the original hydraulic radius. In extreme cases the low flow channel may be totally obstructed, so that the Manning n becomes irrelevant at all upstream levels below the obstructing blocks.

In short, the values of Manning n fitted by residual flow calibration will depend significantly on the type of model applied. However, the rating curve is also a processed form of recorded external data, so because all models will need to comply with this as well as the recorded variation of levels at each end of the reach, there is reason to think that the *ratio* of the Manning n values fitted to the verification and calibration curves should be the same as that found here – that is 0.040/0.045.

Therefore the conclusion that riparian resistance clearly *decreased* in the test reach between October 2006 and August 2008 should *not* be dependent on the modelling platform.

19. Discussion

19.1 Remaining Difficulties

As already reported, this study has established that existing modelling techniques are sufficiently sensitive to detect changes in hydraulic resistance corresponding with riparian vegetation modification as recently undertaken within and near the Vintage Reserve. It follows that use of correct roughness factors is required if flood predictions are to be accurate.

However, there are two remaining difficulties in identifying which roughness factors are "correct" from the evidence of this study:

1. The location of the primary gauging site for the study within the Vintage Reserve, right in the middle of the reach undergoing modification of the riparian vegetation. It is also not helpful that the higher floods all overflow upstream of the gauging site, so an unknown proportion of the flood flows are excluded from gaugings.

2. An apparent lack of consistency between the riparian resistance values obtained by field calibration and those reported in the literature.

The following discussion deals with these matters separately.

Figure 32. Riparian planting looking upstream from above Vintage Reserve gauging site

19.1.1 Vintage Reserve Gaugings

There is clear photographic evidence that riparian vegetation modification is significant in the immediate vicinity of the Vintage Reserve gauging station. Figure 32 illustrates riparian planting, and Figure 33 illustrates riparian vegetation clearance. Depending on which dominates, the riparian resistance may be going up or down. Figure 33 also shows fallen trees partially obstructing the low flow channel, which will raise the low flow resistance until the obstructions are removed or washed away.

If this succession of incidence and removal of blocking debris is a natural feature of the stream, the bandwidth of a long established rating curve will indicate the scale of this effect. However if there is drastic human intervention such as that indicated in Figures 32 and 33, rating observations alone cannot distinguish between the impacts of that intervention and normal loop rating effects. To make that distinction, residual flow techniques are required.

Figure 33 Riparian vegetation clearance and low flow channel obstructions looking downstream from below Vintage Reserve gauging site

At the Border Road bridge (see Figure 34), the problem of channel overflow does not arise, as the road embankments force all (probable) flood flows under the bridge. The bridge also provides a safe platform for flood gauging in all conditions.

Figure 34 shows some vegetation at the bridge cross-section, but this tends to be lower than at the Vintage Reserve site, with a good representation of grasses which vary less in resistance properties than tall vegetation. The shading effect of the bridge also tends to discourage profuse growth directly underneath, and the bridge area appears to be excluded from the interventions planned for the vegetation in the reserve, creating more consistency in riparian vegetation cover. Finally (and importantly) the flow appears to change from a flatter to steeper grade under the bridge, reducing the influence of vegetation on the relationship between flow and upstream level.

Figure 34 The cross-section at the Border Road bridge, looking downstream.

Border Road is therefore clearly superior to the Vintage Reserve as a site for long term monitoring of river flows, with the only weakness being possible erosion of the bed, which would enlarge the cross-section and modify the rating. Any risk of this could be minimised by stabilising the cross-section using concrete, either informally by grouting or formally by constructing a low broad-crested weir.

The Vintage Reserve gauge could be maintained, but only as a secondary site recording water levels without regular accompanying attempts at gauging. The two gauges would then continue to offer slope measurements between sites, but with Border Road being the primary flow measurement site.

19.1.2 Inconsistencies Between Calibration and Values from Literature

The calibrated values of a Riparian Resistance gave a relative resistance of 10.0 for a calibrated low flow Manning n of 0.045 – in other words, a Manning value of about 0.45 for the riparian resistance. Values from literature appear to be typically only one-quarter to one-third of these values.

While it is attractive to be able to use literature-based values directly, this situation is no different from that applying to granular resistance, in which (see Equation (15) in Section 10.1.2) the calibrated low flow Manning n of 0.045 corresponds to an equivalent grain diameter of 2781 mm or 2.781 m! No granular material remotely approaching this size is in evidence in the Opanuku low flow channel, and the discrepancy is conventionally explained (e.g. in Henderson [1966]) by the introduction of “form resistance” in addition to granular resistance.

In practice, this means that only prismatic uniform channels in granular material have resistance predictable purely by reference to the grain size, and as vegetation resistance literature reports tend to deal only with measurements under prismatic uniform flow conditions, it may well be that the same applies to channels with riparian resistance.

With vegetation, the equivalent of “form resistance” could arise from

1. The existence of major bed irregularities under the vegetation – see Figures 32 and 33
2. Heterogeneity – a tall canopy may be dominant visually and therefore taken to characterise the vegetation, but dense undergrowth and a tall canopy combined are likely to obstruct flow considerably more than a monocultured test plot of tall canopy alone.
3. Tall vegetation typically extends laterally, so a resistance value cannot really be applied only to the point where such vegetation emerges from the ground. An example is the tree in the centre of Figure 32, which will clearly obstruct flood flows through the main low flow channel even though it is growing outside that channel. This does not conform well to the basic subchannel model shown in Figure 7.
4. Elastic properties may vary for trees of the same height.

With respect to the last point, experiments with the stem wave speed gave a match with this field resistance calibration for a stem wave speed of 0.5 m/s, about ten times the default value found from literature. However this higher value is still far below elastic wave speeds measured in dry timber, which are of the order of 1000 m/s, and the literature covers experiments with very few tree species, so there appears to be considerable room for experimentation to find stem wave speeds in species common in New Zealand.

19.2 The Residual Flow Approach to Roughness Calibration

Standard roughness calibration techniques generally assume a flow profile and seek to match observed level hydrographs by adjusting roughness parameters such as the Manning n values. Differences between modelled and observed level hydrographs are minimised in some sense, after which the Manning n values are said to be calibrated.

However this does not address the minimisation of errors in the assumed flow profiles, even though field measurements of flows are usually far more difficult than those of levels. For example, what is the use of an exact match in levels if the assumed flood flows through the channel were derived solely from an approximate hydrological catchment runoff model? A rating curve from a gauged cross-section offers some improvement, but it is well known (see Section 15.3.1) that flows at a given section are affected by water surface slope and acceleration as well as the water level, particularly in large flood events, so significant flow errors result from heavy reliance on rating curves.

For hydropower work, the accurate modelling of flows is paramount, as any forecasting of future generating capacity depends on close matching of tributary flows as well as station flows. To improve forecasting accuracy, an improved roughness calibration technique has been developed which concentrates attention on the minimisation of flow errors by virtually eliminating model level errors. This is done by setting the measured levels as boundary conditions at stub tributaries set up at each profile measurement point.

This ensures virtually perfect matching of profile levels, but at the expense of allowing uncontrolled inflows and outflows through the tributaries as required to maintain the exact level match. However, while accurate tributary inflow and outflow measurements may not be available from the field for calibration, in most cases it is safe to assume by definition that they are small compared with the main channel flow, so that approximate estimates are quite adequate. For example, the flow in a 150mm pipe is likely to be well under 1% of the flood flow from a catchment of several square kilometres.

Once roughness values are fitted which produce main channel flows falling within the range of measurement error at calibrated gauging stations, and which reduce the tributary inflows and outflows to small residual amounts (after taking into account reasonable estimates of any major tributary flows) the Manning n values can be accepted as calibrated.

Because this method achieves calibration by the minimisation of residual inflows and outflows left after the progressive removal of all other model errors, it is called the “residual flow approach”. If such residuals are all negligible compared with concurrent main channel flows, the calibration can be seen as highly accurate.

Section 15 above presents an example of this approach for the Opanuku Stream. Note that calibration is possible by this approach only if at least two level hydrographs are available to provide the required surface level measurements, and if a loop rating is allowed for the gauging site as discussed in Section 15.3.1.

20. Conclusions

1. Flood levels are sensitive to variations in riparian roughness.
2. This sensitivity is significant with respect to potential flood damage costs, particularly at flood levels where lateral channel overflows start to occur.
3. Riparian vegetation resistance can be calibrated accurately in a natural river reach by using models based on close monitoring of levels and flows in flood events.
4. Such calibrated resistance estimates can then be transferred to comparable channels with reasonable confidence.
5. The Opanuku Stream offers a suitable experimental test reach between Border Road and the Vintage Reserve, subject to recommended correction of a number of identified data collection problems.
6. Vegetation resistance models based on simplified experiments on homogeneous single species plots do not at present match riparian resistance measurements, except in simplified channels which closely resemble the experimental channels.
7. For progress on predictive reliability, further work is required on the effects of bed irregularities, species heterogeneity, lateral vegetation extension and stem elastic properties.
8. Between floods observed in October 2006 and August 2008, there was a measurable decrease of about 10% in the hydraulic resistance of the test reach, expressed in terms of the Manning n.
9. This period coincided with significant replacement of exotic riparian vegetation by native plantings along the test reach, but some of the resistance decrease may also be attributable to seasonal effects and the replacement of mature growth with immature plantings.

References

Abbott, M.B. and Larsen, J. (1985) Modelling circulations in depth-integrated flows Part 2: A reconciliation J. Hydraul. Res., 23(5): 397-420

Ackers P. (1958) Resistance of fluids in channels and pipes, Hydraulic Research Paper No.2, H.M. Stationery Office, London.

Anon (1961) Modern Computing Methods H.M. Stationery Office, London.

Barnes, H.H. (1967). Roughness Characteristics of Natural Channels. U.S. Geological Survey Water-Supply Paper 1849.

Barnett, A.G. (1985) The Tauranga harbour study – hydrodynamic aspects Proc. Australasian Conference on Coastal and Ocean Engineering, Christchurch, 1985 Vol. 2: 465-474.

Barnett, A.G., Lindberg, S, Syme, W.J. and Shankar, U (1991). A Rigorous Hydraulic Approach to Urban Drainage Modelling, Proc. Int. Symposium on Urban Stormwater Management, Sydney, February 1992 pp 290-293.

Barnett, A.G. (1998) The Museum of New Zealand – flood protection lessons Proc. 1998 IPENZ Conference, Auckland, Vol. 3, 113-118.

Barnett A.G. (2002). Resistance Computation in Compound Channels. Proc. 2002 Modelling Conference, Auckland, Nov 2002 pp. 143-151.

Barnett , A.G. (2008). Hydraulic Effects of Riparian Planting. Barnett & MacMurray Ltd.

Barnett, A.G. and Hellberg, C. Residual Flow Modelling: An Advance in Channel Resistance Calibration. Paper 3370, Proc. 34th IAHR World Congress, Brisbane, Australia June-July 2011 (On CD).

Bates, P.D. (2004). Remote sensing and flood inundation modeling. Hydrol. Process. 18:2593-2597.

Beven, K.J., 1993. Prophecy, reality and uncertainty in distributed hydrological modeling. Adv. Wat. Res., 16(1): 41-51.

Cao, Z., Meng, J. Pender, G. and Wallis, S. (2006). Open Channels Flow Resistance and Momentum Flux in Compound Open Channels. J. Hydraul. Eng., 132(12): 1272-1282.

Chow, V.T. (1959). Open Channel Hydraulics. International edition. McGraw Hill, London.

Cowan, W.L. (1956). Estimating hydraulic roughness coefficients. Agr. Eng., 37(7): 473–475.

Department for Environment, Food and Rural Affairs and the Environmental Agency DEFRA/EA (2003a). Reducing uncertainty in river flood conveyance, Interim Report 2: Review of methods for estimating conveyance. UK.

DEFRA/EA (2003b). Reducing Uncertainty in River Flood Conveyance Roughness Review. UK.

DEFRA/EA (2004). Reducing uncertainty in river flood conveyance, Phase 2: Conveyance Manual. UK.

Ervine D.A. and Ellis J. (1987). Experimental and Computational Aspects of Overbank Floodplain Flow., Transactions of the Royal Society of Edinburgh: Earth Sciences, Vol. 78, pp 315–475.

Ervine, D.A., Babaeyan-Koopaei, K. and Sellin, H.J. (2000). Two-dimensional Solution for Straight and Meandering Overbank Flows. J. Hydraul. Eng., 126(9): 653-669.

Fathi-Moghadam, M. and Kouwen N, (1997). Non-rigid, non-submerged vegetation roughness in flood plains. J. Hydraul. Eng., 123: 51-57

Flippin-Dudley, S.J., Abt, S.R., Bonham, C.D., Watson, C.C. and Fischenisch, J.C. (1998). Evaluation of Flow-Resistance Equations for Vegetated Channels and Floodplains. U.S. Army Corps of Engineers, Technical Report EL-98-2, Washington, D.C.

Fread, D.L. and Smith, G.F. (1978). Calibration technique for 1-D unsteady flow model. J. Hydr. Div., 104(7): 1027-1044.

Freeman, G.E., Rahmeyer, W.H. and Copeland, R.R. (2000). Determination of resistance due to shrubs and woody vegetation. Technical Report, ERDC/CHL TR 025, U.S. Army Engineer Research and Development Center, Vicksburg, MS.

French, R.H. (1994). Open-Channel Hydraulics. McGraw-Hill, USA.

GHD (2006) Opanuku/Oratia Streams Catchment, Final Report (Consulting Report)

Helmiö, T. (2004) Flow resistance due to lateral momentum transfer in partially vegetated rivers. Wat. Res. Res., W05206, doi:10.1029/2004WR003058.

Helmio¨, T. (2002). Unsteady 1D flow model of compound channel with vegetated floodplains. J. Hydrol., 269(1– 2): 89–99.

Henderson, F.M. (1966). Open Channel Flow. Macmillan Series in Civil Engineering, Macmillan Company, New York.

Hicks, D.M. and Mason, P.D. (1991). Roughness characteristics of New Zealand Rivers. Water Resources Publications, LLC, Englewood, CO.

HYDRA Software Ltd (2012) www.auloshydraulics.com

Ibbit, R.P. and O'Donnell, T., (1974). Designing conceptual catchment models for automatic fitting methods. IAHS-AISH No. 101: 461-475.

James C.S. and Wark J.B., (1992). Conveyance Estimation for Meandering Channels. HR Wallingford Ltd. Report SR 329, pp. 1-91.

Järvelä, J. (2002). Determination of flow resistance of vegetated channel banks and floodplains. In Bousmar D. and Zech Y. (editors), River Flow 2002. Lisse, Swets & Zeitlinger, pp. 311-318.

Jowett I.G. and Thompson S.M. (1992) Book Review, New Zealand Journal of Marine and Freshwater Research, Vol. 26 pp. 285-286.

Khatibi, R.H., Williams, J.R. and Wormleaton, P.R. (1997). Identification problem of open-channel friction parameters. J. Hydraul. Eng., 123(12), 1078–1088.

Kidson , H R. L., Richards, K.S. and Carling, P.A. (2006). Hydraulic model calibration for extreme floods in bedrock-confined channels: case study from northern Thailand. Hydrol. Process., 20(2): 329 – 344.

Klaassen, G.J. and Zwaard, J.J. 1974. Roughness coefficients of vegetated floodplains. J. Hydraul. Res., 12(1): 43-63.

Knight, D. W. (1999). Flow mechanisms and sediment transport in compound channels. Int. J. Sediment Res., 14(2): 217–236.

Knight, D. W., and Sellin, R. H. J. (1987). The SERC flood channel facility." J. Inst. Water Environ. Manage., 41(4): 198–204.

Knight, D.W., and Shiono, K. (1996) River channel and floodplain hydraulics, In Floodplain Processes [Eds Anderson, Walling and Bates], Chapter 5, J. Wiley, 139-181.

Knight, D.W. (2006). River flood hydraulics: theoretical issues and stage-discharge relationships. Chapter 17. in: Knight, D.W. and Shamseldin A.Y. (eds) River basin modelling for flood risk mitigation. Taylor & Francis.

Knight, D.W., Demetriou, J.D. and Hamed, M.E., (1983). Hydraulic analysis of channels with flood plains, Proceedings Int. Conf. on Hydraulic Aspects of Floods and Flood Control, British Hydromechanics Research Association, BHRA, Cranfield, Sept., Paper E1, 129-144.

Kouwen, N. (1992) Modern approach to design of grassed channels, J. Irrig. And Drain. Engrg., ASCE, 118(5), 733-743.

Kouwen N. (1988). Field estimation of the biomechanical properties of grass. J. Hydraul. Res., 26: 559–568.

Kouwen N. and Li R-M. (1980). Biomechanics of vegetated channel linings. J. Hydr. Div., 106: 1085-1103.

Kouwen N. and Unny T.E. (1973). Flexible roughness in open channels. J. Hydr. Div., 99: 713-728.

Kouwen, N. and Fathi-Moghadam, M. (2000). Friction factors for coniferous trees along rivers. J. Hydraul. Eng., 126 (10): 732-740

Li, R.-M. and Shen, H.W. (1973). Effect of tall vegetations on flow and sediment. J. Hydr. Div., 99(5): 793–814.

Lindner, K. (1982). Der Strömungswiderstand von Pflanzenbeständen. Mitteilungen 75. Leichtweiss-Institut für Wasserbau, Technische Universität Braunschweig. [Doctoral thesis].

Mason, D.C., Cobby, D.M., Horritt, M.S. and Bates, P.D. (2003). Floodplain friction parameterization in two-dimensional river flood models using vegetation heights derived from airborne scanning laser altimetry. Hydro. Process., 17: 1711–1732.

Mertens, W. (1989), Zur Frage hydraulischer Berechnungen naturnaher Fliessgewa¨sser, Wasserwirtschaft, 79(4): 170– 179.

Naot, D., I. Nezu, and H. Nakagawa (1993). Hydrodynamic behavior of compound rectangular open channels. J. Hydraul. Eng., 119(3), 390–408.

Nguyen, H. T. and J. D. Fenton (2005). Identification of roughness for flood routing in compound channels, Proc. 31st Congress, Int. Assoc. Hydraulic Engng and Res., Seoul, Korea, 11-16 September, 2005, Published on CD.

Nicholas, A. and McLelland, S. (2004). Computational fluid dynamics modelling of three-dimensional processes on natural river floodplains. J. Hydraul. Res., 42: 131-143.

Petryk, S., and Bosmajian, G. (1969). Drag on cylinders in open channel flow. Ph. D thesis, Colorado State University, USA.

Petryk, S., and Bosmajian, G. (1975). Analysis of flow through vegetation. Journal of the Hydraulics Engineering, 101(7): 871-884.

Pezzinga, G. (1994). Velocity distribution in compound channel flows by numerical modeling. J. Hydraul. Eng., 120(10): 1176–1198.

Righetti, M., and A. Armanini (2002). Flow resistance in open channel flows with sparsely distributed bushes, J. Hydrol., 269: 55-64.

Shamseldin A.Y. (2008) Hydraulic Resistance of Vegetation: Ref. 13024.00, Uniservices Ltd, University of Auckland.

Sellin, R.H.J., 1964, A laboratory investigation into the interaction between the flow in the channel of a river and that over its floodplain, La Houille Blanche, No.7, 793-802.

Shiono K. and Knight D.W. (1990). Mathematical Models of Flow in Two or Multi-Stage Straight Channels. International Conference on River Flood Hydraulics, Paper G1, pp. 229-238.

Shiono K., Muto Y., Knight D.W. and Hyde A.F.L. (1999). Energy Losses due to Secondary Flow and Turbulence in Meandering Channels with Overbank Flow. J. Hydraul. Res., 37(5): 641-664.

Shiono, K. and Knight, D.W. (1991). Turbulent open channel flows with variable depth across the channel, J. Flu. Mech., . 222: 617-646.

Smart, G. (1992). Stage-discharge discontinuity in composite flood channels. J. Hydraul. Res., 30(6): 817–833.

Sofialidis, D., and Prinos, P. (1998). Compound open-channel flow modeling with nonlinear low-Reynolds *k*- models. J. Hydraul. Eng., 124(3): 253–262.

Sofialidis, D., and Prinos, P. (1999). Numerical study of momentum exchange in compound open channel flow. J. Hydraul. Eng., 125(2):152–165.

Stoesser, T., Wilson, C., Bates, P., and Dittrich, A. (2003). Application of a 3D numerical model to a river with vegetated floodplains. J. Hydroinform., 5: 99–112.

Thompson, G.T. and Roberson, J.A. (1976). A Theory of Flow Resistance for Vegetated Channels. Trans., ASAE ,19(2): 288-293.

Tsihrintzis, V. A., (2001). Discussion on variation of roughness coefficients for unsubmerged and submerged vegetation., J. Hydraul. Eng., 127(3), 241–244

Tsujimoto, T. (1999). Fluvial processes in streams with vegetation. J. Hydraul. Res., 37(6), 789–803.

U.S. Army Corps of Engineers(USACE) (1991). Hydraulic Design of Flood Control Channels. Engineer Manual, No. 1110-2-1601.

U.S. Army Corps of Engineers(USACE) (1997). Hydraulic impacts of riparian vegetation. Technical Report EL-97-9..

US Department of Agriculture (USDA) (1954). handbook of channel design for soil and water conservation.

US Department of Agriculture (USDA) (1954). handbook of channel design for soil and water conservation.

Vojinovic, Z. and Abbott, M.B. (2012) Flood Risk and Social Justice. IWA Publishing, London.

Werner M.G.F. and Lambert, M.F. (2007). Comparison of modelling approaches used in practical flood extent modeling. J. Hydraul. Res., 45(2): 202–215

Wiggert, J.M. Taylor, M.R. and Contractor D.N. (1976). Optimization of an implicit flow routing model. Int. Symp. On Unsteady flow in Open Channel., University of New Castle-on Tyne, BHRA Fluid Mechanics, Cranfield, Bedford, England.

Williamson, J. (1951) The laws of flow in rough pipes, La Houille Blanche, 6(5):738

Wilson, C.A.M.E. and Horritt, M.C., (2002). Measuring the flow resistance of submerged grass. Hydrol. Process., 16: 2589–2598.

Wu, Fu-Chen, Hsieh, W.S. and Chou, Yi-Ju (1999). Variation of roughness coefficients for unsubmerged and submerged vegetation. J. Hydraul. Eng., 125(9):934–942.

Yang, K , Cao; S, and Knight, D.W. (2007). Flow Patterns in Compound Channels with Vegetated Floodplains. J. Hydraul. Eng., 133 (2): 148-159.

Yen (2002). Open channel flow resistance. J. Hydraul. Eng., 128(1): 20-39.

Appendix 1

List of Computer Files

Section 8:

AULOS Result Files: OpaExam2.rpt (Exam2), Opa_2007fineExam2.rpt (high resolution)

Spreadsheets: OpaExam2.xls (plots), Examwork2.xls (balancing flow)

Section 9:

Cross-sections: Xsection locations.xls

Aerial Photo: Opanuku.bmp

Raw Lidar data: 40Composite_DTM.xyz, 41Composite_DTM.xyz, 42Composite_DTM.xyz

Composite in NZMG: CompositeNZMG.xyz

Terrain 1mx1m grid: NZMG1m.grd

Section 11:

AULOS Result File: OpaQ100Ddn.rpt

Rating Spreadsheet: Q100Rating.xls

Section 12:

HYCEMOS-U Files: HY_INRainP.zzz (Power rainfall), HY_INRainC.zzz (Candia rainfall)

AULOS Result Files: OpastudyT40.rpt, OpastudyT.rpt, OpastudyT44.rpt

Spreadsheet: OpaResidCum.xls (plots)

Section 13:

Spreadsheet: CalibvsVerif.xls (plot)

Section 14:

Rating Spreadsheet: AllGaugingsMSL.xls

Section 15:

AULOS Result Files: Opa06W42.rpt (runoff n=0.042), Opa06X.rpt (calibrated model n=0.045)

Spreadsheets: OpaCalib0608X.xls (Calibration vs observed), OpaResidCum08X.xls (residuals)

Section 16:

HYCEMOS-U Files: HY_INRainP08.zzz (Power rainfall), HY_INRainC08.zzz (Candia rainfall)

AULOS Result Files: Opa08W42.rpt (runoff n=0.042), Opa08X4min.rpt (calibrated model n=0.040)

Spreadsheets: OpaCalib0608X.xls (Calibration vs observed), OpaResidCum08X.xls (residuals)

Section 17:

Exam2 Spreadsheets: OpaExam2.xls (plots), Examwork2.xls (balancing flow)

AULOS Result Files: Opa08WDdn.rpt (Drawdown),
Opa08W455min.rpt, Opa08X45.rpt (n=0.045),
Opa08Wrr85min.rpt, Opa08Xrr8.rpt (rr=8),
Opa08WS0025min.rpt, Opa08XS002.rpt (S=0.002)

Spreadsheet: OpaCalib0608X.xls (Rating Curves)

Section 18:

AULOS Result Files: Opa08X1hr.rpt, Opa08X1hr.ags (water level 1m grid series at 1 hour intervals)

AULOS Grid Files: Opa08X0hry0.grd (depths at 0 hours), Opa08X13hry0.grd (depths at 13 hours)

Terrain Grid File: 1to5000A4.grd (Terrain 1m grid of study area)

Surfer mapping file: Aerial10m+1mto5000A4.srf (Maps to scale 1:5000 on portrait A4 page)

AULOS Result File: Opa08Xhalfmin.rpt (Opa08X run, saving net inflow results every 30 seconds)

AULOS Out File: Opa08XhalfminBC7dp.rpt (ASCII table of boundary flows to 7 decimal places)

Spreadsheet: VolcompX1hr7dp.xls (Volume balances at 1 hour intervals, to 7 decimal places)